SNOWMELT WATER INFILTRATION INTO FROZEN SOIL IN RED RIVER OF THE NORTH BASIN

A Dissertation
Submitted to the Graduate Faculty
of the
North Dakota State University
of Agriculture and Applied Science

By

Debjit Roy

In Partial Fulfillment of the Requirements
for the Degree of
DOCTOR OF PHILOSOPHY

Major Department:
Agricultural and Biosystems Engineering

March 2018

Fargo, North Dakota

North Dakota State University
Graduate School

Title

SNOWMELT WATER INFILTRATION INTO FROZEN SOIL IN RED RIVER OF THE NORTH BASIN

By

Debjit Roy

The Supervisory Committee certifies that this ***disquisition*** complies with North Dakota State University's regulations and meets the accepted standards for the degree of

DOCTOR OF PHILOSOPHY

SUPERVISORY COMMITTEE:

Dr. Xinhua Jia
Chair

Dr. Dean D. Steele

Dr. Zhulu Lin

Dr. Xuefeng Chu

Approved:

04/10/2018
Date

Dr. Sreekala Bajwa
Department Chair

ABSTRACT

Infiltration into frozen soils is an important process in the hydrological cycle. Though infiltration occurs at the soil surface, it is affected by many factors, e.g. soil water content, temperature, and hydraulic conductivity. Understanding the snowmelt water infiltration processes into frozen soil helps to address issues about runoff generation and spring flooding in seasonally frozen area like Red River of the North basin (RRB). In this study, the methods of soil water release curve (SWRC) development, the effect of soil water content on frozen soil infiltration, and the variation of hydraulic conductivity for different RRB soils in frozen and unfrozen conditions were examined and evaluated. The objectives of this study were: (1) to construct SWRC using combined HYPROP and WP4 method, (2) to evaluate the soil water and temperature effects on the infiltration into frozen soil, and (3) to compare predicted hydraulic conductivity of three frozen soils of RRB with measured values using minidisk infiltrometer. It was found that HYPROP+WP4 combined method produced acceptable SWRC of RRB soils compared to other available traditional methods. However, shrinking and swelling of clay content of the soils might cause difference with in-situ measurement. Infiltration into frozen soil depended on initial soil water contents. The drier the frozen soil, the higher the infiltration rate. Soil water content changed gradually with rising temperature in a dry soil but in a frozen wet soil, it was very rapid due to the phase changing of water. The Horton infiltration model was fitted with measured frozen soil infiltration data with good agreement. Hydraulic conductivity of frozen soils decreased with an increase in soil water contents, but it was also subjected to sand and clay contents of the soil. Simple nonlinear regression model fitted with measured data and resulted reasonable agreement compared to Motivilov model. Freeze-thaw cycles altered the soil pore distribution, decreased the infiltration rate and hydraulic conductivity of frozen soils.

ACKNOWLEDGEMENTS

At the very beginning, I am feeling proud to express my gratitude and thanks to my advisor, Xinhua Jia, PhD, PE. It is her constant effort and support which made this work possible. I am very grateful to her for the worthy guidance, valuable suggestion, and constructive criticism throughout the program duration.

I would like to give my sincere thanks to Dr. Dean D. Steele, Dr. Zhulu Lin, and Dr. Xuefeng Chu for being the honorable members of my PhD supervisory committee, for spending their valuable time and effort to evaluate my research work, and for sharing their thoughts, ideas and precious comments and suggestions.

It is my pleasure to express special thanks to Dr. Dongqing Lin, James Moos, Sheldon Tuscherer, Connor Yaggie, Rohit Pathak, Kelsey Kolar, Mojtoba Ahmadi, Qiang Li, and Hannah Bye for their kind support and help throughout the study. Besides, I thank all the faculty and staff of ABEN department of NDSU as well as all employee of Elllingson Companies.

I thank my wife, Taposhi Rani Shil, my parents, Binoy Kumar Roy and Shikha Rani Shil, my parents-in-laws, Krishna Kanta Shil and Asha Rani Shil, my siblings, Anindita and Riya, my two kids, Arijit and Abhismit, for their well wish, prayer and care, encouragement and inspiration during my stay in NDSU.

And, above all, I am grateful to almighty God. Without the blessings, it would be impossible to complete my work successfully.

DEDICATION

To

My Wife, ***Taposhi Rani Shil,***

Sacrificed impossible to make my honor possible

"Still waters run deep. Shallow waters run dry frequently."

-Thomas County Cat

TABLE OF CONTENTS

ABSTRACT iii

ACKNOWLEDGEMENTS iv

DEDICATION v

LIST OF TABLES xi

LIST OF FIGURES xii

LIST OF APPENDIX FIGURES xiv

1. GENERAL INTRODUCTION 1

1.1. Background 1

1.2. Snowmelt water infiltration 2

1.2.1. Importance of snowmelt water infiltration 4

1.2.2. Factors affecting snowmelt water infiltration 4

1.3. Snowmelt water infiltration processes 6

1.3.1. Water movement through frozen soil 8

1.3.2. Freeze-Thaw (FT) cycle 10

1.3.3. Temperature variation and heat transfer in frozen soil 11

1.3.4. Hydraulic conductivity in frozen soil 13

1.4. Infiltration equations and models 15

1.4.1. Horton infiltration equation 15

1.4.2. Kostiakov equation 15

1.4.3. Philip equation 15

1.4.4. Green-Ampt equation 16

1.4.5. HYDROL-INF model 16

1.4.6. DRAINMOD model 17

1.4.7. HYDRUS model 18

1.5. Water infiltration measurement 18
1.5.1. Ring infiltrometer 18
1.5.2. Tension infiltrometer 20
1.5.3. Rainfall simulator 23
1.6. Objectives of the dissertation study 24
1.6.1. Specific objectives of the research 25
1.7. Organization of the dissertation 25
1.8. Reference 26
2. DEVELOPMENT AND COMPARISON OF SOIL WATER RELEASE CURVES FOR THREE SOILS IN THE RED RIVER VALLEY OF THE NORTH, USA 32
2.1. Abstract 32
2.2. Introduction 33
2.3. Materials and methods 36
2.3.1. Soils 36
2.3.2. HW method 37
2.3.3. HTP method 40
2.3.4. SWRC fitting 41
2.3.5. SWRC difference 42
2.4. Results and discussion 42
2.4.1. Fargo silty clay soil 45
2.4.2. Glyndon silty loam soil 45
2.4.3. Hecla sandy loam soil 46
2.4.4. SWRC difference 47
2.4.5. Variability of SWRC in soil textural classes 50
2.4.6. Bulk density changes 52

2.5. Conclusion 53
2.6. Acknowledgements 54
2.7. References 55
3. INFILTRATION INTO FROZEN SILTY CLAY LOAM SOIL WITH DIFFERENT SOIL WATER CONTENTS IN THE RED RIVER OF THE NORTH BASIN 59
3.1. Abstract 59
3.2. Introduction 60
3.3. Materials and methods 64
3.3.1. Soil and soil properties 64
3.3.2. Initial soil water contents 66
3.3.3. Soil water and temperature sensors 66
3.3.4. Sensor calibration 67
3.3.5. Soil packing and freezing 68
3.3.6. Experiments 69
3.3.7. Measurements 70
3.3.8. Goodness of fit 72
3.3.9. Horton infiltration model: fitting with observed data 74
3.4. Results and discussion 74
3.4.1. Sensor data quality checking 74
3.4.2. Infiltration rate over time 76
3.4.3. Observed data fitting with Horton infiltration model 78
3.4.4. Soil water changes with temperature 80
3.4.5. SWRC comparison: before and after experiments 85
3.5. Conclusion 87
3.6. Acknowledgement 88

3.7. References 88

4. HYDRAULIC CONDUCTIVITY MEASUREMENT OF THREE SOILS IN THE RED RIVER OF THE NORTH BASIN IN FROZEN AND UNFROZEN CONDITIONS BY USING MINIDISK INFILTROMETER 93

4.1. Abstract 93

4.2. Introduction 94

4.3. Materials and methods 98

4.3.1. Soils and soil properties 98

4.3.2. Soil water release curve and soil freezing curve 99

4.3.3. Experiment conditions 102

4.3.4. Instrumentation 102

4.3.5. Experiment preparation: soil packing and freezing 103

4.3.6. Experiment setup and measurement 105

4.3.7. Relationship between k and θ_v: nonlinear regression model 108

4.3.8. Comparison to Motivilov model 108

4.3.9. Goodness of fit and root mean square error 109

4.4. Results and discussion 109

4.4.1. k comparison: frozen and unfrozen conditions 110

4.4.2. Relationship between k and θ_v: fitted model 112

4.4.3. Fitted model vs. Motivilov model 114

4.4.4. Freeze-thaw effect on k measurement 116

4.5. Conclusion 117

4.6. Acknowledgement 119

4.7. References 119

5. GENERAL CONCLUSIONS 123

APPENDIX. INFILTRATION MEASUREMENT IN FROZEN AND UNFROZEN SOILS 125

LIST OF TABLES

Table | Page

1. Percent of sand, clay, silt and bulk densities of the soil samples 37
2. Best fit estimated van Genuchten parameters by HYPROP and WP4 (HW) method and hanging column, Tempe cell, and pressure plate method (HTP). 42
3. Variation in α and n van Genuchten fitting parameter reference value ranges for soils in this study and soils from the same textural classes 50
4. Comparison of soil bulk density (g cm^{-3}) for the three soils using HYPROP and hanging water column, Tempe cell, and pressure plate (HTP) methods 53
5. Soil hydraulic property parameters from soil water release curve. 65
6. Percent of sand, clay, silt and bulk densities of the soil samples 99
7. Soil hydraulic properties from soil water release curve 100
8. Mean measured hydraulic conductivity, k (cm/min) for different soil types, initial soil water contents (θ_{inital}), and frozen/unfrozen conditions 110

LIST OF FIGURES

Figure — Page

1. HYPROP® assembly (Schindler et al., 2010). 38

2. Fitted SWRCs using best estimated van Genuchten parameters with HYPROP+WP4 (HW) dataset for (a) Fargo soil, (c) Glyndon soil, (e) Hecla soil and with hanging column, Tempe cell, and pressure plate (HTP) dataset for (b) Fargo soil, (d) Glyndon soil, and (f) Hecla soil. 43

3. Comparison between fitted SWRCs of HYPROP and WP4 (HW) and hanging column, Tempe cell, and pressure plate (HTP) datasets for (a) Fargo soil, (b) Glyndon soil, and (c) Hecla soils. 44

4. Comparison of absolute values of volumetric water content differences (%) between fitted SWRCs of HYPROP+WP4 (HW) and hanging column, Tempe cell, and pressure plate (HTP) datasets for (a) Fargo soil, (b) Glyndon soil, and (c) Hecla soils. 48

5. Comparison of combined datasets between measured SWRCs of HYPROP and WP4 (HW) and hanging column, Tempe cell, and pressure plate (HTP) methods for (a) Fargo soil, (b) Glyndon soil, and (c) Hecla soils. 49

6. Soil water release curve (SWRC) of silty clay loam soil used in the study and developed by HYPROP and WP4 methods. 65

7. Schematic of the experimental setup. 69

8. Infiltration rates over total duration of experimental runs, plotted for (a) Run 1, 2, and 3 of initial water content permanent wilting point (θ_{pwp}); (b) Run 4, 5, and 6 of initial water content between θ_{pwp} and water content at field capacity (θ_{fc}), θ_{mid}; and (c) Run 7, 8, and 9 of initial water content θ_{fc}. 73

9. Volumetric water content (θ_v) vs. dielectric permittivity (DP) relationship during 5TE sensor calibration (Sensor 1). 75

10. Comparison between measured and calculated volumetric water content for Sensor 4 for (a) before all experiments, phase 1 and (b) after six experiments, phase 2. 76

11. Infiltration rate vs. time over 60-minute duration of experiments for: (a) Run 1, 2, and 3 with initial water content of permanent wilting point (θ_{pwp}); (b) Run 4, 5, and 6 with initial water content between θ_{pwp} and field capacity (θ_{fc}); and (c) Run 7, 8, and 9 with initial water content θ_{fc} 77

12. Infiltration rate vs. time by Horton infiltration model, plotted for different initial water contents at permanent wilting point, between permanent wilting point and field capacity, and field capacity in Eq. 3.8, Eq. 3.9, and Eq. 3.10, respectively. 79

13. (a) Volumetric soil water content (θ_v) vs. time and (b) soil temperature vs. time, plotted for experimental Run 6 with initial water content condition between permanent wilting point (θ_{pwp}) and field capacity (θ_{fc}). The vertical straight lines indicate: (1) starting time of soil freezing and datalogging, (2) starting time of experimental run, (3) ending time of experimental run, and (4) ending time of datalogging.....81

14. Volumetric soil water content (θ_v) vs. temperature, plotted for (a) Run 1, 2, and 3 with initial water content of permanent wilting point (θ_{pwp}); (b) Run 4, 5, and 6 with initial water content between θ_{pwp} and field capacity (θ_{fc}); and (c) Run 7, 8, and 9 with initial water content θ_{fc} at depths of 11 cm, 17 cm, and 23 cm. 84

15. Comparison between pre-experiment and post-experiment soil water release curves (SWRC). 86

16. Soil release curves (SWRC) developed by HYPROP+WP4 combined methods for (a) Colvin soil, (b) Fargo soil, and (c) Hecla soils; Soil freezing curves (SFC) for (d) Colvin soil, (e) Fargo soil, and (f) Hecla soils. 101

17. Schematic of experimental setup. 106

18. Hydraulic conductivity (k) vs. volumetric water contents (θ_v) relationship by Eq. 4.12, Eq. 4.13, and Eq. 4.14, plotted for Colvin, Fargo and Hecla soils, respectively. 113

19. Measured k values by minidisk infiltrometer plotted against calculated k values by Eq. 4.12, Eq. 4.13, and Eq. 4.14 in 1:1 plot for (a) Colvin, (b) Fargo, and (c) Hecla soils, respectively. Measured k values by minidisk infiltrometer plotted against calculated k values by Motivilov model in 1:1 plot for (d) Colvin, (e) Fargo, and (f) Hecla soils, respectively. 115

20. Mean hydraulic conductivity (k) values plotted for 3, 6, and 9 freeze-thaw (FT) cycles for Colvin soil with initial soil water content in between permanent wilting point and field capacity (θ_{mid}). 117

LIST OF APPENDIX FIGURES

Figure Page

A1. Field tests in frozen condition (North Moorhead, spring 2014). 125

A2. Field tests in unfrozen condition (North Moorhead, fall 2014). 126

A3. Field tests in frozen condition (North Moorhead, spring 2015). 126

A4. Field tests in unfrozen condition (North Moorhead, summer 2015). 126

A5. Field tests in unfrozen condition (North Moorhead, fall 2015). 127

A6. Field tests in frozen condition (North Moorhead, spring 2016). 127

A7. Field tests in frozen condition (Fairmount, fall 2014). 127

A8. Field tests in frozen condition (Fairmount, spring 2016). 128

A9. Field experiments: unfrozen vs frozen condition (North Moorhead, all years).....128

1. GENERAL INTRODUCTION

1.1. Background

Snowmelt water infiltration into frozen soil is an important but complicated process that can affect surface water runoff and groundwater recharge. It is estimated that snowmelt water contributes to yearly surface runoff volume by about 80-85% in seasonally frozen areas (Gray and Granger, 1987). Snowmelt water contributes directly to the hydrology of the snow-covered area. It has a direct relation with the runoff generation from snow melting during spring time, so it has a prime role to create devastating spring flooding and drainage problem. On the other hand, snowmelt water may be the source of water for irrigation and household purposes during spring time in seasonally frozen areas. Spring season crop growing also depends on snowmelt water infiltration into frozen soil. Snowmelt water infiltration into soil enhances better growing environment, good water trafficability, timely planting, good compactness of soil, easy movement of planting machineries and increased production for crops.

Understanding of snowmelt water infiltration into frozen soil and knowledge about the total processes help to get better ideas about water conservation, runoff generation, spring flooding, soil physical and thermal properties in seasonally frozen soil. Also, snowmelt water infiltration process is important to soil water conservation. Many factors, such as soil moisture, soil temperature, snow cover water release rate, porosity, soil cracks, snowmelt infiltrating water energy content, presence or absence of macro-pores, and complex processes of heat and mass transfer through the frozen soils affect the total infiltration process into frozen soils. In northern hemisphere, nearly 60 percent of the land surfaces are seasonally frozen, and North Dakota is a part of that area. There is no simple and clear answer on how water infiltrates into frozen soil.

The lack of understanding of the infiltration process into frozen soil is the major limiting factor affecting spring flood forecasting.

In recent years, during the spring flood events in the Red River of the North Basin (RRB), flood forecasting was unable to predict accurately flood water level. The Red River of North originates from the confluence of the Bois de Sioux and Otter Trail rivers at Wahpeton, North Dakota and Breckenridge, Minnesota. The flow line of Red River is considered as the border between two U.S. states, North Dakota and Minnesota. It flows to north through the valley of the Red River and continues to Manitoba, Canada. Then the river goes farther north and falls into Lake Winnipeg. Lake Winnipeg is actually part of the Hudson Bay watershed including the Nelson River. On the river path, Red River passes through some major localities of North Dakota and Minnesota states like Fargo, Moorhead, and Grand Forks. The flood forecasting computer models did not consider or have data to forecast the infiltration into frozen dry soil (MPRnews, 2013). But, any error in flood prediction can cause significant financial losses and threaten 200,000 lives in the Fargo-Moorhead metro area as well as people and animals in the entire basin.

The complete realization about the infiltration process into frozen soils could have a broad impact to the hydrological field for the entire and especially in permafrost regions. It would help to better understand the runoff processes and flooding events in winter and spring. Properly adjusted numerical infiltration model could be used to predict actual runoff peaks to prevent damage from floods or to prevent overestimation of runoff.

1.2. Snowmelt water infiltration

Infiltration is defined as “the process whereby water enters the surface strata of the soil and moves downward toward the water table” (Wisler and Brater, 1949, pp. 175). The amount of

water absorbed into the soil in a given time is called infiltration rate. The capability of soil to absorb water at maximum infiltration rate under a given condition is called infiltration capacity. The total infiltration process indicates the water movement mechanism into soil profile under different forces like gravity and capillary suction and therefore is very important for the hydrology studies (Bedient and Huber, 1988). Infiltration is an important fundamental factor in the field of hydrology. It defines a drainage basin ability to absorb water and release of that water to stream flow. The infiltration of water from rain or snow melting into soil mostly depends on the infiltration capacity character of the soil. The water first removes the soil water deficiency and then the excess water moves downward and adds with ground water.

However, according to Gray et al. (2001), infiltration process occurs in a different way if the ground is frozen and covered with snow than that under the unfrozen and uncovered conditions. This process is very complex and involves heat and mass transfer and phase changes. Studies of snowmelt water infiltration into frozen soils are relatively scarce. There is no simple and clear answer on how water infiltrates into frozen soil. Despite the large amount of empirical studies and modeling attempts, the full process of infiltration in frozen soil is not completely understood. Numerous observations have showed that during snowmelt period, most of melted water retains within the top 0 to 30 cm depth of uncracked soils. Granger et al. (1983) referred the entire soil depth as ‘zone of infiltration’. Snowmelt water infiltration into uncracked frozen soil mostly depends on the distribution of ice within the “zone of infiltration”. For this reason, uncracked frozen soils which have significantly different textures and land use, but have similar moisture regime during melting period, can have a similar infiltration rate. Snowmelt water infiltration into frozen soils has strong relationship with “effective or air-filled porosity” of “the

zone of infiltration". If porosity or macro-pore numbers increases, infiltration capacity of that frozen soil also significantly increases (Granger et al., 1983).

1.2.1. Importance of snowmelt water infiltration

The process of snowmelt infiltration into frozen soil is important in predicting surface runoff and flooding (Zheng et al., 2001). Rainfall or snowmelt is the main cause of severe flooding events in many seasonally frozen areas in spring time. During the 2013 spring flood event in the Red River of the North Basin (RRB), the floodwater was several meters below the level initially forecasted by the National Weather Service (NWS). In 2013, flood protection sandbag dikes were built in Fargo, but the floodwater level did not even get close to most of the sandbag dikes. NWS hydrologists figured out that computer models predicted higher floodwater level than the actual event according to the snow equivalent water amount. The cause for the difference between the predicted and actual flood stage could be due to the computer prediction model's inability to account for frozen dry soil that absorbed as much as half of the snowmelt through infiltration. There is a critical weakness in the flood prediction model because its computer model did not consider or have data to forecast the infiltration into frozen soil (MPRnews, 2013). It is very clear that snowmelt water in spring time infiltrates into the frozen soil in the RRB, and the infiltration rate and amount will determine the time and magnitude of the spring flood (peak runoff) in RRB.

1.2.2. Factors affecting snowmelt water infiltration

Snowmelt water infiltration involves complex processes of heat and mass transfer through the frozen soils. Many factors, such as soil moisture, soil temperature, snow cover water release rate, porosity, soil cracks, snowmelt water infiltrating energy content, and presence or absence of macro-pores, affect the total infiltration process (Granger et al., 1983). Hydraulic

conductivity of frozen soil is one of the governing factors that affecting infiltrability of water along the soil profile with ice (Stahli, 1999). Snowmelt water infiltration into frozen soils is a complicated process that can affect surface water runoff and the groundwater recharge. In frozen soils, the infiltration rate is determined mainly by soil temperature, soil-water content (in water and ice), the porosity and the snow cover above the soil. Infiltration occurs mainly through macro-pores and is driven by the moisture conditions if macro-pores are missing. According to Bengtesson et al. (1992), water infiltration in frozen soils after snow melting mainly occurs in macro-pores and along cracks, especially for clayey soils. A severely cracked heavy-textured clay soil can absorb large amounts of water (Granger et al., 1983). For a unit area, infiltration amount can be higher than the snow equivalent water amount due to interflow to and through cracks from outside the area. Due to presence of cracks, snowmelt water mostly enters into the cracks and cannot produce significant runoff flow at the field edge. If the fields are heavily cracked during fall, it is expected that most of snowmelt water will be infiltrated through the cracks. Zheng et al. (2001) found that variation of infiltration rates mostly depended on soil water profile phase change, temperature difference and heat exchange and transfer between atmosphere and soil.

In properly drained soil, better aeration can take place to help microbial activity, soil porosity can be improved and provide better soil structures. Compare to undrained soil, gravitational water is removed from soil profile continuously in drained soil. It increases the pore space within the soil and creates greater water storage capacity. Better pore space is the indication of good soil structure, and good soil structure can hold more water by adding additional storage capacity. The additional storage capacity allows more water to infiltrate into the soil (Irwin & Whiteley, 1983). Snowmelt water infiltration into frozen soils has a strong

relationship with “effective” or “air-filled” porosity of “the zone of infiltration”. If porosity or macro-pore numbers increases, infiltration capacity of that frozen soil also significantly increases (Granger et al., 1984). A good drainage condition increases infiltration rate into soil due to extra pore space and increases the soil water storage. Surface runoff is created when the precipitation amount exceeds the total sum of evapotranspiration and soil water holding capacity during a storm event. In poorly or undrained soil, surface runoff peaks are high due to less water holding capacity of the soil. Drainage removes gravitational water, creates more pore space for additional water storage through infiltration within the soil profile and result reduced runoff peak (Carlson, 2011). If the soil is properly drained in winter, it also reduces soil structure damage during winter season. In spring, drained soils dry out rapidly and get warmer faster than undrained soil during spring (Gardner et al., 1994; Carlson, 2011). Bulk density is one of the important soil properties that influence infiltration. When soil becomes more compact, bulk density increases and it restricts soil water movement and infiltration capacity of the soil. The drained soil has lower bulk density than the undrained soil or poorly drained soil (Fausey and Baker, 2003), so water can infiltrate more in subsurface drained soils than that of undrained soils. Drainage can create effect on hydrology, by allowing more infiltration into soil due to increased porosity, and by increasing moisture storage capacity (Sands, 2010).

1.3. Snowmelt water infiltration processes

In cold region hydrology, frozen soil is a key component which has direct effects on infiltration and indirect effects on heat transfer from and to snowpack lying on the soil surface. Frozen soil infiltration is a complicated hydrological process that contributes to crop water intake, surface runoff generation and ground water recharge in northern latitudes. However,

information about infiltration processes in frozen soils are significantly limited comparing to non-frozen soil infiltration processes.

A land surface is considered as seasonally frozen when minimum annual temperature is below 0°C (Saito et al., 2007; Lundberg et al., 2015). In northern cold region, more than half of the land surface is seasonally frozen and snow melting is a major hydrological event in this area. There are three categories of infiltration in frozen soil (Granger et al. 1984). The first one is "unlimited" infiltration where soil is deeply cracked, containing macro-pores so that it has high infiltration ability. This is very common in clay soils of agricultural fields with continuous cropping pattern or in coarse dry sand. Most of the snowmelt infiltrate under this condition and consequently, very small or no surface runoff produces after infiltration. "Limited" infiltration happens in uncracked soil and depends on snow cover, ice content distribution within soil profile and presence of impermeable layer within zone of infiltration. When an ice layer forms on the frozen soil surface or within shallow depth of soil, it limits melt water downward movement and causes "Restricted" infiltration. Infiltration amount is very negligible under this condition, water may pond on soil surface or evaporates. The situation can be caused if soil freezes just after a rainfall or snowmelt event. Frozen soil infiltration is different than that of unfrozen soil because of infiltrating water re-freezing and melting of ice content within a soil profile (Flerchinger et al., 2005). When the soil surface is frozen, snowmelt infiltration depends not only the permeability of the soil but also the ice content distribution along the soil profile (Ireson et al, 2013). Around the world, frozen soil causes devastating floods and soil erosion after rainfall or quick snowmelt events, because frozen soil restricts the infiltration into frozen soil by reducing soil infiltration capacity and then infiltration excess water creates huge runoff even after a slight rainfall or snowmelt event. Heat and water transport interaction, above the frozen soil surface and within

the soil, and the ice contents affect permeability of frozen soil. In frozen soil, downward movement of infiltrated water from frozen soil surface during thawing period is higher in unsaturated soil having low ice content and with the presence of cracks. On the other hand, infiltration amount and rate are comparatively low if the soil is at saturation with high ice formation in soil profile and with no crack presence in soil (Mackay, 1983). Infiltrability of frozen dry fine sand soil reduced to one order of magnitude compared to unfrozen soil though infiltration in frozen condition started with high value (Engelmark, 1988). Iwata et al. (2011) observed that in cold winter, if a large amount of (rain) water stored on soil surface, froze due to air temperature fall and resulted in a frozen ice layer on soil surface, that ice layer would impede snowmelt infiltration.

1.3.1. Water movement through frozen soil

Frosting due to soil freezing regulates the infiltration capacity and permeability of frozen soil. When soil temperature decreases below 0°C, soil starts to freeze from surface. So, the soil water contents along the soil profile gradually reduce and change to ice contents. Permeability and infiltration capacity greatly decrease with increase in ice contents formation within the soil profile. Granger et al. (1984) reported that the amount and distribution of ice contents within the 0-30 cm of uncracked frozen Prairie soil profile ("Zone of infiltration") is the dominant factor that affects water infiltration during melting time. Soils having significantly different texture and land use but having similar soil water content may have same infiltration amount during the time of snow melting (Granger et al., 1984). The flow path tortuosity increases due to formation of ice in soil, because soil water in large pores freezes first and restricts water movement in those pores. As a result, infiltration capacity of that frozen soil reduces (Lundberg et al., 2015). But water can still infiltrate into frozen soil even after freezing if the soil is not wetted to saturation

during the time of freezing (Flerchinger et al., 2005; He et al., 2015). The pore size distribution of "zone of infiltration" also affects the melt water infiltration in frozen soil (Granger et al., 1984). He et al. (2015) reported that snowmelt water infiltration during spring greatly governs by air-filled porosity of top 10 cm soil, and soil moisture content of top 30 cm soil that were stored in fall. An ice layer (i.e. frosting) is formed on soil surface or within shallow depth of soil just after freezing of water from rain or snowmelt, can limit water infiltration into frozen soil. Direct runoff created from snowmelt or ice content within the soil profile can contribute to stream flow and ground water recharge during spring. If the soil is deeply frozen, it results in less infiltration and large surface runoff compared to shallow depth frost in winter. However, this is not true for all cases, sometimes deep frost cannot produce much snowmelt runoff. Therefore, soil frost does not necessarily have a prime role in large flood during spring. According to frost type (Flerchinger et al., 2005), concrete frost occurs in bare and fine textured agricultural soil. Many ice lenses form within the soil profile and make the soil very hard for water infiltration as like concrete. The ice layer formations turn the frozen soil almost impermeable and water can barely infiltrate into it (Zuzel and Pikul, 1987). During the melting period, if the ice lenses contribute water to the soil profile, infiltration rate can be the same as unfrozen soil. Land management practices, such as, tillage, effects on soil moisture and soil temperature. Unfrozen soil near surface was found wetter and warmer in no-tillage condition compared to conventional tillage practice (Parkin et al., 2013). Land use also has some control on snow cover accumulation and the amount of soil moisture during freezing. As infiltration in frozen soil is directly associated to porosity of infiltration zone, if macro-pore numbers can be increased, more infiltration can occur from snow accumulation.

1.3.2. Freeze-Thaw (FT) cycle

Zheng et al. (2001) conducted several infiltrometer tests to examine infiltration characteristics during three different soil freezing stages (i.e. “transient freeze-thaw stage, steady freezing stage and thawing stage”) in a winter season. They fitted the results from infiltration tests into the Kostiakov (1932) empirical infiltration equation. The results reported that at “transient frost stage”, the frozen layer in the soil affected the accumulative infiltration amount and the initial infiltration rate, but it did not create any effect on final rate of infiltration. At “steady freezing stage”, when the frost depth increased, final infiltration rate decreased, and accumulative infiltration decreased. At “thawing stage”, accumulative infiltration amount and the final rate of infiltration increased with thawing depth.

Freezing and thawing, one of the important phenomenon of the frozen soil, are the results of heat and water transport exchanges which also are controlled by environmental and climatic factors at frozen soil surface-atmosphere boundary. Freezing and thawing cycles change physical properties of frozen soil by creating stress fractures, affect aggregate stability of soil and then results in changes of hydraulic properties of soil. Soil aggregate stability increases with freezing, but it degrades during thawing process (Dagesse, 2013). During freezing, ice forms within the soil pores, restricts soil permeability due to water movement to freezing front and results in frost heave. With the ice presence in soil, temperature is strongly related to soil matric potential. Soil water can sustain in equilibrium with ice below freezing temperature due to negative potentials. With the temperature decrease at freezing front, more water freezes as ice that changes the soil water potential to more negative. When liquid water content in soil decreases, it creates a gradient between unfrozen liquid water contents and soil water potentials so that liquid water moves from wet zone to freezing front and soil starts to dry due to freezing. In frozen soil, the

soil matric potentials and liquid water contents are related to osmotic potential and temperature. Soil freezing characteristics curve is analogous to soil water release curve for unfrozen soil and is generally considered valid for frozen situation (Flerchinger et al., 2005; Ireson et al., 2013). It is not that simple in soil freezing and thawing cycle that after crossing critical temperature, unfrozen soil becomes impermeable frozen soil. Presence of salt in soil pore and capillary forces that attract water to soil particle affect the decrease of freezing point in frozen soil. As soil consists of different pore sizes, soil freezing point greatly depends on pore size distribution of soil and at the same time, water and ice can exist in various sized pores. Ireson et al. (2013) reported that due to this reason, water in large pores freezes faster than that in small pores and water in small pores thaw earlier than that in large pores. If the soil is unsaturated before freezing, all three phases of water i.e. ice, liquid and vapor, can be present within the pore space. In a frozen soil, soil pore spaces reduce due to soil water freezing and causes significant decrease in water infiltration and increase in surface runoff. During freezing, soil water redistribution due to pore size distribution depends on soil texture and thus, soil texture is an important soil physical property related to frozen soil infiltrability. Al-Houri et al. (2009) found that frozen soil infiltrability was less than 5% after 2-hour drainage, 21% after 4-hour drainage and 30% after 24-hour drainage of unfrozen soil infiltrability in loam soil. They also observed that frozen sandy loam soil infiltrability was 4% of unfrozen soil infiltrability after 24 hours drainage period. Repeatedly occurred freeze-thaw cycles decreased penetration resistance of a clay loam soil at 0-30 cm depth in northern Montana (Jabro et al., 2014).

1.3.3. Temperature variation and heat transfer in frozen soil

In frozen soil, due to a high number of large pores, the water at the beginning is infiltrating at a higher rate and more time is needed to saturate the soil (to fill up the large pores).

With more and more water infiltrating into the ground, soil receives more heat and starts to behave like an unfrozen soil (Granger et al., 1983; Bengtesson et al., 1992). For small pores, water movement is only possible when the soil temperature is higher or equal to 0°C. Compared to water, ice's thermal conductivity is four times larger, but its heat capacity is only one-half of that of water. Therefore, heat is transported quickly in frozen soil than that in unfrozen soil due to its higher thermal conductivity.

During frozen soil infiltration, water moves downward in the subsurface depending on heat transport. At deep layers from the soil surface, heat is transported by conduction or by convection. The heat transfer in frozen soil depends on latent heat, water vapor heat flow, soil hydraulic conductivity, soil thermal conductivity, soil heat capacity, fusion latent heat and vaporization latent heat. Frozen soil has different phases, existing in soil profile and those are ice, liquid and vapor. Those phase changes are dynamic, and their relationships are very complicated, depending on soil profile moisture distribution, phase of soil water and soil temperature (Ireson et al., 1999). Water infiltrating into frozen soil transports latent heat and sensible heat, initiates melting of ice to liquid water and therefore, increases soil ground temperature to 0°C. When soil thaws, the freshly melted ice water at the thawing front moves downwards due to the soil matric potential difference between unfrozen layer at thawing front and frozen layer below thawing front (Mackay, 1983). Soil texture is also a dominant factor that influence thermal processes in frozen soil and control heat diffusion in the frozen soil. The amount of latent heat from soil retention capacity also depends on soil texture (Bayard et al., 2005).

There are different models to simulate infiltration process into frozen soil. Zhang et al. (2007) developed a one-dimensional model for frozen soil connecting hydrological processes

and thermal processes together. The model can simulate soil and water interaction processes within frozen soil. The freezing process can move water from deep soil layer to upper soil layer, and then, the relocated water freezes near the frost front. During the winter when the freezing process continues, the total water in deeper soil layers will be moved to the upper soil layer.

1.3.4. Hydraulic conductivity in frozen soil

Hydraulic conductivity of frozen soil is considered very low but may not be that low at temperature just below 0°C (Mackay, 1983). When water freezes continuously from macro-pores to micro-pores, ice content forms within soil pores and hydraulic conductivity also reduces for the frozen soil. During freezing, with the ice formation in pore, matric potential increases and hydraulic conductivity reduces. As a reverse process, during thawing, soil matric potential decreases as ice melts in small pores with temperature increment, the hydraulic conductivity increases (Ireson et al., 1999). Near or at 0°C, hydraulic conductivities are similar in both frozen and unfrozen soil, but with temperature decrease, hydraulic conductivity reduces due to ice content formation that restrict water flow through pore space. If the soil is unsaturated during freezing, the soil can conduct water through it.

In a frozen soil, frozen active layer can be at saturation or over saturation, but other layers are below saturation and even drier. During freezing, the upper part of frozen active layer is unsaturated and is always subjected to many freeze-thaw cycles (Mackay, 1983). When pore water starts to freeze and form ice, soil water potential drops down and becomes negative. The gradient created between water potential and liquid ice contents moves the soil moisture to the freezing front within the soil profile. The movement of soil moisture to freezing zone and ice accumulation is governed by unsaturated hydraulic conductivity of the soil. Water cannot move, or it can move less to freezing front if the soil unsaturated hydraulic conductivity is low. Very

dry and coarse-grained soils have low unsaturated hydraulic conductivity compared to fine textured soil (Flerchinger et al., 2005). During frozen soil infiltration, unsaturated hydraulic conductivity can be calculated from available porosity of soil, assuming that hydraulic conductivity and soil water retention characteristics of frozen soil are similar to those of unfrozen soil (Flerchinger et al., 2005). The hydraulic conductivity of frozen soil mostly depends on the conditions of soil before it is frozen, or a snow cover occurs on soil surface (Fouli et al., 2013). If the soil remains dry or has less soil water content in fall before winter starts, and if the soil does not get any released water from snow cover melting that infiltrates into the soil and refreezes, then the soil will be permeable and can conduct water until it gets saturated from snowmelt in spring. But if the soil is wet or nearly saturated before it freezes, it should have low permeability. If snowmelt happens due to sudden temperature rise in winter, the melt water can refreeze into the soil profile after entering it. This results in reduction of infiltration capacity of soil before spring melt. In seasonally frozen areas, snowmelt infiltration in spring is subjected to frozen soil condition due to variation of hydraulic conductivity (Lundberg et al., 2015).

A single event of freeze-thaw cycle creates extensive network of cracks and ice lenses in clay soil which increases hydraulic conductivity, and it continues to increase with more freeze-thaw cycles. However, after three cycles, hydraulic conductivity becomes stable. On the other hand, soil pressure reduces soil cracks during thawing and reduces hydraulic conductivity (Othman et al., 1993). Freeze-thaw cycles decrease the void ratio of frozen soil by creating soil porosity like micro-pore or micro-cracks which also helps to increase hydraulic conductivity in frozen clay soil (Kim and Daniel, 1992). But the scenario is different in granular soils. With ice content increasing close to 100% saturation during freezing, the open pore spaces of frozen granular soil decrease and thus, hydraulic conductivity decreases (Andersland et al., 1996).

1.4. Infiltration equations and models

Many infiltration equations are available for infiltration measurements. Most of those are empirical in nature and developed based on field observation. Few of those are widely used and well known.

1.4.1. Horton infiltration equation

Horton (1940) infiltration equation, named according to its developer Robert E. Horton, is an empirical equation for measuring infiltration rate or volume. Horton considered that infiltration starts with a constant rate (f_0) and decreases exponentially with time (t). After soil saturation reduces a certain value, the infiltration rate become constant (f_c).

$$f = f_c + (f_0 - f_c)e^{-kt} \tag{1.1}$$

where f is the infiltration capacity (cm/min), f_0 is initial infiltration capacity (cm/min), f_c is final infiltration capacity (cm/min), t is the time, and k is empirical constant (min^{-1}).

1.4.2. Kostiakov equation

Kostiakov developed the empirical equation in 1932 considering that the infiltration rate over time is a power function. Zheng et al. (2001) used this equation for their infiltration into frozen soil experiment as follows:

$$H = At^{-\lambda} + f \tag{1.2}$$

where H is the infiltration rate (mm/min), t is the time (min), f is the steady infiltration rate (mm/min), A is related to the infiltration rate near the beginning of infiltration ($A+f$ is the infiltration rate after 1 min of ponding) and λ is an empirical coefficient.

1.4.3. Philip equation

Using analytical solutions of unsaturated flow equation, Philip (1957) developed a method for measurement of infiltration capacity and cumulative infiltration volume.

$$f = (0.5)At^{-1/2} + B \tag{1.3}$$

$$F = At^{-1/2} + Bt \tag{1.4}$$

where *f* is the infiltration capacity (cm/min), *F* is the cumulative infiltration volume (cm) and *A* and *B* are constants related to soil type and water movement.

1.4.4. Green-Ampt equation

Green-Ampt (1911) equation was derived from the Darcy's law equation. The parameters of this equation are relatively difficult to measure. The infiltration rate and amount can be calculated using the Green-Ampt equation:

$$f = K_s\left(1 + \frac{S \times IMD}{F}\right) \tag{1.5}$$

where *f* is the infiltration rate, K_s is the hydraulic conductivity in the wetted zone, *S* is the capillary suction at the wetted zone, *F* is the cumulative infiltration and *IMD* is the initial moisture deficit. The cumulative infiltration can be found by integrating infiltration rate (*f*) over time (*t*). i.e. $f = dF/dt$. Then Eq. 1.5 becomes as:

$$K_s t = F - (S \times IMD) \times log_e\left(1 + \frac{F}{S \times IMD}\right) \tag{1.6}$$

1.4.5. HYDROL-INF model

Chu and Marino (2006) developed an infiltration-runoff model based on Green-Ampt infiltration calculation method. The model is very useful for applied hydrological studies. The developed model is a Windows® based model including easily useable windows interface. They named the model as "HYDROL-INF" model. The model can simulate infiltration into and within soil profile which is considered layered with randomly distributed soil moisture content. It can also simulate surface runoff resulted from the rainfall event after satisfying soil infiltration capacity. The model can consider both dry periods with no rainfall and wet periods for stable or

unstable rainfall. The windows operating system interface helps to make the total modeling processing easy for the model user. These include data input, data processing, model running, and output processing. To make the model user friendly, some "hydrologic tools/calculators" were included in the modeling process. The model developer will add other hydrologic models for infiltration and runoff simulation comparison and useful hydrologic calculation tools in updated version of the model.

1.4.6. DRAINMOD model

The hydrological model, DRAINMOD in its original form, is widely used and well established for prediction and simulation of water table and discharge fluctuation in surface and subsurface drainage systems. The original DRAINMOD cannot be used for simulation of drainage in cold region, because it does not take into account the freezing and thawing cycles in frozen soil profile. In frozen soil, the water flow is greatly influenced by the freezing and thawing cycle which affects the water table fluctuation and discharge fluctuation. The freezing-thawing cycle controls snow melting. The infiltration rate is lower in frozen soil than that of unfrozen soil. So, during the rainfall event in winter and early spring, runoff is comparatively higher in frozen soil due to less infiltration. The soil moisture retention curves are similar between unfrozen soil and periodically or seasonally frozen soil. Even soil drying process in frozen soil follows the same trend of soil freezing process. The snow cover or frost depth affects the soil surface temperature. The temperature and heat transfer, and exchange between atmosphere and soil, influences the movement of water within the soil profile. So, snowmelt water infiltration is greatly and directly dependent on soil temperature in frozen soil. Luo et al. (2006) modified the original DRAINMOD model to predict and simulate water table and discharge fluctuation in surface and subsurface drainage systems considering freezing and

thawing cycle of frozen soil, soil temperature and heat exchange, snowmelt water infiltration and accumulation. They also evaluated the effects of freezing and thawing cycles, snow melting and accumulation processes for less drained soil.

1.4.7. HYDRUS model

HYDRUS model is developed by Simunek et al. (2012), which is a very effective and useful model option for heat and water flow simulation. The model algorithms are based on Richards equation. It uses mass-lumped linear finite element method to solve the equation numerically for saturated and unsaturated flow. HYDRUS model can be used for predicting and simulating different hydrological process like rainfall, snowfall, evaporation, transpiration, infiltration, root zone water accumulation, soil moisture holding capacity, capillary movement of water in soil, drainage, irrigation, groundwater movement and storage, and all directional movement of flow within soil profile. The models can simulate infiltration capacity and surface runoff considering the applied water flux threshold of the soil. Also, if the soil initial and specific conditions are available for the soil profile and vegetative covers, those can adjust evaporation and transpiration processes between potential and actual values.

1.5. Water infiltration measurement

Different instruments (e.g. infiltrometer) based on different principles are used to measure infiltration across the world. The major types of infiltrometer are: Ring infiltrometer, tension infiltrometer, and rainfall simulator.

1.5.1. Ring infiltrometer

Ring infiltrometer is widely used for measurement of water infiltration into soil. It can be made from metal or plastic cylinders. The cylinders are thin-wall, open to each end and have outside-beveled cutting edge at bottom side. There are different types of ring infiltrometers used

in the field measurements. Those are “Single ring or pressure infiltrometer”, “Double ring or concentric ring infiltrometer”, “Twin or dual ring infiltrometer” and “Multiple ring infiltrometer” (Reynolds et al., 2002). The diameters and heights can be varied from 10 to 50 cm and 5 to 20 cm, respectively. However, whether smaller or larger size of cylinders used for infiltration measurements are based on experimental purposes. Bagarello et al. (2009) measured saturated hydraulic conductivity, K_s, by using a constant pressure head ring infiltrometer where the metal ring was inserted at shallow depth of soil and pressure head was maintained the same or constant inside the ring. Single ring pressure infiltrometer can be used with different ponding depths, but the ponding depths influences the parameter estimation of hydraulic conductivity (Elrick et al., 1990). Single ring infiltrometer measures the infiltration with lateral and vertical components. Chowdary et al (2006) reported that even with a double ring infiltrometer, lateral movement of water could not be eliminated but could be managed.

Infiltration experiments in frozen soils can be performed using a double ring infiltrometer with the combination of sensors for soil temperature and water content measurement. To determine the infiltration rate, one can observe the decline of water in the infiltrometer. To determine the hydraulic conductivity, a similar installation can be used, with the difference that the water level is held constant. Water can be added until an equilibrium is reached. Then a specified equation can be used to determine the hydraulic conductivity. Kane and Stein (1983) found similar shapes between infiltration curves of frozen soils and unfrozen soils during their infiltration tests in seasonally frozen soil with different moisture contents. They used double ring infiltrometers for their tests. Also, at freezing time, double ring infiltrometer experiments showed that rate of water infiltration and soil water content within the soil profile are inversely related to each other (Lee and Molnau, 1982; Kane and Stein, 1983).

1.5.2. Tension infiltrometer

Tension infiltrometers or disc infiltrometer are used for measuring unsaturated soil properties like soil capillary properties and properties for conductivities. Capillary and gravity force are two most important factors that influence the infiltration into soil. In clay soil, capillary force dominates most and in sandy soil, infiltration occurs mainly due to gravitational force (Deurer et al., 2008). In ring infiltrometer test, water is ponded on soil surface under atmospheric pressure. When soil pores are filled with water, infiltration rate becomes stabilized and infiltration rate is then measured. For this reason, infiltration rate is fast at the beginning and becomes slower with time. But the problem is that, a good portion of water infiltrates through macro-pores (i.e. cracks and wormholes) and reduced the amount of water infiltrates into the soil matrix. Tension infiltrometer controls the infiltration rate by a negative suction pressure or tension and the infiltration is usually slower than natural infiltration. So, water does not infiltrate through soil cracks and wormhole and the maximum portion of water goes through soil matrix. Tension infiltrometer has variable range of tension and by changing the suction pressure or tension, one can easily control the infiltration rate into soil. Before using for field measurement, tension infiltrometers should be checked for leaks. If there is any leak, suction will not be sustained. Assembly of the tension infiltrometer and filling with water should be done before field use. A graduated container for water, a disc attached at the bottom of the container and an air bubble tower are the major components of tension infiltrometer (Latorre et al., 2013). The tension or disc infiltrometer is getting popular among the researchers, because, it is easy to handle in field application. A good number of soil-water properties, such as sportivity and hydraulic conductivity, can be determined or estimated from cumulative infiltration curve by tension or disc infiltrometer (Moret-Fernández et al., 2009; 2012).

Minidisk infiltrometer is a smaller version of tension infiltrometer (Decagon Devices, Inc., Pullman, WA). It consists of a single tube combines with a bubble tower and water reservoir. It is a portable type tension infiltrometer and can be used for quick measurements of infiltration and hydraulic properties of soil. The device is divided into upper and lower chamber. Both chambers have to be filled with water for infiltration measurement. The upper chamber or bubble tower controls suction. The water from lower chamber infiltrates into soil under a selected suction. The infiltration rate measurement can be obtained from labeled lower chamber. This type of infiltrometer is useful for laboratory experiments for infiltration rate and hydraulic properties measurements. The length of the minidisk infiltrometer is 32.7 cm and diameter of the tube is 3.1 cm. It consists of 4.5 cm diameter disk which is 3 mm thick. It has a suction range from 0.5 to 7 cm depending on soil types.

Zhang (1997) proposed a two-term numerical solution which also derived from Philips equation for "sorptivity" and "hydraulic conductivity" estimation. The Philip infiltration equation is only valid for vertical water movement and also only for a very short infiltration time. Practically, for cumulative infiltration measurement, the very short duration is not appropriate to estimate sorptivity. In Zhang's numerical solution, there are two non-dimensional constants which can be determined from soil retention parameters, minidisk infiltrometer parameter and initial moisture content of soil. He found excellent agreement between the estimated and theoretical values of sorptivity and hydraulic conductivity. The theoretical values were obtained from van Genuchten, Gardner, Russo and Zhang and van Genuchten methods. In most comparisons, the relative error was within 5%, but the proposed method can be used only for homogeneous soil. On the other side, Dohnal et al. (2010) found that Zhang's proposed numerical solution which in now used in minidisk infiltrometer of Decagon Device cannot

perform well for the soils having "n" value less than 1.35. They showed that Zhang's solution actually overestimated hydraulic conductivity values for n < 1.35 soils that are mostly clay, sandy loam or silty loam soils. They proposed a newly formulated expression for calculating hydraulic conductivity of soils in the range of 1 < n < 1.35 based on nonlinear optimization of 16 soils having n < 1.35, different disk sizes and disk pressure heads. Li et al. (2005) did steady infiltration rates comparisons among different soil crusts using trickle irrigation method and minidisk infiltrometer. For minidisk infiltrometer, they used Zhang's formula to calculate steady infiltration rate which is actually hydraulic conductivity component of that formula. They reported that minidisk infiltrometer was a good method to estimate field infiltration rates (i.e. hydraulic conductivity) from laboratory results. With Minidisk infiltrometer, the infiltration rates are calculated with the help of a spreadsheet available from Decagon Devices which is based on (Zhang, 1997) by fitting the parameters C_1 and C_2 of the Phillip equation:

$$I = C_1\, t\ + C_2\, \sqrt{t} \tag{1.7}$$

where I is the cumulative infiltration (cm), t is time (min), the slope of the curve C_1 is a function of the hydraulic conductivity k (cm min^{-1}), and C_2 is a function of sorptivity (cm $min^{-1/2}$). The hydraulic conductivity is calculated as:

$$k = \frac{C_1}{A} \tag{1.8}$$

where A (cm min^{-1}) is obtained from:

$$A = \frac{11.65(n^{0.1} - 1)\ e^{[2.92(n-1.9)\alpha h]}}{(\alpha r_d)^{0.91}}\ if\ \ n \geq 1.9 \tag{1.9}$$

$$A = \frac{11.65(n^{0.1} - 1)\ e^{[7.5(n-1.9)\alpha h]}}{(\alpha r_d)^{0.91}}\ if\ \ n < 1.9 \tag{1.10}$$

in which h (cm) is a given suction, r_d (cm) is the radius of the disk, and α and n are van Genuchten parameters based on the soil type. Minidisk infiltrometer can be used for a suction range from -0.5 to -6 cm. If van Genuchten parameters are not available for a specific soil, a table of those parameters for twelve soil textural classes can be obtained from Carsel and Parrish (1988). For the hydraulic conductivity measurement of soils having n<1.35, an improved version of Zhang (1997) equation by Dohnal et al. (2010) can be used, which is:

$$k = \frac{C_2(\alpha r_d)^{0.6}}{11.65(n^{0.82}-1)\ e^{[34.65(n-1.19)\alpha h]}}\ \ if\ \ n < 1.35 \qquad (1.11)$$

1.5.3. Rainfall simulator

Rainfall simulator, a kind of infiltration measuring tool, has the advantage of reproducing a natural rainfall event artificially with similar intensity, rain droplet sizes and energy (Abudi et al., 2012). This tool can be easily relocated in different places, less expensive comparing other tools and is the faster data collection facility. Rainfall simulators are in two types (Aksoy et al., 2012): pressured and non-pressured. Non-pressured simulator creates rain drops and smaller energy flux than natural events; Pressured rainfall simulator results in higher intensities than that of natural rainfall events with nozzle spraying (Abudi et al., 2012). In soil erosion and rainfall-runoff investigations, both pressured and non-pressured rainfall simulators can be used (Guerrant et al., 1990; Wierda & Veen, 1992). The relationship among the resulting infiltration, soil cover, micro-topography, and soil crust were studied by using rainfall simulators (Battany & Grismer, 2000; Freebairn & Gupta, 1990).

The Cornell sprinkler infiltrometer is a rainfall simulator type infiltrometer which is combined with a single ring infiltrometer (Ogden et al., 1997). It is relatively cheap and is a simple portable tool that can be used to produce same size rain droplets with similar intensity of

natural rainfall for rapid measurement of soil infiltration. It can wet the soil by similar process as natural rainfall and can consider the soil roughness influence on infiltration. It consists of a portable rainfall simulator which is placed on an infiltration ring. This single metal ring has a diameter of 241 mm and it is inserted into the soil up to 7 cm depth for field infiltration measurement (Cornell Sprinkler Infiltrometer User's Manual). Before starting a new infiltration measurement, the sprinkler vessel was placed on the ring and water level in the vessel was measured. After starting the test, in every time interval, water outflow from the ring was measured and so is the runoff volume.

The simulated rainfall rate (R) was measured by following equation (Cornell Sprinkler Infiltrometer User's Manual):

$$R = [H_1 - H_2] / T_f \quad (1.12)$$

where H_1 is the beginning water level, H_2 is the ending water level in the infiltrometer vessel; and T_f is the time required for lowering down water level from H_1 to H_2.

The runoff rate (RO_t, cm/min) was determined by the following equation:

$$RO_t = V_t / (457.30*t) \quad (1.13)$$

where 457.30 cm^2 is the area of the ring, V_t is the runoff volume and t is the time interval for which runoff water was collected. Then, the infiltration rates (I_t) was determined by the difference between the rainfall rate and runoff rate:

$$I_t = R - RO_t \quad (1.14)$$

1.6. Objectives of the dissertation study

The research project focused on snowmelt infiltration characteristics into frozen soil. The research evaluated the frozen soil response to infiltration, the effects of soil properties like soil moisture on frozen soil infiltration and the change of hydraulic conductivity in frozen soil

compared to unfrozen soil. The project also evaluated the available methods for developing soil water release curves for different soils in the Red River Valley.

1.6.1. Specific objectives of the research

Soil water release curves for three North Dakota soils from Red River Valley were constructed by the HYPROP and WP4 dew-point potentiameter combined method and compared with other traditional methods. Infiltration in frozen soils was measured by using Cornell Sprinkler infiltrometer and evaluated at three initial soil moisture contents for a silty clay loam soil of Red River Valley. Hydraulic conductivity in frozen and unfrozen conditions were estimated from the cumulative infiltration curves by Minidisk infiltrometer for three soils in the Red River Valley of the North.

1.7. Organization of the dissertation

The dissertation consists of five chapters in total. The chapters are: general introduction, three consecutive chapters regarding the findings in this study, and a general conclusion. In addition, the general abstract gives the findings and critical observation summary of all manuscripts and experiments conducted in this dissertation research. The first chapter, the general introduction states the background of the research, statement of problems, related literature reviews, and the goal and specific objectives of the research taken under this dissertation. The first chapter describes a combined method of developing soil water release curves by Hyprop evaporation and WP4 dew-point potentiometer methods for three RRB soils, and compares those soil water release curves by traditional methods. The second chapter shows the results of infiltration experiments into a frozen silty clay loam soil with three initial soil water contents, and evaluates the effect of soil water content and temperature on frozen soil infiltration. The third chapter presents the hydraulic conductivity measurement of three frozen soils of RRB

with three initial soil moisture contents before freezing, comparison between hydraulic conductivity values of frozen and unfrozen soils, effect of freeze-thaw cycle on hydraulic conductivity. A Minidisk infiltrometer is used to measure hydraulic conductivity. The general conclusion chapter presents the general outcomes from the studies, performed in this dissertation. All references, cited in the text, are listed at the end of each chapter except the general conclusion, the general conclusion does not have any reference list. Finally, all field infiltration tests conducted by using the Cornell Sprinkler infiltrometer in various locations, for frozen and unfrozen conditions, are included in the appendix.

1.8. Reference

Abudi, I., Carmi, G., & Berliner, P. (2012). Rainfall simulator for field runoff studies. *Journal of Hydrology,* 454–455(0), 76-81. doi:http://dx.doi.org/10.1016/j.jhydrol.2012.05.056

Aksoy, H., Unal, N. E., Cokgor, S., Gedikli, A., Yoon, J., Koca, K., Eris, E. (2012). A rainfall simulator for laboratory-scale assessment of rainfall-runoff-sediment transport processes over a two-dimensional flume. *CATENA, 98*(0), 63-72. doi:http://dx.doi.org/10.1016-/j.catena.2012.06.009

Al-Houri, Z.M., Barber, M.E., Yonge, D.R., Ullman, J.L., & Beutel, M.W. (2009). Impacts of frozen soils on the performance of infiltration treatment facilities. *Cold Regions Science and Technology.* 59:51-57

Andersland, O.B., Wiggert, D.C., & Davies, S.H. (1996). Hydraulic conductivity of frozen granular soils. *Journal of Environmental Engineering*. 122(3):212-216

Bagarello, V., Iovino, M., Palazzolo, E., Panno, M., & Reynolds, W. D. (2006). Field and laboratory approaches for determining sodicity effects on saturated soil hydraulic conductivity. *Geoderma, 130*(1-2), 1-13. doi:10.1016/j.geoderma.2005.01.004

Battany, M. C., & Grismer, M. E. (2000). Development of a portable field rainfall simulator for use in hillside vineyard runoff and erosion studies. *Hydrological Processes*, 14(6), 1119-1129. doi:10.1002/(SICI)1099-1085(20000430)14:6<1119::AID-HYP8>3.0.CO;2-O

Bayard, D., M., Stahli, A., Parriaux & H., Fluhler. (2005). The influence of seasonally frozen soil on the snowmelt runoff at two Alpine sites in southern Switzerland. *Journal of Hydrology.* 309:66-84

Bedient, B.P. & Huber, W.C. (1988). *Hydrology and Floodplain Analysis*. New York, USA: Addison-Wesley Publishing Company.

Bengtsson, L., Seuna, P., Lepisto, A., & Saxena, R. K. (1992). Particle movement of melt water in a subdrained agricultural basin. *Journal of Hydrology* 135: 383-398.

Carlson, G. (2011). Tile drainage impact. SDSU iGrow: South Dakota State University. Available on: http://igrow.org/agronomy/corn/tile-drainage-imapct. Assessed 03 December 2013.

Carsel, R. F., and Parrish, R. S. (1988). Developing Joint Probability-Distributions of Soil-Water Retention Characteristics. *Water Resources Research,* 24(5), 755-769. doi:10.1029/-WR024i005p00755

Chowdary, V. M., Rao, M. D., & Jaiswal, C. S. (2006). Study of infiltration process under different experimental conditions. *Agricultural Water Management, 83*(1–2), 69-78. doi:http://dx.doi.org/10.1016/j.agwat.2005.09.001

Chu, X., and Marino, M. A. (2006). Simulation of infiltration and surface runoff - A Windows-based hydrologic modeling system HYDROL-INF. In *Proc.* World Environmental and Water Resources Congress, 1-8. Graham, R.: ASCE.

Dagesse, D.F. (2013). Freezing cycle effects on water stability of soil aggregates. *Can. J. Soil Sci.* 93:473-483

Deurer, M., Clothier, B., Green, S., & Gee, G. (2008). Infiltration rate, hydraulic conductivity, preferential flow. In *Soil Science: Step-by-Step Field Analysis*, 221-234. S. Logsdon, D. Clay, D. Moore and T. Tsegaye (editiors), Madison, WI, USA: Soil Science Society of America, Inc.

Dohnal, M., Dusek, J., & Vogel, T. (2010). Improving hydraulic conductivity estimates form minidisk infiltrometer measurements for soils with wide pore size distributions. *Soil Sci. Soc. Am. J.* 74:804-811

Elrick, D. E., Reynolds, W. D., Geering, H. R., & Tan, K.A. (1990). Estimating steady infiltration rate times for infiltrometers and permeameters. *Water Resources Research, 26*(4), 759-769. doi:10.1029/WR026i004p00759

Engelmark, E. (1988). Rates of infiltration into frozen and unfrozen fine sand. *Can. J. Earth Sci.* 25:343-347

Fausey, N.R. & Barbara, J. B. (2003). Effects of subirrigation on soil properties. ASAE Paper Number: 032086. St. Joseph, Mich.: ASAE.

Flerchinger G.N., Lehrsch, G.S., McCool, D.K. (2005). Freezing and Thawing processes. In *Encyclopedia of Soils in the Environment*, Hillel D (ed.). Elsevier: Ltd, Oxford, UK:104-110

Fouli, Y., Cade-Menun, B.J., & Cutforth, H.W. (2013). Freeze-thaw cycles and soil water content effects on infiltration rate of three Saskatchewan soils. *Can. J. Soil. Sci*. 93:485-496

Freebairn, D. M., & Gupta, S. C. (1990). Microrelief, rainfall and cover effects on infiltration. *Soil and Tillage Research,* 16(3), 307-327. doi: http://dx.doi.org/10.1016/01671987-(90)90104L

Gardner, W.K., Drendel, M.F., & McDonald, G.K. (1994). Effects of subsurface drainage, cultivation and stubble retention on soil porosity and crop growth in a high rainfall area. *Australian Journal of Experimental Agriculture* 34:411-418.

Granger, R.J., D. M. Gray & G.E. Dyck. (1984). Snowmelt infiltration to frozen Prairie soils. *Can. J. Earth. Sci*. 21:669-677

Gray, D. M. & Granger, R. J. (1987). Frozen soil: the problem of snowmelt infiltration. In. Y.S. Fok (Ed.), *Proc. Int. Conf. Infiltration Development and Application*, pp. 179-188, Honolulu, Hawaii: Water Resource Research Center, University of Hawaii

Gray, D.M., Toth, B., Zhao, L., Pomeroy, J. W., and Granger, R. J. (2001). Estimating areal snowmelt infiltration into frozen soils. *Hydrological Processes* 15: 3095-3111.

Guerrant, D. G., Miller, W. W., Mahannah, C. N., & Narayanan, R. (1990). Infiltration evaluation of four mechanical rainfall simulation techniques in Sierra Nevada watersheds. JAWRA *Journal of the American Water Resources Association*, 26(1), 127-134. doi:10.1111/j.1752-1688.1990.tb01357.x

He, H., Dyck, M.F., Si, B.C., Zhang, T., Lv, J., & Wang, J. 2015. Soil freezing-thawing characteristics and snowmelt infiltration in Cryalfs of Alberta, Canada, *Geoderma Regional.* 5:198-208

Ireson, A.M., van der Kamp, G., Ferguson, G., Nachshon, U., & Wheater, H.S. (2013). Hydrogeological processes in seasonally frozen northern latitudes: Understanding, gaps and challenges. *Hydrogeology Journal*. 21:53-66

Irwin, R.W., & Whiteley, H.R. (1983). Effects of land drainage on stream flow. *Canadian Water Resources Journal* 8(2):88-103.

Iwata, Y., Nemoto, M., Hasegawa, S., Yanai, Y., Kuwao, K., & Hirota, T. (2011). Influence of rain, air temperature and snow cover on subsequent spring-snowmelt infiltration into thin frozen soil layer in northern Japan. *Journal of Hydrology*. 401:165-176

Jabro, J.D., Iversen, W.M., Evans, R.G., Allen, B.L., & Stevens, W.B. (2014). Repeated freeze-thaw cycle effects on soil compaction in a clay loam in Northern Montana. *Soil Sci. Soc. Am. J.* 78:737-744

Kane, D. L., & Stein, J. (1983). Water movement into seasonally frozen soils. *Water Resour. Res.* 19: 1547–1557.

Kim, W., & Daniel, D.E. (1992). Effects of freezing on hydraulic conductivity of compacted clay. 1992. *J. Geotech. Engrg*. 118(7):1083-1097

Lee, H. W. & Molnau, M. P. (1982). Infiltration into frozen soils using simulated rainfall. ASABE Paper No. 82–2048. St. Joseph, Mich.: ASAE.

Li, X., Gonzalez, A., and Sole-Benet, A. (2005). Laboratory methods for the estimation of infiltration rate of soil crusts in the Tabernas Desert badlands. *Catena.* 60:255-266

Lundberg, A.L., Ala-Aho, P., Eklo, O., Klove, B., Kvaerner, J., & Stumpp, C. (2015). Snow and frost: Implication for spatiotemporal infiltration patterns- a review. *Hydrol. Process.* 30:1230-1250

Mackay, J.R. (1983). Downward water movement into frozen ground, western arctic cost, Canada. *Can. J. Earth Sci.* 20:120-134

Moret-Fernández, D., & González-Cebollada, C. (2009). New method for monitoring soil water infiltration rates applied to a disc infiltrometer. *Journal of Hydrology, 379*(3–4), 315-322. doi:http://dx.doi.org/10.1016/j.jhydrol.2009.10.017

Moret-Fernández, D., Latorre, B., & González-Cebollada, C. (2012). Microflowmeter–tension disc infiltrometer: Part II – Hydraulic properties estimation from transient infiltration rate analysis. *Journal of Hydrology, 466–467*(0), 159-166. doi:http://dx.doi.org/10.1016/-j.jhydrol.2012.04.047

MPRnews. (2013). Why was the Fargo flood forecast off by so much? Fargo, North Dakota: Minnesota Public Radio. Available at: http://minnesota.publicradio.org/-display/web/2013/05/01/regional/fargo-flood-forecast. Accessed 10 October 2013.

Ogden, C. B., van Es, H. M., & Schindelbeck, R. R. (1997). Miniature Rain Simulator for Field Measurement of Soil Infiltration. *Soil Science Society of America Journal, 61*, 1041-1043. doi:10.2136/sssaj1997.03615995006100040008x

Othman, M.A. & Benson, C.H. (1993). Effect of freeze-thaw on the hydraulic conductivity and morphology of compacted clay. *Can. Geotech. J*. 30:236-246

Parkin, G., von Bertoldi, A.P., & McCoy, A. J. (2013). Effect of tillage on soil water content and temperature under freeze-thaw conditions. *Vadose Zone J*.:1-9

Reynolds, W.D., Elrick, D.E., & Youngs, E.G. (2002). 3.4.3.2: Ring or cylinder infiltrometers (Vadose zone). In *Methods of Soil Analysis: Part 4 Physical Methods*, 818-820. W.A. Dick, Madison, Wisconsin, USA: Soil Science Society of America, Inc.

Saito, K., Kimoto, M., Zhang, T., Takata, K., & Emori, S. (2007). Evaluating a high-resolution climate model: Simulated hydrothermal regimes in frozen ground and their change under the global warming scenario, *J. Geophys. Res.* 112: 1-19 doi: 10.1029/2006JF000577.

Sands, G. R. (2010). Drainage fact sheet. University of Minnesota Extension: University of Minnesota. Available on: http://www.extension.umn.edu/distribution/cropsystems/-M1292.html. Assessed 03 December 2013.

Scherer, T., Kandel, H., Sands, G., & Hay, C. (2013). Frequently asked questions about subsurface (tile) drainage. AE1690: North Dakota State University.

Simunek, J., van Genuchten, M. Th., & Sejna, M. (2012). HYDRUS: Model use, calibration, and validation. *Trans. ASABE* 55(4): 1261-1274.

Stahli, M. (1999). Soil moisture redistribution and infiltration in frozen sandy soils. *Water Resources Research,* 35(1):95-103

Viessman, W. and Lewis, G. L. (2003). *Introduction to Hydrology*. 5th ed. New Jersey, USA: Pearson Education, Inc.

Wierda, A., & Veen, A. W. L. (1992). A rainfall simulator study of infiltration into arable soils. *Agricultural Water Management*, 21(1–2), 119-135. doi: http://dx.doi.org/10.1016/0378-3774(92)90087-D

Wisler, C. O. & Brater, E. F. (1949). *Hydrology*. New York, USA: John Willey and Sons, Inc.

Zhang, X. & Sun, S. F. (2011). The impact of soil freezing/thawing processes on water and energy balances. *Adv. Atmos. Sci.* 28(1):169-177.

Zhang. R. (1997). Determination of soil sorptivity and hydraulic conductivity from the disk infiltrometer. *Soil Sci. Soc. Am. J.* 61:1024-1030

Zheng, X., Van Liew, M. W., & Flerchinger, G. N. (2001). Experimental study on infiltration into a bean stubble field during seasonal freeze-thaw period. *Soil Science* 166(1):3-10.

Zuzel, J.F. & Pikul, J.L. (1987). Infiltration into a seasonally frozen agricultural soil. *Journal of Soil and Water Conservation*. 42:447-450

2. DEVELOPMENT AND COMPARISON OF SOIL WATER RELEASE CURVES FOR THREE SOILS IN THE RED RIVER VALLEY OF THE NORTH, USA[1]

2.1. Abstract

A soil water release curve (SWRC) describes the critical and soil-specific relationship between soil water content and matric potential. In this study, soil moisture and corresponding matric potentials were measured using (1) a new method by HYPROP and WP4 dewpoint potentiometer, and, (2) the traditional method by hanging water column, Tempe cell, and pressure plate. The SWRCs were developed for Fargo silty clay, Glyndon silty loam, and Hecla sandy loam soils by using the van Genuchten model. The goodness of fit between the fitted SWRC and the measured data agreed well with R^2 between 0.91 and 0.98. The comparison for the fitted SWRCs showed that the SWRCs for Hecla sandy soil provided the best agreement while Glyndon soil had the best match in terms of slope and shape. The SWRCs for Fargo silty clay soil did not provide a good match between the two methods. The difference in water content between the two fitted SWRCs was less than 2% for Glyndon and Hecla sandy loam soils. However, Fargo silty clay had a 4.5-5% difference for 66% of the measurements, possibly due to the different bulk densities caused by shrinkage and swelling nature of the clay soil. Since the best fitted van Genuchten parameters were within the reference range that was acceptable for the

[1] The material in this chapter was co-authored by Debjit Roy and Xinhua Jia, Dean D. Steele and Dongquing Lin, and was accepted in the *Soil Science Society of America Journal* as manuscript number S-2017-09-0324-OR.R1. Debjit Roy had primary responsibility for collecting data, analyzing the data collected, interpreting the results, and developing the conclusions that are advanced here. Debjit Roy also drafted and revised all versions of this chapter. Co-authors served as technical and editorial consultants in the development of the manuscript represented by this chapter.

same type of soils, the HYPROP and WP4 can be used to develop SWRCs that are comparable to the traditional laboratory methods for the three soils in the Red River Valley of the North, USA.

2.2. Introduction

Soil moisture and soil matric potential are two important properties in crop-soil-water management studies. The relation between soil matric potential and soil water content is unique in nature for each soil (Miller and Gardiner, 2001), and can be explained by the soil water release curve (SWRC), also known as soil water retention curve, soil characteristics curve or soil moisture characteristics curve (Hillel, 1998). The SWRC is considered the most important relationship and critical input data for understanding unsaturated soil behavior and modeling (Patil and Rajput, 2009; Sreedeep and Singh, 2011; Malaya and Sreedeep, 2012). All properties of unsaturated soil, e.g. unsaturated hydraulic conductivity, are strongly correlated with SWRC (Burckhard et al., 2000; Fredlund and Rahardjo, 1993; Erzin and Erol, 2007; Vanapalli et al., 1996). The SWRC knowledge plays a very significant role for irrigation application and management, rainfall and runoff generation processes, rainfall infiltration and wetting front movement, and groundwater dynamics (Zhan and Ng, 2004; Fuentes et al., 2009; Hillel, 1998). It is also needed in water dynamics for subsurface agricultural drainage systems and in civil and environmental engineering studies, such as construction, wastewater treatment, and solute transport projects (Sreedeep and Singh, 2011; Malaya and Sreedeep, 2012).

Many methods have been used to determine the SWRC directly or indirectly, such as insertion tensiometers, high performance tensiometers, pressure-plate apparatus or pressure membrane extractors, pressure cell, electrical resistance sensors, thermal conductivity sensors, centrifuges, transistor or thermocouple psychrometers, filter paper, hanging water columns and

dewpoint potentiometer (Dane and Topp, 2002; Sreedeep and Singh, 2011). However, matric potential obtained from different methods may differ at the same scale or may be irregular for different soil moisture ranges (Cancela et al., 2006; Bittelli and Flury, 2009; Solone et al., 2012). The advantages and limitations of various methods have been reported by numerous researchers. For example, the pressure plate method has failed to achieve equilibrium in fine textured soil due to soil shrinkage during drying, as the pressure plates may fail to stay in contact with the soil samples (Bittellli and Flury, 2009; Solone et al., 2012). In addition, higher soil moisture contents due to shrinkage are found using the pressure plate method, compared to the dew point method. In contrast, the two methods agreed well for sandy soils due to lack of shrinkage. In loam or sandy loam soils, matric potentials were systematically measured by the hanging water column, psychrometer, and pressure plate method for one complete SWRC curve by Fujimaki and Inoue (2003). Furthermore, Schindler et al. (2012) did not find any systematic deviations for a range of soil samples when comparing the matric potentials measured by evaporation vs. those measured by equilibrium methods. Schelle et al. (2013) also found that the hanging water column method and HYPROP® evaporation method had good agreement over the wet to moderate moisture range, with the dew point method used to measure the moisture content in the dry range.

The traditional laboratory and field methods for soil matric potentials and water content determination are time consuming and sometimes very expensive. For some laboratory methods, special training on handling specific apparatus and tedious data collection procedures are required. Therefore, a convenient, hands-free and automated way of developing SWRC using fewer laboratory methods is one of the main objectives for many researchers. Combinations of different well-established laboratory and field methods as well as the latest improved methods (e.g. HYPROP® evaporation method) for SWRC construction have been tested in several types

of soils in several regions (Maček et al., 2013; Schelle et al., 2013; Schindler et al., 2012), but no study has been conducted for the soils in the Red River Valley of the North Basin (RRB).

The soils of the RRB are unique in nature as they contain shrinking/swelling clays and are poorly drained (Caine, 1903; Nikiforoff et al., 1939). In recent years, subsurface drainage (or tile drainage) systems have become popular in the RRB (Scherer et al., 2013). Installation of tile drainage systems in agricultural fields has agronomic, environmental and economic benefits. In the RRB, the burgeoning tile drainage industry requires a readily available knowledge base of the soil hydraulic properties of the RRB soils, including the SWRCs of those soils, for the design, installation, and modeling of subsurface drainage/subsurface irrigation systems. If the SWRCs of these soils can be constructed quickly and easily, a database for RRB soil properties can be developed and can be accessed instantly for necessary information. Therefore, it is very important to develop SWRCs for the RRB soils using relatively straightforward and expeditious measurement techniques.

The HYPROP® laboratory evaporation method (UMS GmbH, Germany) for constructing SWRC is a relatively new and simple method. This method can determine soil matric potentials and corresponding soil water contents continuously by using two high precision miniature tensiometers and sample weight changes with time. These tensiometers are installed at two depths inside a soil core of 250 mL held within the soil-sampling ring. This method is very suitable to measure better quality soil matric potential data for SWRC, especially those close to the saturation between 0 to -100 kPa ranges. A large amount of data can be measured with respect to time, and a comparatively accurate and continuous SWRC can be developed if another instrument, the WP4 dewpoint potentiometer (Decagon Devices, Pullman, WA, USA), is used to measure the soil matric potentials in the dry range. The basic principle of the WP4 dewpoint

potentiometer is the equilibration of soil liquid phase and relative humidity in the air above the sample in a closed chamber (Gee et al., 1992; Scanlon et al., 2002; Campbell et al., 2007). Maček et al. (2013) demonstrated that a combination of two simple and inexpensive methods could give a good measurement of soil matric potential for developing a complete SWRC. They used the HYPROP evaporation method for the wet range (0 to -100 kPa) and the WP4 dewpoint potentiometer for the dry range (-100 to -300,000 kPa).

The relationship between soil water content and soil matric potential is very complex and difficult to describe by a simple model (Hillel, 1998). Many models and equations for fitting the SWRCs have been proposed and developed (Leong and Rahardjo, 1997). Among those, the van Genuchten (1980) equation (VG) for describing the SWRC is very well accepted and widely used. In this study, SWRCs were developed for Fargo silty clay, Glyndon silty loam and Hecla sandy loam soils using two methods: (i) HYPROP combined with WP4 (HW) and (ii) the traditional method using hanging water column, Tempe cell and pressure plate (HTP). The fitted SWRCs utilizing the simple HW method vs. fitted SWRCs developed from the traditional HTP method were compared in order to determine if the simple method is a valid approach and is a good alternative method for developing SWRCs for soils in the RRB region.

2.3. Materials and methods

2.3.1. Soils

Fargo silty clay soil (fine, smectitic, frigid Typic Epiaquerts) was collected at about 8 km north of Gardner, Cass County (47°10'22.7"N, 96°54'01.3"W) North Dakota. Glyndon silty loam soil (coarse-silty, mixed, superactive, frigid Aeric Calciaquolls) was collected from a field in Rush river township, Cass County (47°02'57.5"N, 97°05'30.0"W), 40 km from Fargo, North Dakota. The coordinates of the Hecla sandy loam soil (sandy, mixed, frigid Oxyaquic

Hapludolls) sampling site were 46°02'47.2"N, 98°06'14.7"W, about 4.8 km straight south and about 0.8 km west of the Oakes Irrigation Research Site, Dickey County, North Dakota. Soil samples in the top 15 cm were taken from the field. They were air dried, ground using a soil grinder, and sieved through a 2-mm screen before measurements. The prepared and disturbed soil samples were used to develop the SWRCs in the laboratory by HYPROP®, WP4, pressure plate, Tempe cell and hanging water column methods. Limited by the amount of soils, the HYPROP method was run 4 times on Fargo, 2 times on Glyndon, and 2 times on Hecla soils. The WP4 method was applied three times at each water content for all three soils. Data from all cycles were pooled and used in constructing the soil SWRC curve. The particle size distribution (%sand, %silt, and %clay) measured of particle size analysis was done by the hydrometer method (Bouyoucos, 1951) and the results are presented in Table 1. The bulk density of each soil was obtained from Web Soil Survey (NRCS, 2017) for the specific soil. Volumetric water contents were calculated from gravimetric water contents and soil specific bulk densities.

Table 1. Percent of sand, clay, silt and bulk densities of the soil samples

Soil	USDA Soil Textural Classification	Sand (%)	Clay (%)	Silt (%)	Bulk density (g cm^{-3})
Fargo	Silty clay	5	48	47	1.09
Glyndon	Silt Loam	37	20	43	1.18
Hecla	Sandy loam	70	14	16	1.31

2.3.2. HW method

The HW combination method was used to measure soil matric potential and corresponding water content for all three soils in this study. The HYPROP measuring assembly contains a sensor unit with a stainless-steel soil-sampling ring (250 mL) connected to a desktop computer installed with HYPROP data evaluation software (Figure 1).

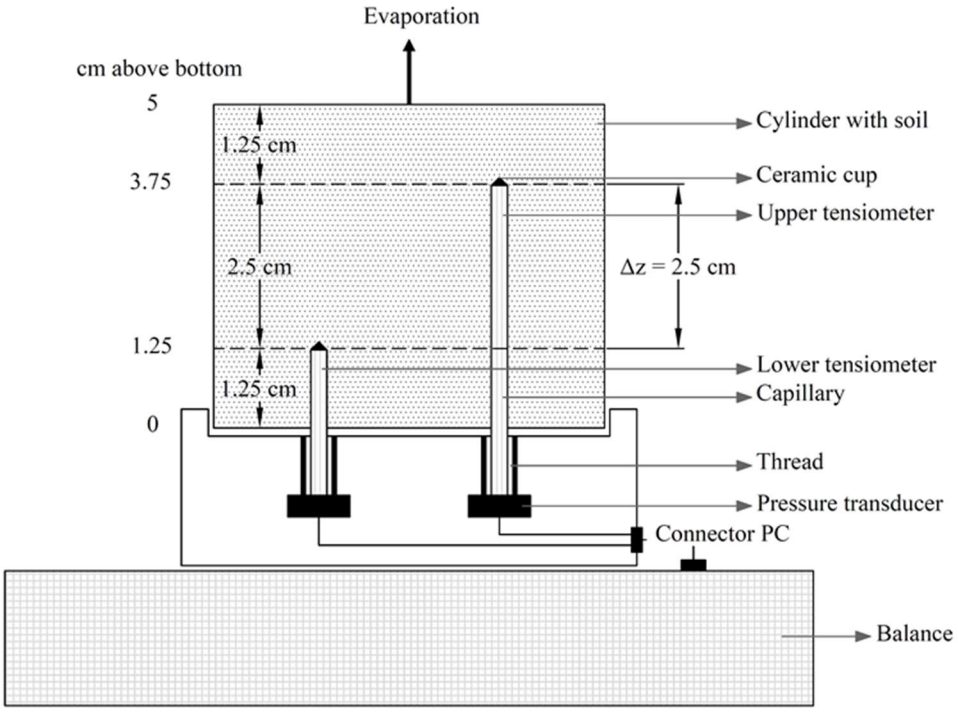

Figure 1. HYPROP® assembly (Schindler et al., 2010).

At regular intervals, five sets of sensor units were connected in series, and weighed one at a time on a laboratory balance. On the first day of the experiment, soil samples were weighted on an hourly interval. After the first day, depending on soil type, the weight measurement interval for clayey soils was three times per day and for sandy soils, it was once per day (UMS, 2010). The sensor unit had two tensiometers, a soil sampling ring, pressure transducer, temperature sensor, and plug connector. The tensiometers measured soil matric potentials at two different depths in every ten minutes. The measurement of matric potentials ranged between 0 to approximately -100 kPa, while in this study, the matric potential ranged from -0.1kPa to -48 kPa for Hecla, from -0.1 kPa to -78 kPa for Glydon silty loam, and from -0.1 kPa to -110 kPa for Fargo soil. The pressure transducer measured the soil matric potential as an analogue signal. Soil sample matric potential and weight change data were recorded continuously until matric

potential collapsed (too dry) in both tensiometers. The dry density and final water content of the soil samples were also measured. The process from soil preparation to tensiometer collapse usually took about two weeks to complete. In order to shorten the drying time, a 100 W incandescent light was placed above the five soil core samples, and a small desk fan was located at 0.3 m away from the samples to circulate the air above the soil samples. This combination reduced the process to 4-5 days for a clayey soil and even shorter for a sandy soil. Soil sample collection, preparation and measurement procedures in this study were conducted according to the HYPROP manual guidelines (UMS, 2010).

The WP4 dewpoint potentiometer determines the soil water matric potentials in a closed chamber by measuring the relative humidity of the air above a sample using the chilled mirror method. The measurement range by the WP4 dewpoint potentiometer is from 0 kPa to -300,000 kPa, while in this study, the matric potential ranged from -40 kPa to -1263 kPa for Hecla, from -54 kPa to -983 kPa for Glydon silty loam, and from -52 kPa to -1484 kPa for Fargo soil. This method is suitable to measure the matric potentials in the dry range, which are important to construct a full SWRC curve. Various amounts of water (0.5, 1.0, 1.5, 2.0, 2.5 and 3.0 g, respectively) were added to the air-dried soil samples (10 g each) with three replicates at each soil water condition as part of the sample preparation. Before starting the measurement procedure by the WP4 dewpoint potentiometer instrument, the WP4 chamber was calibrated and adjusted with a standard 0.5 molar KCl solution. Sample preparation and all measurement procedures were executed according to the operator manual (Decagon Devices, 2003). The combined dataset of soil matric potentials and soil water contents by HYPROP and WP4 methods is referred to as the HW dataset.

2.3.3. HTP method

The hanging water column method was performed with a Haines apparatus where wet soil samples were kept on a porous plate with hydraulic contact to the bulk water (Dane and Topp, 2002). The top of each soil sample was kept at atmospheric pressure when the pressure of the bulk water was reduced to a sub-atmospheric level, which created subsequent hydraulic head reduction and caused water to flow from soil samples to the column. The suction head of the hanging water column method is limited from 0 to -8.5 m, or 0 kPa to -83.4 kPa. In the Tempe cell method, the air pressure inside the cell was raised to be above atmospheric pressure so that water was forced to drain out from the soil samples via the porous plate (Dane and Topp, 2002). Simple SWRCs of the undisturbed soil samples within the range between 0 kPa and -100 kPa can be constructed by the Tempe cell method (Soil Moisture Equipment Corp., 1995). The pressure plate method could minimize the limitation of the hanging water column and the Tempe cell methods since the pressure plate method can withstand high pressure. The pressure plate method can do soil moisture extraction from soil samples for the range between -100 kPa and -1500 kPa (Eijkelkamp Agrisearch Equipment, 2009). In this study, soil matric potential measurement ranges were from -0.1 kPa to -20 kPa by hanging water column method, from -20 kPa to -50 kPa by Tempe cell method, and from -100 kPa to -1500 kPa by pressure plate for all three soil types. Soil matric potentials and water content measurement by hanging water column, Tempe cell, and pressure plate methods on the Fargo, Glyndon and Hecla soils were conducted by the soil physics lab at North Dakota State University. The combined dataset was referenced as the HTP dataset for each soil.

2.3.4. SWRC fitting

SWRCs were developed by using the van Genuchten (1980) equation:

$$\theta(\Psi) = \theta_r + (\theta_s - \theta_r)[1 + (\alpha|\Psi|)^n]^{-m} \quad (2.1)$$

where Ψ is the soil matric potential in kPa, θ_r and θ_s are the residual and saturated volumetric water contents in $cm^3\ cm^{-3}$, respectively, α is related to the reciprocal value of the air entry matric potential in kPa^{-1}, n is a measure of pore size distribution, and m is a fitting parameter which can be written simply as $m = 1 - 1/n$. The values of α, n and m are directly dependent on the shape of the $\theta(\Psi)$ curve (or the SWRC). The value of Ψ at air entry point was measured from the reciprocal value of air entry point as air entry value = 1/α in kPa.

Ψ and θ measured for the Fargo, Glyndon and Hecla soils in the combined HW and HTP datasets, were plotted as θ vs. Ψ. Best fit parameters (α, n, and m) were estimated for the VG model of SWRC using "Excel Solver®" (Wraith and Or, 1998) and are reported in Table 2. To measure the goodness of fit between the measured and the predicted datasets, coefficients of determination (R^2) were obtained for each dataset used for a soil. The R^2 value explained how well the predicted values matched with measured values. The R^2 value was determined by following equation:

$$R^2 = \left[\frac{\sum_{i=1}^{N}(Observed\ value - Observe\quad mean)(Measured\ value - Measure\quad mean)}{\sqrt{\sum_{i=1}^{N}(Observed\ value - Observe\quad mean)^2}\sqrt{\sum_{i=1}^{N}(Measued\ value - Measure\quad mean)^2}}\right]^2 \quad (2.2)$$

For comparison purpose, SWRCs were constructed for a Ψ range between 0 kPa and -1500 kPa (permanent wilting point for crops) using the best fit VG parameters for each combined dataset of the respective soils.

2.3.5. SWRC difference

The absolute differences (AD) between the soil moisture values measured by the HW and the HTP methods and the predicted values on the corresponding fitted SWRCs can be computed as:

$$AD = | \theta_{measured} - \theta_{fitted} | \quad (2.3)$$

where $\theta_{measured}$ is the HW method or the HTP method and θ_{fitted} is the corresponding fitted SWRC value.

Table 2. Best fit estimated van Genuchten parameters by HYPROP and WP4 (HW) method and hanging column, Tempe cell, and pressure plate method (HTP).

Soil	Method	α (kPa^{-1})	n	m
Fargo Soil	HW	0.33	1.19	0.16
	HTP	0.47	1.14	0.13
Glyndon Soil	HW	0.12	1.45	0.31
	HTP	0.16	1.39	0.28
Hecla Soil	HW	0.14	1.85	0.46
	HTP	0.24	1.58	0.37

2.4. Results and discussion

The simple HW method provided sufficient measured θ data between the wet (from 0 kPa to -100 kPa) and the dry (above -100 kPa to -300,000 kPa) Ψ ranges, which can get a better estimation of VG parameters. The traditional HTP method using the hanging column, Tempe cell, and pressure plate measured the θ and Ψ between -10 kPa and -1500 kPa ranges with fewer measured data points (11 data points). Best fitting parameters of the VG model for all datasets and for all soils are reported in Table 2. The estimated fitting parameters of the HW dataset were different from those of the HTP dataset. The comparison of the fitted SWRCs from the HW and traditional HTP datasets for each of soil types is shown in Figure 2, while the fitted HW and HTP SWRCs for the Fargo, Glyndon and Hecla soils are shown in Figure 3.

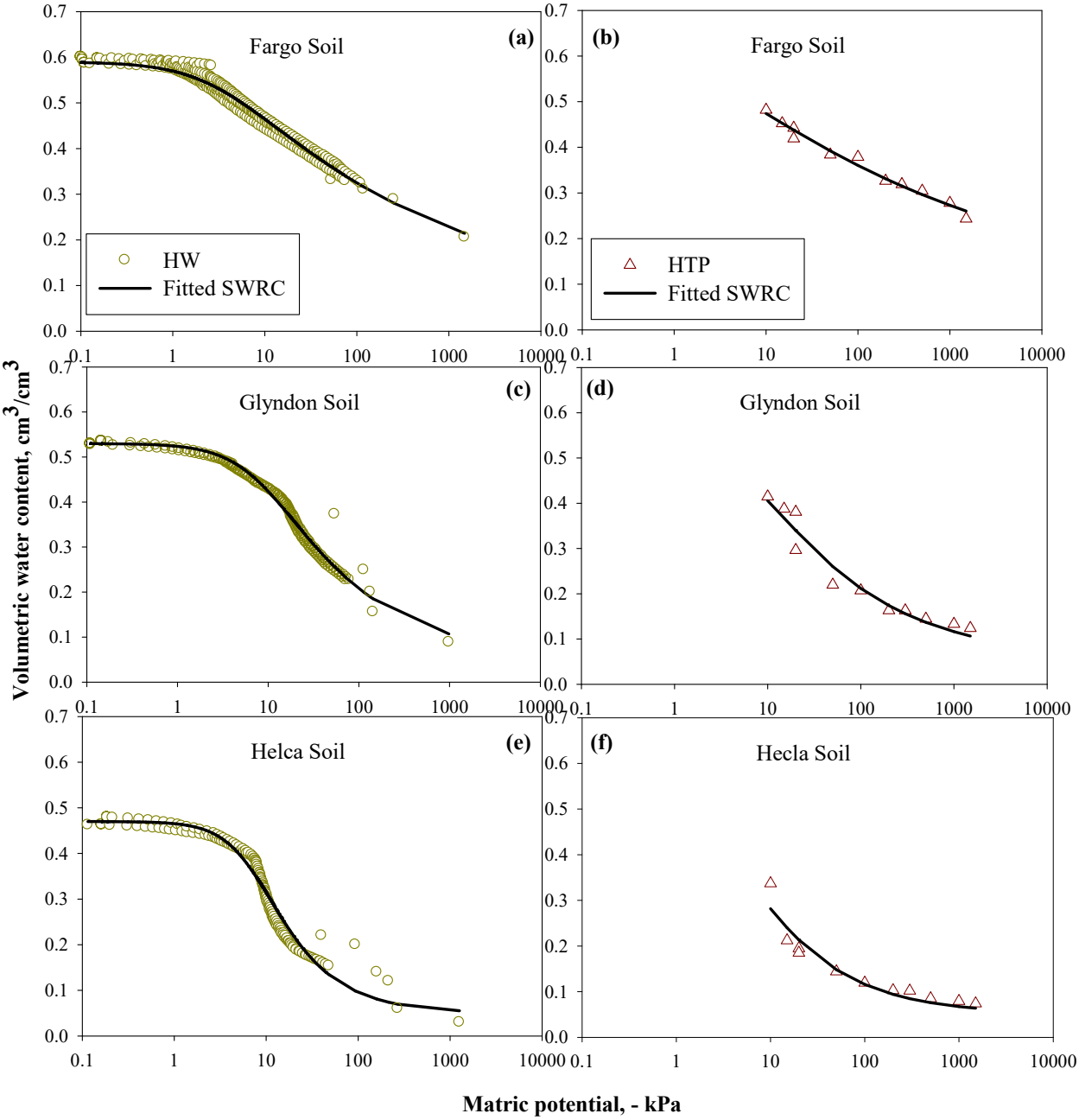

Figure 2. Fitted SWRCs using best estimated van Genuchten parameters with HYPROP+WP4 (HW) dataset for (a) Fargo soil, (c) Glyndon soil, (e) Hecla soil and with hanging column, Tempe cell, and pressure plate (HTP) dataset for (b) Fargo soil, (d) Glyndon soil, and (f) Hecla soil.

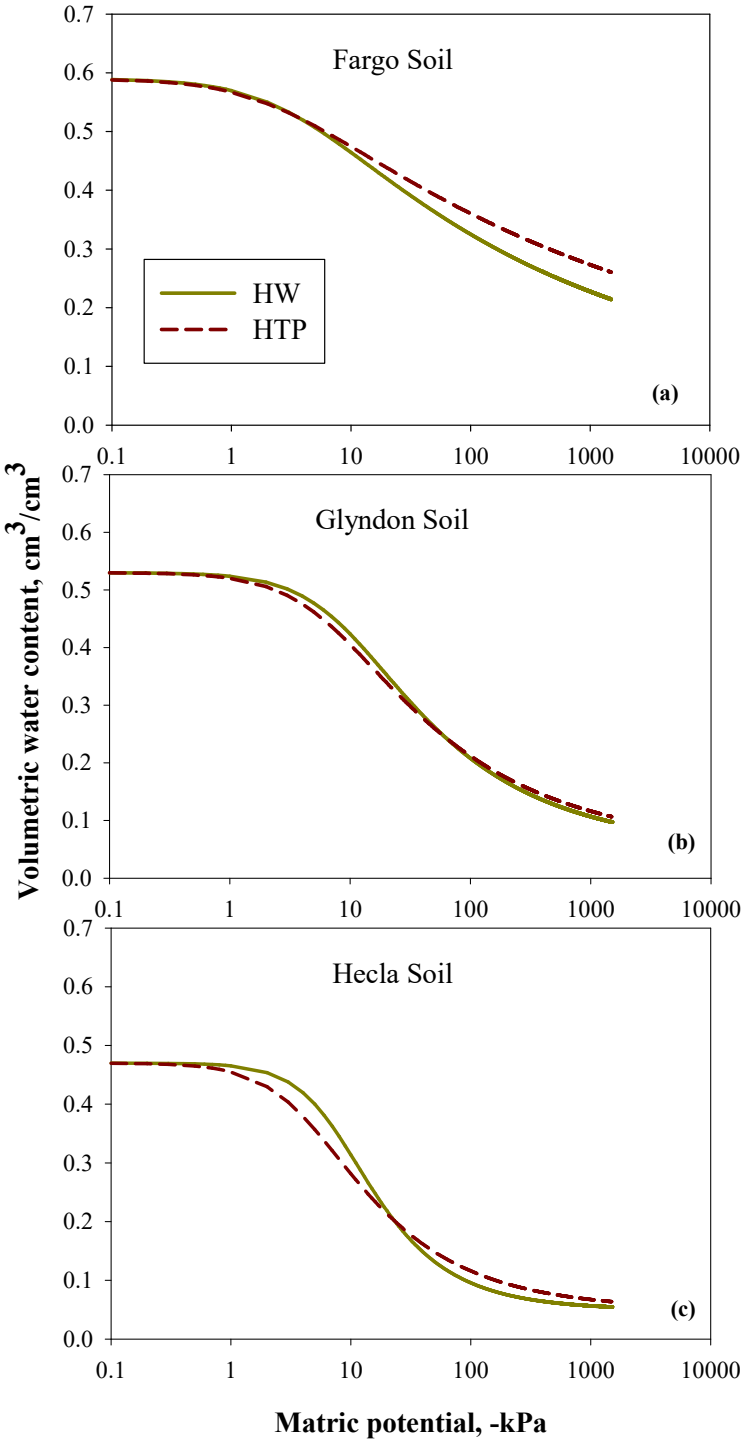

Figure 3. Comparison between fitted SWRCs of HYPROP and WP4 (HW) and hanging column, Tempe cell, and pressure plate (HTP) datasets for (a) Fargo soil, (b) Glyndon soil, and (c) Hecla soils.

2.4.1. Fargo silty clay soil

The HYPROP® data of four drying cycles and WP4 data of three drying cycles were used to create the HW dataset for the Fargo soil. The SWRCs according to the VG equation were fitted using the best fitting parameters (Table 2) with HW dataset (Figure 2a) and HTP dataset (Figure 2b). The R^2 between original and fitted data points was approximately 0.98 for both HW and HTP datasets, which indicated that the fitted SWRCs agreed well with the measured datasets. Comparison between the two fitted SWRCs showed a close agreement up to Ψ value of -10 kPa and then the two SWRCs showed differences in values until the end of the curve at -1500 kPa (Figure 3a). The shape of the SWRC of HW decreases faster after -10 kPa Ψ compared to that of HTP. Field capacity (θ_{fc}) at -33 kPa values were 0.39 cm^3 cm^{-3} and 0.41 cm^3 cm^{-3} and permanent wilting point (θ_{pwp}) at -1500 kPa values were 0.21 cm^3 cm^{-3} and 0.26 cm^3 cm^{-3} for the SWRCs of HW and HTP datasets, respectively. The difference between the two θ_{pwp} values was higher (0.05 cm^3 cm^{-3}) compared to the θ_{fc} values difference (0.02 cm^3 cm^{-3}) because the gap between the two SWRCs continuously increased at the dry θ range. The air entry Ψ value difference between the two SWRCs was less than 1 kPa (i.e. 0.96 kPa) for the SWRCs of HW and HTP datasets.

2.4.2. Glyndon silty loam soil

The HW dataset contained data from two HYPROP® drying cycle experiments and three WP4 drying cycle experiments on the Glyndon silty loam soil. The R^2 value was 0.98 for the HW dataset. The fitted SWRC matched well with measured values (R^2 = 0.95) for the HTP dataset. The two fitted SWRCs were almost identical for the entire Ψ range and both SWRCs followed a similar slope (Figure 3b). Among the three soils used in this study (Fargo, Glyndon, and Hecla), the fitted SWRCs constructed from datasets HW and HTP for Glyndon soil

displayed the closest match with respect to shape and slope, although some differences existed. The air entry Ψ value of 8.3 kPa for fitted SWRC of HW dataset and 6.25 kPa for the fitted SWRC of the HTP dataset was slightly different as it varied by 2.05 kPa. For comparison purposes, the HYPROP® instrument has an accuracy of ±0.15 kPa in pressure measurement (UMS, 2010). The differences of both θ_{fc} at -33 kPa (0.309 cm^3 cm^{-3} for HW dataset and 0.294 cm^3 cm^{-3} for HTP dataset) and θ_{pwp} at -1500 kPa (0.097 cm^3 cm^{-3} and 0.106 cm^3 cm^{-3} for HW and HTP datasets, respectively) were comparatively very small (approximately 0.01 cm^3 cm^{-3}).

2.4.3. Hecla sandy loam soil

The Hecla soil HW dataset also contained two drying cycle datasets from the HYPROP® method and three drying cycle datasets from the WP4 method. The fitted SWRC for the Hecla HW dataset had the steepest slope compared to any other SWRCs developed for other soils (Figure 2c). The R^2 between the measured and the predicted values was 0.96 for the fitted SWRC with the HW dataset. The Hecla soil HTP dataset had somewhat poorer agreement with R^2 = 0.91. In Figure 3c, the fitted SWRC of the HTP dataset started descending sooner than that of HW dataset after approximately -1 kPa suction. Both SWRCs intersected with each other at approximately -23 kPa Ψ value and then the fitted SWRC of the HTP dataset went above the fitted SWRC of the HW dataset for the rest of the Ψ range with relatively small differences in values. The θ_{fc} at -33 kPa was found greater (0.174 cm^3 cm^{-3}) for the SWRC of the HTP dataset than that for the SWRC of the HW dataset (0.165 cm^3 cm^{-3}), though the difference between the two θ_{fc} values was not considerably high (0.01 cm^3 cm^{-3}). Similarly, the difference between the θ_{pwp} values at -1500 kPa for the two SWRCs was 0.01 cm^3 cm^{-3}, which was 0.054 cm^3 cm^{-3} for SWRC of HW dataset and 0.063 cm^3 cm^{-3} for SWRC of HTP dataset. The difference (2.98 kPa)

between the air entry Ψ values of the two SWRCs created variation in SWRC shapes, as it was 7.14 kPa for SWRC of HW dataset while it was 4.16 kPa for the SWRC of the HTP dataset.

2.4.4. SWRC difference

The difference in soil moisture content between the predicted values of the two fitted SWRCs for each soil can be expressed as a histogram (Figure 4). The maximum and minimum of soil moisture differences between the fitted SWRCs by the HW and HTP methods are also reported in Figure 4 for each soil. The histogram represents the number of data points for a specific range of θ difference. From Figure 4a, the Fargo soil showed that 19% of the total data points had a difference in the 4.1-4.5% range while 66% of the data points had a θ difference in the 4.5-5.0% range. The rest of the data points fell inside the 0-4.0% difference. As discussed earlier (Figure 3a), the two fitted SWRCs for Fargo soil showed a higher θ difference in θ prediction after Ψ = -10 kPa. The gap kept increasing between the two SWRCs until those reached the end of Ψ data range at -1500 kPa. For the Glyndon silty loam soil, all the differences between the two fitted SWRCs in θ predictions were within the 0-2.0% range (Figure 4b). The largest class of data points (78%) occurred in the range of 0.9-1.0%. According to our earlier discussion in Figure 3b, the two fitted SWRCs for the Glyndon silty loam soil were best matched among the three soils in terms of shape and slope. For Hecla soil, 22%, 76%, and 2% of data points were within the θ prediction difference of 0-1.0%, 1.1-2.0%, and 2.1-4.5%, respectively (Figure 4c). The two SWRCs had some shape differences for certain Ψ ranges as shown in Figure 3c. The measured water contents by both HW and HTP methods were plotted together for the same matric potential range in Figure 5 for all three soils. The comparison between measured SWRCs show where the two methods agree and where the methods diverge for Fargo soil (Figure 5a), Glyndon soil (Figure 5b) and Hecla Soil (Figure 5c).

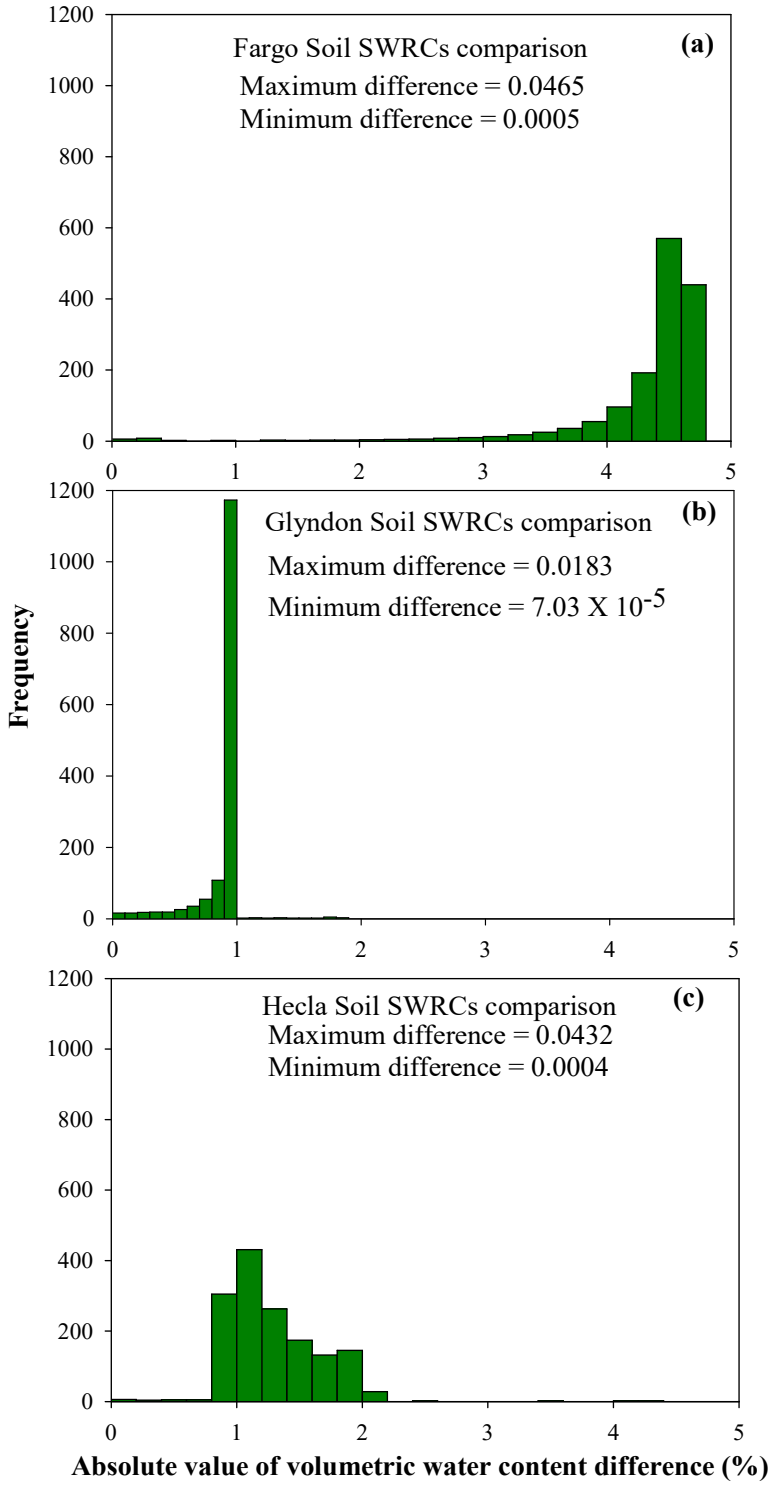

Figure 4. Comparison of absolute values of volumetric water content differences (%) between fitted SWRCs of HYPROP+WP4 (HW) and hanging column, Tempe cell, and pressure plate (HTP) datasets for (a) Fargo soil, (b) Glyndon soil, and (c) Hecla soils.

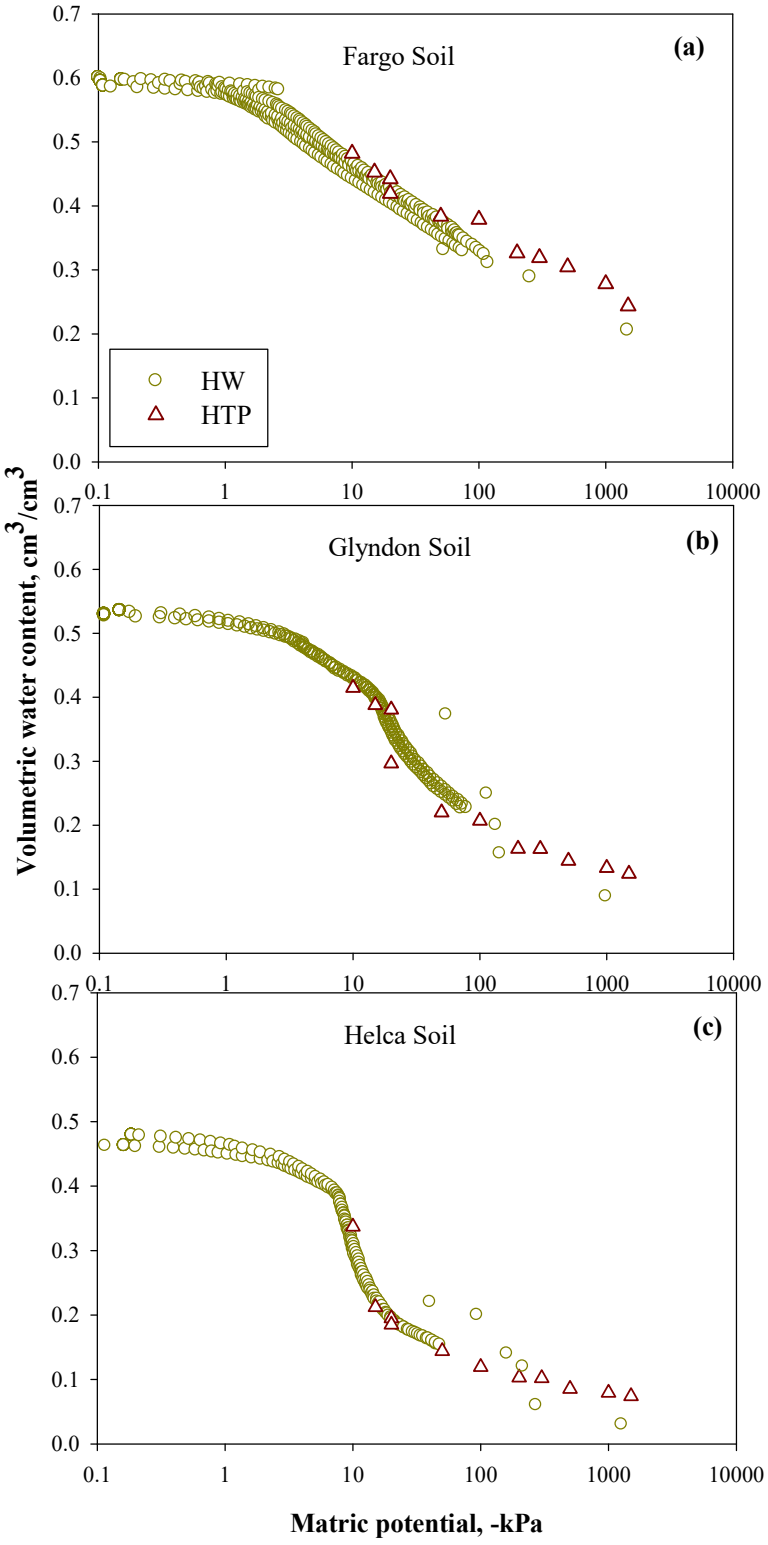

Figure 5. Comparison of combined datasets between measured SWRCs of HYPROP and WP4 (HW) and hanging column, Tempe cell, and pressure plate (HTP) methods for (a) Fargo soil, (b) Glyndon soil, and (c) Hecla soils.

2.4.5. Variability of SWRC in soil textural classes

According to Tuller and Or (2004), it is anticipated that the SWRC relationship may vary substantially for the same soil textural class due to variation in fitting parameters α (reciprocal value of air entry Ψ) and pore size distribution parameter, n. The VG SWRC model fitting parameters for the same soils in this study are presented in Table 3, and compared with other soils from the literature (Rawls et al., 1982; Carsel and Parrish, 1988; and Leij et al., 1996). The fitting parameters of the SWRC model for different methods in this study are also included in Table 3. The α and n values shown in Table 3 from Rawls et al. (1982) were later modified by van Genuchten et al. (1991). The unit of the α value for the fitted SWRCs in this study was in kPa^{-1} (Table 2), but converted to cm^{-1} (Table 3) for comparison with values in the literature.

Table 3. Variation in α and n van Genuchten fitting parameter reference value ranges for soils in this study and soils from the same textural classes

Soil	USDA Soil Textural Classification	Method[1]	α (cm^{-1})	n
Fargo	Silty clay	Rawls et al. (1982)	0.029	1.13
		Carsel and Parrish (1988)	0.005	1.09
		Leij et al. (1996)	0.023	1.39
		HW	0.033	1.19
		HTP	0.046	1.14
Glyndon	Silt loam	Rawls et al. (1982)	0.048	1.21
		Carsel and Parrish (1988)	0.020	1.41
		Leij et al. (1996)	0.012	1.39
		HW	0.012	1.45
		HTP	0.016	1.39
Hecla	Sandy loam	Rawls et al. (1982)	0.068	1.32
		Carsel and Parrish (1988)	0.075	1.89
		Leij et al. (1996)	0.021	1.61
		HW	0.014	1.85
		HTP	0.024	1.58

[1] Values from the literature are for the soil textural classes indicated; values from HYPROP+WP4 (HW) and hanging column, Tempe cell, and pressure plate (HTP) are for the Fargo, Glyndon, and Hecla soils used in this study.

From table 3, it can be seen that the α and n values had a wide range for the same soil textural class. The α values in Table 3 varied from 0.005 to 0.029 cm^{-1} for silty clay soil, from 0.012 to 0.048 cm^{-1} for silt loam soil, and from 0.021 to 0.075 cm^{-1} for sandy loam soil. As reported by Porebska et al. (2006), a soil which differed more in its sandy composition resulted in a higher α value. The HW dataset fitted SWRC for the Fargo soil had an α value (0.033 cm^{-1}) slightly above the upper end of the reference value for silty clay soil. The HTP dataset fitted SWRC had the α value (0.046 cm^{-1}), which is much higher than the upper end of the reference value. For the Glyndon soil, the α value of the fitted SWRC of HW exactly matched with the lower end of the silt loam soil reference value range and the α value of HTP SWRC fell within the silt loam soil reference value range, specifically very close to the lower end of the range. A smaller value of α, falling outside of the lower end of the sandy loam soil reference value range, was found for the fitted HW SWRC in the Hecla soil, but it fell inside the range of the sandy loam soil for the fitted HTP SWRC.

Similar to the α values, the reference value ranges of n also ranged as 1.09-1.39 for silty clay soil, 1.21-1.41 for silt loam soil, and 1.32-1.89 for sandy loam soil. These findings are similar to what Porebska et al. (2006) found, a soil with higher sand content tends to have a higher n value. The fitted pore size distribution parameter n for SWRCs of the HW and HTP datasets for each soil fell within the corresponding ranges of reference values except for the HW SWRC of the Glyndon silty loam soil. The n value was slightly higher than the upper end of the silt loam soil reference value range.

The shape and slope differences of SWRCs for the same textural class of soil may be attributed to the availability of measured data points, deviations in measurements due to inappropriate handling of instruments, variation of finer particles in soil texture (Schindler et al.,

2012; Schelle et al., 2013), shrink-swell phenomena of clay soil (Patil and Rajput, 2009), and other unexplained reasons. The swelling and shrinking characteristics of the Fargo soil of the RRB expanded the soil volume at saturation and reduced the soil volume at the permanent wilting point. While the soil samples were packed into the columns according to the pre-defined bulk density for the hanging column, Tempe cell, and HYPROP methods, but due to the column size difference, the larger the column, the higher the expansion and contraction of the soil column. This expansion and reduction of soil volume, especially with the HYPROP method due to its larger column size, changed the θ_s and θ_{pwp}, which led to a comparatively large difference between two fitted SWRCs for Fargo soil compared with that of other soils. A small measurement error near the soil saturation can cause a significant change in the shape of the SWRCs (Vogel et al., 2000).

2.4.6. Bulk density changes

When using HYPROP to develop soil water release curve, the option of oven dried soil weight is chosen to calculate the bulk density and the associated volumetric water content. Because of the soil swelling, soil was expanded beyond the ring during saturation. Extra soil was removed before starting the experiment, and the bulk density of the soil core was reduced and smaller than the originally packed value, or values from other methods with a confined soil core during the wetting process (Tempe Cell, Hanging Column, and Pressure Plate). The resulting bulk density for the HYPROP and the HTP is listed in Table 4, while WP4 applied the same bulk density as the HTP method.

As one can see that the sandy soil had a small bulk density difference, while a clayey soil had the largest difference. For Fargo soil, the bulk density was 1.08 g cm^{-3} in the HTP method, but decreased to 0.90 g cm^{-3} in the HYPROP method, a significant 16% difference. A potential

increase of 2 to 24% from shrinkage to plastic limit for a clay soil was reported by Ito and Azam (2010). In the HYPROP experiment, though the soils were packed according to the defined bulk density, the soil was wetted to saturation without any constraints in which the soil swelling cannot be prohibited. A simple change of the bulk density will affect the measured moisture content as well as the associated matric potential. Further research in using the HYPROP method should incorporate the swelling and shrinkage relationship (Cornelis et al., 2006; Schindler et al., 2015), or constrain the soil core during the wetting process to prevent swelling and maintain the same bulk density as comparable methods.

Table 4. Comparison of soil bulk density (g cm^{-3}) for the three soils using HYPROP and hanging water column, Tempe cell, and pressure plate (HTP) methods

Soil Type	HYPROP	HTP	Difference	% Difference
Fargo silty clay	0.90	1.08	-0.18	-16.44
Glyndon silty loam	1.08	1.18	-0.11	-8.90
Hecla sandy loam	1.26	1.31	-0.06	-4.20

2.5. Conclusion

The simple HYPROP and WP4 dewpoint potentiometer method constructed a better SWRC because of the improved measurement ranges for estimating van Genuchten fitting parameters. In this study, the predicted soil moisture content via fitted SWRCs agreed well with the measured data by the HYPROP+WP4 method with R^2 values of 0.98, 0.98, and 0.96 for Fargo, Glyndon and Hecla soils, respectively. The predicted soil moisture contents agreed well with the measured data by the traditional hanging column + Tempe cell + pressure plate laboratory method with R^2 values of 0.98, 0.95, and 0.91 for Fargo, Glyndon and Hecla soils, respectively. This indicated that both the simple and traditional methods are suitable to estimate the van Genuchten parameters.

Comparing the two fitted SWRCs by the two methods, we found that Glyndon silty loam and Hecla soils had the best fitted SWRCs in terms of shape and slope. The soil moisture difference for Glyndon silty loam soil between the two SWRCs was only 0.9-1.0% for 78% of the data points. For Hecla soil, the soil moisture difference was 1.1-2.0% for 76% of the data points. The fitted SWRCs for Fargo soil did not show a good match in terms of shape and slope due to the presence of clay and its swelling and shrinkage nature in the Red River Valley. For the Fargo soil, 66% of the data points showed a 4.5-5.0% difference.

The simple combined HYPROP and WP4 produced good quality data over the entire wet and dry soil moisture range to develop the SWRCs. It saves at least half the time, applies simpler procedures, and is considered as an acceptable approach for replacing the traditional laboratory method. The results may be further improved if the soil bulk density could be possibly maintained the same among different methods.

2.6. Acknowledgements

The authors wish to thank Mr. Joel Bell and Dr. Thomas DeSutter of Soil Science for providing the soil samples and the data from the traditional methods. This project is supported by NASA ROSES Project 13-WATER13-0036, USDA National Institute of Food and Agriculture project 2015-68007-23193, ND Soybean Council, ND Water Resources Research Institute, ND Agricultural Experimental Station, and USDA Hatch project ND01475. The authors would like to express their gratitude to Ms. Debra Baer for her assistance for this work. We also want to thank the reviewers and the associate editor for their valuable comments.

2.7. References

Bittelli, M., and Flury, M. (2009). Errors in water retention curves determined with pressure plates. *Soil Sci. Soc. Am. J.* 73:1453-1460.

Bouyoucos, G. J. (1951). A recalibration of the hydrometer method for making mechanical analysis of soils. *Agron. J.* 43:434-438.

Burckhard, S.R., Pirkl, D., Schaefer, V.R., Kulakow, P., & Leven, B. (2000). A study of soil water-holding properties as affected by TPH contamination. In *Proc. Conf. on Hazardous Waste Research*, Great Plains/Rocky Mountain Hazardous Substance Research Center, Manhattan, pp. 356–359, KS, USA.

Caine, T.A. (1903). Soil survey of the Fargo area, North Dakota. Field Operation of the Bureau of Soils, USDA.

Campbell, J.J., Smith, D.M., & Teare, B.L. (2007). Application of a dew point method to obtain the soil water characteristics. In *Experimental Unsaturated Soil Mechanics* (ed. T. Schanz, pp 71-77), Springer, New York.

Cancela, J.J., Dafonte, J., Martinez, E.M., Cuesta, T.S., & Neira, X.X. (2006). Assessment of a water activity meter for rapid measurements of soil water potentials. *Biosyst. Eng.* 94: 285-295.

Carsel, R.F., & Parrish, R.S. (1988). Developing joint probability distributions of soil water retention characteristics. *Water Resour. Res.* 24:755-769.

Cornelis, W.M., Corluy, J., Medina, H., Diaz, J., Hartmann, R., Van Meirvenne, M., & Ruiz, M.E. (2006). Measuring and modeling the soil shrinkage characteristic curve. *Geoderma* 137(1-2): 179-191.

Dane, J.H. & Topp, G. C. (editors). (2002). *Methods of Soil Analysis: Part 4-Physical Methods.* Wisconsin, USA: Soil Science Society of America, Inc.

Decagon Devices. (2003). WP4 Dewpoint Potentiometer Operator Manual, version 2.1. Pullman Washington, USA: Decagon Devices.

Eijkelkamp Agrisearch Equipment. (2009). 15 Bar Pressure Plate Extractor Operating Instruction, Giesbeek, The Netherlands.

Erzin, Y., & Erol, O. (2007). Swell pressure prediction by suction methods. *Eng. Geol., Science Direct.* 92(3-4):133–145.

Fredlund, D. G., & Rahardjo, H. (1993). Soil mechanics for unsaturated soils, Wiley, NY.

Fuentes, C., Zavala, M., & Saucedo, H. (2009). Relationship between the storage coefficient and the soil-water retention curve in subsurface agricultural drainage systems: water table drawdown. *J. Irrig. Drain. Div. Am. Soc. Civ. Eng*. 135(3):279–285.

Fujimaki, H. & Inoue, M. (2003). A flux-controlled steady-state evaporation method for determining unsaturated hydraulic conductivity at low matric pressure head values. *Soil Sci.* 168: 385-395.

Gee, G.W., Campbell, M.D., Campbell, G.S., & Campbell, J.H. (1992). Rapid measurement of low soil water potentials using a water activity meter. *Soil Sci. Soc. Am. J.* 56:1068-1070.

Hillel, D. (1998). *Environmental soil physics*. San Diego, USA: Academic Press.

Ito, M., and S. Azam. 2010. Determination of swelling and shrinkage properties of undisturbed expansive soils. Geotechnical and Geological Engineering 28(4): 413-422.

Leij, F.J., Alves, W.J., van Genuchten, M.Th., & Williams, J.R. (1996). The UNSODA unsaturated hydraulic database. EPA/600/R-96/095, U.S. Environmental Protection Agency, Cincinnati, OH.

Leong, E.C., & Rahardjo, H. (1997). Review of soil-water characteristics curve equations. *J. Geotech. Geoenviron. Eng.* 123(12):1106-1117.

Maček M., Smolar, J., & Petkovšek, A. (2013). Extension of measurement range of dewpoint potentiometer and evaporation method. In *Proc. 18th International Conference on Soil Mechanics and Geotechnical Engineering*, 1137-1142, Paris, France: The French Society for Soil Mechanics and Geotechnical Engineering (CFMS).

Malaya, C., & Sreedeep, S. (2012). Critical review on the parameters influencing soil-water characteristic curve. *J. Irrig. Drain Eng.* 138(1):55-62.

Miller, R.W., & Gardiner, D.T. (2001). *Soils in Our Environment.* 9th ed. New Jersey, USA: Prentice Hall, Inc.

Nikiforoff, C.C., Hasty, A.H., Swenson, G.A., Gray, A.L., Fieger, E.A., Hill, S., Newman, H.C., Mattson, C.H., Hide, J.C., & Kneen, E. (1939). Soil survey (Reconnaissance) of the Red River Valley area, Minnesota. Bureau of Chemistry and Soils, USDA, Series 1933, No 25, April.

NRCS. (2017). Web Soil Survey. Available online at https://websoilsurvey.sc.egov.usda.gov/. Accessed [March/20/2017].

Patil, N.G., & Rajput, G.S. (2009). Evaluation of water retention functions and computer program "Rosetta" in predicting soil water characteristics of seasonally impounded shrink-swell soils. *J. Irrig. Drain Eng.* 135(1):286-294.

Porebska, D., Slawinski, C., Lamorski, K., & Walczak, R. T. (2006). Relationship between van Genuchtchn's parameters of the retention curve equation. *Int. Agrophys*. 20: 153-159.

Rawls, W.J., Brakensiek, D.L., & Saxton, K.E. (1982). Estimating soil water properties. *Transactions of the ASAE* 25(5):1316-1320.

Scanlon, B.R., Andraski, B.J., & Bilskie, J. (2002). Water potential: miscellaneous methods for measuring matric or water potential. In *Methods of Soil Analysis. Part 4-Physical Methods* (eds. J.H. Dane and G.C. Topp), pp 643-670. Soil Science Society of America, Madison, WI.

Schaap, M. G., Leij, F. L., & Van Genuchten, M. Th. (2001). Rosetta: a computer program for estimating soil hydraulic parameters with hierarchical pedotransfer functions. *J. Hydrol.* 251:163–176.

Schelle, H., Heise, L., Janicke, K., & Durner, W. (2013). Water retention characteristics of soils over the whole moisture range: a comparison of laboratory methods. *Eur. J. Soil Sci.* 64:814-821.

Scherer, T., Kandel, H., Sands, G., & Hay, C. (2013). Frequently asked questions about subsurface (tile) drainage. AE1690: North Dakota State University.

Schindler, U., Muller, L., da Veiga, M., Zhang, Y., Schlindwein, S., & Hu, C. (2012). Comparison of water retention functions obtained from the extended evaporation method and the standard methods sand/kaolin boxes and pressure plate extractor. *J. Plant Nutr, Soil Sci.* 175:527-534.

Schindler, U., Doerner, J., & Mueller, L. (2015). Simplified method for quantifying the hydraulic properties of shrinking soils. *J. Plant Nutr, Soil Sci.*178 (1): 136-145.

Soil moisture Equipment Corporation. (1995). Tempe Pressure Cell Operating Instruction, Santa Barbara CA, USA: SOILMOISTURE.

Solone, R., Bittelli, M., Tomei, F., & Morari, F. (2012). Errors in water retention curves determined with pressure plates: effects on the soil balance. *J. Hydrol.* (Amsterdam). 470-471: 65-74.

Sreedeep, S., & Singh, D. N. (2011). Critical review of the methodologies employed for soil suction measurement. *Int. J. Geomech*. 11(2): 99-104.

Tuller, M., & Or, D. (2004). Water retention and characteristic curve, in *Encyclopedia of Soils in the Environment*, vol. 4 (edited by D. Hillel): pp. 278–289.

UMS. 2010. HYPROP User Manual, version 01/2010. Berlin, Germany: UMS.

van Genuchten, M. T. (1980). A closed form equation for predicting the hydraulic conductivity of unsaturated soils. *Soil Sci. Soc. Am. J.* 44:892–898.

van Genuchten, M.Th., Leij, F.J., & Yates, S.R. (1991). The RETC code for quantifying the hydraulic functions of unsaturated soils, US Environmental Protection Agency, Ada, Oklahoma.

Vanapalli, S.K., Fredlund, D.G., Pufahl, D.E., & Clifton, A.W. (1996). Model for the prediction of shear strength with respect to soil suction. *Can. Geotech. J.,* 33(3):379–392.

Vogel, T., van Genuchten, M.T., & Cislerova, M. (2000). Effect of the shape of the soil hydraulic functions near saturation on variably-saturated flow predictions. *Adv. Water Resour.* 24(2): 133-144.

Wraith, J. M., & Or, D. (1998). Nonlinear parameter estimation using spreadsheet software. *J. Nat. Resour. Life Sci. Educ.* 27:13-19.

Zhan, T.L.T., & Ng, C.W.W. (2004). Analytical analysis of rainfall infiltration mechanism in unsaturated soils. *Int. J. Geomech*. 4(4): 273–284.

3. INFILTRATION INTO FROZEN SILTY CLAY LOAM SOIL WITH DIFFERENT SOIL WATER CONTENTS IN THE RED RIVER OF THE NORTH BASIN[2]

3.1. Abstract

Predicting surface runoff and flooding in seasonally frozen areas such as the Red River of the North Basin (RRB) is a challenging task. It depends on the knowledge of the complex process of infiltration in frozen soil, such as phase changes of water, ice content and distribution in the infiltration zone (the top 0-30 cm of the soil profile), soil pore size distribution, soil temperature and freeze-thaw cycles. In this study, laboratory infiltration experiments were conducted using a Cornell sprinkler infiltrometer. The infiltration rates into a frozen silty clay loam soil were measured at three different initial water contents: permanent wilting point (PWP), θ_{pwp}; field capacity (FC), θ_{fc}; and between FC and PWP, θ_{mid}. Volumetric soil water content (θ_v) and soil temperature at three depths were also continuously monitored using sensors. Initial infiltration into frozen soil occurred quickly in the soil with θ_{pwp} because the soil was dry. Initial infiltration was comparatively slower in the soil with θ_{mid}, while water from the melted ice was contributed to the soil over time. Initial infiltration was very slow in the soil with θ_{fc}, because the wet soil had very small pore space, so the soil rapidly reached its saturation after the infiltration started. Horton infiltration equation was fitted with the observed infiltration rates for the soils with three initial water contents and the goodness of fit was evaluated by using the coefficient of

[2] The material in this chapter was co-authored by Debjit Roy and Xinhua Jia, Dean Steele, Xuefeng Chu, and Zhulu Lin, and is under review for possible publication in the *Hydrological Processes* Journal as manuscript number HYP-18-0137. Debjit Roy had primary responsibility for collecting data and the primary developer of the conclusions that are advanced here. Debjit Roy also drafted and revised all versions of this chapter. Co-authors served as proofreader and checked the math in the statistical analysis conducted by Debjit Roy.

determination, R^2 values. The final infiltration rates from the fitted Horton equations were 0.060, 0.010, and 0.027 cm/min for the initial water contents of θ_{pwp}, θ_{mid}, and θ_{fc}, respectively. The soil water content along the soil profile changed with infiltrating water over the time. However, the initial soil water content and melt water from ice due to soil temperature rise regulated the change in soil water content. The θ_v changed gradually in the θ_{pwp} soil, rapidly at 0°C in the θ_{mid} soil and less in the θ_{fc} soil. It was also found that soil aggregate stability was altered by soil packing and freeze-thaw cycles. It changed the soil hydraulic properties and minimized the pore spaces, which reduced infiltration rate over time in the soil with θ_{fc}. Due to less pore spaces, the same soil reached saturation early so that the θ_v did not respond much with temperature rise.

3.2. Introduction

In cold region hydrology, frozen soil is a key component directly affecting infiltration and indirectly affecting heat transfer from and to the snowpack situated on the soil surface. Frozen soil infiltration is a complicated hydrological process that contributes to crop water uptake, surface runoff generation and ground water recharge in northern latitudes. Frozen soil infiltration differs from unfrozen soil infiltration because of infiltrating water re-freezing and melting of ice content within the soil profile (Flerchinger et al., 2005). Soil starts to freeze from the surface when soil temperature drops below 0°C, while the water contents along the soil profile are gradually reduced and converted to ice. Permeability and infiltration capacity are greatly decreased with increases in ice formation within the soil profile. Granger et al. (1984) reported that the amount and distribution of ice, within the 0-30 cm depth of uncracked frozen Prairie soil profile, i.e. “zone of infiltration,” are the dominant factor that affects water infiltration during ice melting. The pore size distribution of “zone of infiltration” also affects the melted water infiltration in frozen soil (Granger et al., 1984). He et al. (2015) reported that

springtime snowmelt water infiltration is greatly governed by the air-filled porosity of the top 10 cm of soil and the soil water content stored during the previous fall season in the top 30 cm of soil. Infiltration rates are inversely related to soil water contents at freezing time (Lee and Molnau, 1982; Kane and Stein, 1983). As soil consists of different pore sizes, the soil freezing point (or, freezing temperature) is greatly dependent on the pore size distribution of soil, and ice and water can coexist in various pores at the same time due to freezing point differences (Ireson et al., 2013). When water molecules stay farther from soil particle, the soil water usually freezes first due to temperature decease, but it will freeze last if water molecules stay closer to soil particles (Williams and Burt, 1974; Six et al., 2004; Fouli et al., 2013). Ireson et al. (2013) reported that due to this reason, water in large pores freezes faster than that in small pores, and water in small pores thaws earlier than that in large pores. The flow path tortuosity increases due to the formation of ice in soil, because soil water in large pores freezes first, and restricts water movement in those pores. As a result, infiltration capacity of that frozen soil diminishes (Lundberg et al., 2015). Many ice lenses form within the soil profile, making the agricultural soil hard during winter time and transforms the frozen soil into an almost impermeable form (Zuzel and Pikul, 1987; Flerchinger et al., 2005). Iwata et al. (2011) observed that in subzero winter, large amounts of rain water stored on soil surfaces can freeze, resulting in a frozen ice layer on the soil surface which impedes snowmelt infiltration. However, water can still infiltrate into the frozen soil even after freezing if the soil is not wetted to saturation during freezing (Flerchinger et al., 2005; He et al., 2015).

Snowmelt water infiltration involves the complex processes of heat and mass transfer through the frozen soils and is very important for estimating snowmelt surface runoff and flood water level prediction (Gray et al., 2001; Zheng et al., 2001). Many factors, such as soil water,

soil temperature, snow cover water release rate, porosity, soil cracks, temperature of infiltrating snowmelt water, and presence or absence of macropores, affect the total infiltration process (Granger et al., 1984). In frozen soils, the infiltration rate is determined mainly by soil temperature, soil-water content (in water and ice), the soil porosity, snowfall time, and snow cover above the soil. Infiltration occurs mainly through the macropores. If macropores are missing, it is driven by the soil water conditions. According to Bengtesson et al. (1992), water infiltration in frozen soils after snow melting mainly occurs in macropores and along cracks, especially for clayey soils. A severely cracked heavy-textured clay soil can absorb large amounts of water (Granger et al., 1984). For a unit area, the infiltration amount can be higher than the equivalent snow cover water due to interflow to and through cracks from the outside of the area. Snowmelt water primarily enters these cracks and cannot produce significant runoff flow at the edge of a field. If the field is heavily cracked during the fall, it is expected that most of the snowmelt water will be infiltrated through the cracks. Zheng et al. (2001) found that variation of infiltration rates mostly depended on soil water profile phase change, temperature difference and heat exchange and transfer between the atmosphere and the soil.

In northern cold regions, more than half of the land surface is seasonally frozen (minimum annual temperature below 0°C) and snow melting is a major hydrological event in such areas (Saito et al., 2007; Lundberg et al., 2015). Freezing and thawing cycles, one of the important seasonally frozen soil phenomena, change the physical properties of frozen soil by creating stress fractures, as well as affect the aggregate stability of soil and facilitate changes in soil hydraulic properties. Soil aggregate stability increases with freezing, but it degrades during the thawing processes (Dagesse, 2013). Granger et al. (1984) observed three types of infiltration into frozen soil: “unlimited” infiltration where soil is deeply cracked and contains many

macropores; “limited” infiltration where soil is uncracked, and “restricted” infiltration where an ice layer forms on the soil surface or within the shallow depth of soil profile. Around the world, frozen soil causes devastating floods and soil erosion after rainfall or quick snowmelt events, because frozen soil restricts the infiltration by reducing soil infiltration capacity and then excess infiltration water creates large runoff volumes even after a light rainfall or snowmelt event. Water infiltrating into frozen soil transports latent heat and sensible heat, initiates melting of ice to liquid water and therefore increases soil ground temperature to be above 0°C. When soil thaws, the freshly melted ice water at the thawing front moves downwards due to a soil matric potential difference between the unfrozen layer at the thawing front and the frozen layer below the thawing front (Mackay, 1983). In frozen soil, the downward movement of infiltrated water from a frozen soil surface during a thawing period is higher in unsaturated soil having a low ice content along with the presence of cracks. Compared with that soil, infiltration amount and rate are extremely low in saturated soil with high ice content in the soil profile lacking cracks (Mackay, 1983). Engelmark (1988) conducted laboratory infiltration experiments on a dry fine sandy soil under frozen and unfrozen conditions and found that the infiltration rate in frozen soil was ten times smaller than that in unfrozen soil. It was also observed that infiltration ability of frozen soil decreased rapidly over time compared to unfrozen soil, though initial infiltration rate was high in frozen soil. In the Red River of the North Basin, frozen dry soils absorbed as much as half of the snowmelt water through infiltration (MPRnews, 2013) and the lack of understanding of the snowmelt water infiltration process is the major limiting factor affecting spring flood forecasting. In the last few years, spring flooding occurred almost yearly, and created a huge financial burden for the RRB.

The objectives of this study were to: (i) measure the infiltration rates into a frozen silty clay loam soil from RRB with three initial soil water contents, (ii) evaluate initial soil water contents influence on the infiltration into that soil, and (iii) further evaluate the effect of temperature on volumetric soil water contents change along the soil profile during infiltration events.

3.3. Materials and methods

3.3.1. Soil and soil properties

The soil used in this experimental study was collected from a tile drained research field in the RRB, located 20 km northeast of Moorhead in Clay County, Minnesota. The soil was classified as silty clay loam with 1% sand, 62% silt and 37% clay contents determined by the hydrometer method (Bouyoucos, 1951). The field bulk density of the soil during the soil collection was 1.25 g/cm^3. A soil water release curve (SWRC) was constructed using the combined datasets from the HYPROP® evaporation method (UMS GmbH, Germany) and the WP4 Dewpoint potentiometer (Decagon Devices, Pullman, WA, USA) method (Maček et al., 2013; Roy et al., 2018), as shown in figure 6. For the construction of SWRC, the van Genuchten (1980) equation was used to describe the relationship between the volumetric water contents and the soil matric potentials. The van Genuchten equation can be expressed as:

$$\theta_v(\Psi) = \theta_r + (\theta_s - \theta_r)[1 + (\alpha|\Psi|)^n]^{-m} \quad (3.1)$$

where θ_v is the volumetric water content in cm^3/cm^3, Ψ is the matric potential in kPa, θ_r is the residual water content in cm^3/cm^3, θ_s is the saturated water content in cm^3/cm^3, α is the air entry point in 1/kPa, and *n* and *m* are soil water retention parameters. The values of α, *n* and *m* are directly dependent on the shape of the $\theta_v(\Psi)$ curve. In Eq. 3.1, m=1-1/n. The equation was fitted with the existing combined dataset of the HYPROP evaporation method and the WP4 Dewpoint

potentiometer method according to the procedures in Wraith and Or (1998) by using the Excel® Solver. The SWRC was used to determine the soil hydraulic property parameters listed in Table 5.

A second SWRC was developed after completing all infiltration experiments by the combined datasets from the HYPROP® evaporation and WP4 Dewpoint potentiometer methods following the same procedure described earlier in this section. Though the same soil was used for the second SWRC, the soil properties were probably changed because the soil went through multiple freeze and thaw cycles and packing.

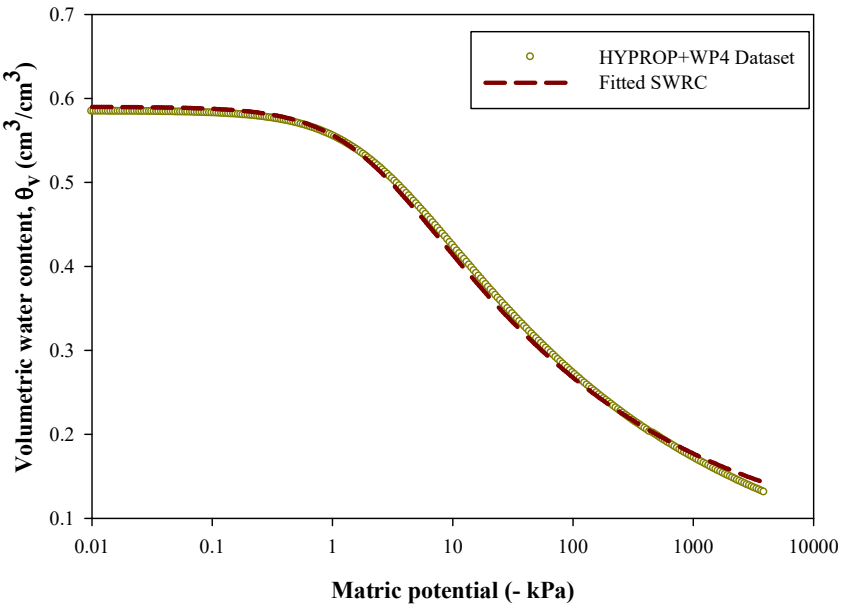

Figure 6. Soil water release curve (SWRC) of silty clay loam soil used in the study and developed by HYPROP and WP4 methods.

Table 5. Soil hydraulic property parameters from soil water release curve.

Soil property	Symbol	Value
Saturated water content (cm^3/cm^3)	θ_s	0.59
Residual water content (cm^3/cm^3)	θ_r	0.05
Air entry point (-1/kPa)	α	0.48
Soil water retention parameter	n	1.23
Soil water retention parameter	m	0.19
Field capacity at -33 kPa (cm^3/cm^3)	θ_{fc}	0.33
Permanent wilting point at -1500 kPa (cm^3/cm^3)	θ_{pwp}	0.17

3.3.2. Initial soil water contents

The infiltration experiments in this study were conducted under three initial soil water contents (by volume). The soil was prepared and packed for one initial soil water condition at a time. The three initial water contents were: (i) permanent wilting point (PWP), θ_{pwp}; (ii) field capacity (FC), θ_{fc}, and (iii) soil water between PWP and FC, $\theta_{pwp} \leq \theta_v \leq \theta_{fc}$, designated as θ_{mid} hereafter. As shown in Table 5, the third volumetric water content θ_{mid} was 0.25 cm^3/cm^3, and the first and second volumetric water contents were 0.17 cm^3/cm^3 (θ_{pwp}) and 0.33 cm^3/cm^3 (θ_{fc}), respectively.

3.3.3. Soil water and temperature sensors

Soil water and temperature were recorded using soil moisture and temperature sensors (Model 5TE, Decagon Devices, Inc. Pullman, WA). The sensor dimensions were 10 x 3.2 x 0.7 cm and the operational temperature range was from -40 to 60°C. The 5TE sensors measure dielectric permittivity of the surrounding medium as a number, instead of direct measurements of volumetric water content and temperature in °C. Therefore, the 5TE sensors were calibrated with the measured volumetric soil water contents to obtain a relationship between the dielectric permittivity values and the volumetric water contents of the testing soil. Standard calibration procedures were followed as described in detail at the manufacturer's website (http://www.decagon.com/en/-support/videos/soil-calibration-video/). Relationships were developed for each sensor and these relationships were then used to calculate the volumetric soil water content. The soil temperature was measured by the 5TE sensors without any further calibration.

Three 5TE sensors were placed at depths of 11, 17, and 23 cm in each soil box to measure the soil water and temperature over the entire duration of the experiments (Figure 7).

One thermocouple was placed at the 15-cm depth to measure the soil temperature at the middle depth of the soil profile as well as at the center of the box. All soil water and temperature sensors were connected to a datalogger (Model CR1000, Campbell Scientific, Inc., Logan, Utah, USA), with a 5-minute data recording interval.

3.3.4. Sensor calibration

The 5TE user manual states that the Topp et al. (1980) equation is used to obtain the corresponding θ_v from the dielectric permittivity. However, Vaz et al. (2013) reported a lower accuracy for the sensors when using the factory supplied calibration relationship compared with a soil-specific calibration. A soil-specific calibration was conducted for the sensors used in this study as described by the manufacturer with the θ_v ranges from 0.03 cm^3/cm^3 to 0.50 cm^3/cm^3. A quadratic relationship was found best-fit for the calibration relationship suggested by the manufacturer, though the sensor dielectric permittivity output and the θ_v often followed a linear relationship (Rosenbaum et al., 2010).

The 5TE specifications state an accuracy of +/- 1°C and further temperature calibrations were not conducted in this study. Kizito et al. (2008), Assouline et al. (2010), and Saito et al. (2009) found that temperatures measured by the 5TE were generally accurate. Therefore, no calibration was needed, so the direct measurements of temperature by the sensors were used in this study.

To ensure that the soil water sensors were measuring volumetric water contents correctly during the experiments, another set of calibrations with the measured volumetric soil water contents were done for the soil water sensors after completing six experimental runs. The double calibrations were to ensure that the soil water sensors measured volumetric water contents accurately throughout the nine experimental runs.

3.3.5. Soil packing and freezing

Two wooden soil boxes (50 x 50 x 30 cm, 2 cm wall thickness) were constructed for soil packing. A small hole created at the center of the box bottom was connected to a drainage tube. The boxes were set up and attached with screws onto two pieces of lumber (nominal 2 x 4 lumber, dimensions 38 mm x 89 mm) to provide a 3.8-cm clearance between the bottom of the box and the floor. Two metal handles were attached opposite each other on the outside of the boxes for ease of moving the boxes. Each empty box weighed approximately 11 kg. A polythene sheet was used to line inside the box, so that the wood would not soak water and change its properties, especially during the freezing and thawing processes.

Soils collected from the field were air-dried, threshed, and passed through a 5-mm sieve before the experiments. Soils were packed consistently to maintain the soil bulk density close to the soil field bulk density. The soil water contents of the air-dried soil were measured using the 5TE soil moisture sensor in order to calculate the required amount of water to be added for the targeted soil water range. The soils were packed layer by layer for every 5 cm, and the calculated amount of water was added to the soil layer, and mixed thoroughly to get a uniform soil water distribution throughout the soil profile. The wooden box was placed on a flat metal cart before packing so that after packing, the heavy box with soil could be easily moved from one place to another. After packing the soil with water, each box was allowed to sit for a few hours for soil settling and soil water stabilizing. During the setting time, the soil box was completely covered with a plastic sheet with few holes to minimize water loss.

A 0.78 m^3 (15 ft^3) chest freezer (120.3 x 76.8 x 84.8 cm, MAYTAG) was used to freeze the soils in the wooden box. The total weight of the loaded box was approximately 100-105 kg. Considering the heavy weight, an overhead crane was used to transfer the box into the freezer.

Soils required two to three days to freeze depending on the initial soil water conditions. The temperature at the center of the soil profile was monitored from the thermocouple readings. When the temperature in the center of the box dropped below 0°C, the soil was considered completely frozen because the freezing process started from the outer to the inner part of the soil box.

3.3.6. Experiments

The experimental setup for infiltration into frozen soil is shown in Figure 7. After the soil was frozen, the box was removed from the freezer and placed again on the metal flat cart using the overhead crane. The frozen soil box was then moved to a convenient place close to a floor drain.

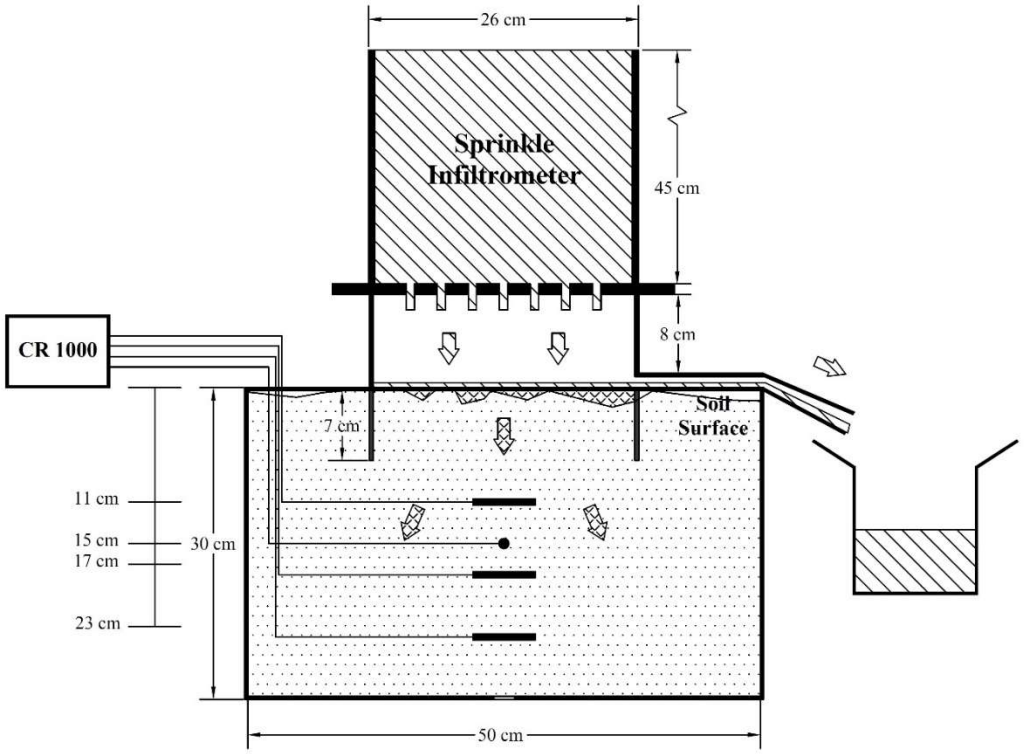

Figure 7. Schematic of the experimental setup.

The infiltration experiments were conducted using a Cornell sprinkler infiltrometer due to its easy handling apparatus for rapid measurements of water infiltration into frozen soil. The total unit consisting of a portable rainfall simulator placed on an infiltration ring (Ogden et al., 1997). The diameter of the single metal ring is 24.1 cm and the height is 18 cm (Cornell Sprinkler Infiltrometer, 2015). The ring was inserted into the soil up to a 7-cm depth so that the lower edge of the round overflow hole (3-cm diameter) was aligned with the soil surface. When experiments were running, an overflow tube was attached to the overflow hole, and was used to collect overflow or runoff water into a plastic container. The ring was inserted into the soil before freezing because inserting the ring in frozen soil was very difficult and could cause soil disturbance.

All sensors (5TE and thermocouple) were placed at different depths along the vertical center line of the box below the inserted ring. A datalogger was connected to the 5TE sensors and the thermocouple after the soil packing and before placing the soil box into the freezer. The soil water and temperature were continuously measured until the end of the infiltration experiments. For each initial soil water condition, three replicated experiments were conducted. In total, nine successful experiments were completed for this study.

A time lapse camera (TimelapseCam®, WINGSCAPES®) was used to take pictures at 15-minute intervals during each experiment. The camera was used during each experiment to assist monitoring progress for long duration experiments.

3.3.7. Measurements

The Cornell sprinkler infiltrometer is a single ring infiltrometer in conjunction of a rainfall simulator (Ogden et al., 1997). It is suitable for conducting infiltration experiments on frozen soils in laboratory settings and can provide a comparable result with measurements in

field environment (Lee and Molnau, 1982). Therefore, in this study, the Cornell sprinkler infiltrometer was used in both laboratory and field experiments.

Before each experiment, the infiltrometer vessel was filled with clear water (tap water) for the infiltration experiment. Based on the measurement, the water temperature ranged between 16-20°C during the experiment, and the electrical conductivity of the tap water was about 985 µs/cm. It was expected that during the infiltration into frozen soil process, because the temperature near the soil surface and water interface was lower, the infiltrating water temperature would also be lower. The vessel was then placed on the ring and initial water level in the vessel was measured after the water surface became stable, which was about 8-10 minutes. After starting the experiment, the water level, overflow, and surface runoff were measured at 3-minute intervals for the first 60 min, then every 30 min for about 540 min (4 hours), and then every 90 min for the rest of the experiment duration. The simulated rainfall rate, runoff rate and the infiltration rate were estimated using the following equations (Cornell Sprinkler Infiltrometer, 2015):

$$R = \frac{[H_1 - H_2]}{T_f} \tag{3.2}$$

$$RO_t = \frac{V_t}{(A*t)} \tag{3.3}$$

$$i_t = R - RO_t \tag{3.4}$$

where, H_1 is the initial water level (cm), H_2 is the final water level (cm) in the infiltrometer, T_f is the time (min) taken for the water level to change from H_1 to H_2, A is the surface area of the ring for infiltration (A = 457.30 cm^2) , V_t is the surface runoff volume in cm^3, t (min) is the time interval, during which surface runoff water was collected, R is the simulated rainfall rate in cm/min, RO_t is the surface runoff rate in cm/min, and i_t is the infiltration rate in cm/min.

During each infiltration experiment, real time soil water and temperature values were recorded with the datalogger. Each experiment was continued until the wetting front reached at the bottom of the soil profile (23 cm) and when soil water content began to change. The total experimental duration varied from 4 to 10 hours. Figure 8 represents the total duration of each run for the three initial water contents. It was observed that, in almost all experiments, the infiltration rates changed considerably over the first 60 minutes and then became stable during the remainder of each experiment. The endpoint at 60 minutes in each experiment is shown in figure 8. Based on this observation, infiltration measurements for a 60-min duration in each experiment were further analyzed and discussed. In some experiments, infiltration rates fluctuated occasionally after the 60-min duration, but compared to the stable or final infiltration rate, those variations were not large enough to be considered. Therefore, 60-min infiltration measurements were used for detailed evaluations.

3.3.8. Goodness of fit

The coefficient of determination (R^2) explains how well the predicted values fitted with the measured values overall. The R^2 value usually ranges between zero and 1. The goodness of fit between the measured and the predicted datasets can be determined by the following equation:

$$R^2 = \left[\frac{\sum_{i=1}^{N} (Observed\ value - Obser \quad mean)(Measured\ value - Measured\ mean)}{\sqrt{\sum_{i=1}^{N} (Observed\ value - Observed\ mean)^2} \sqrt{\sum_{i=1}^{N} (Measued\ value - Measure \quad mean)^2}} \right]^2 \qquad (3.5)$$

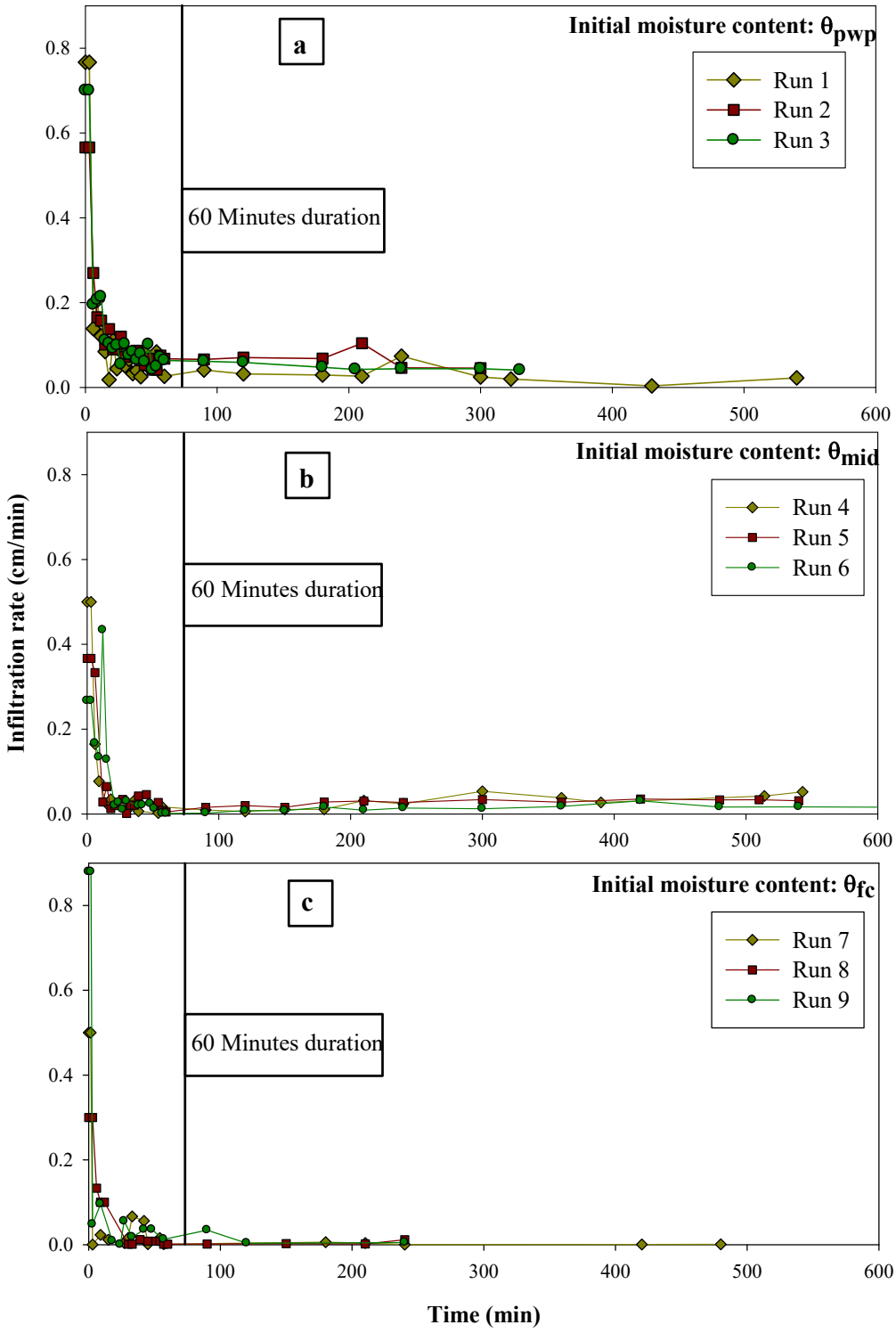

Figure 8. Infiltration rates over total duration of experimental runs, plotted for (a) Run 1, 2, and 3 of initial water content permanent wilting point (θ_{pwp}); (b) Run 4, 5, and 6 of initial water content between θ_{pwp} and water content at field capacity (θ_{fc}), θ_{mid}; and (c) Run 7, 8, and 9 of initial water content θ_{fc}.

3.3.9. Horton infiltration model: fitting with observed data

Horton (1940) infiltration equation, named according to its developer Robert E. Horton, is an empirical equation for measuring infiltration rate or volume. Horton considered that infiltration starts with a constant rate (i_0) and decreases exponentially with time (t). After soil saturation reaches a certain value, the infiltration rate become constant (i_f). The Horton infiltration model (Huffman et al., 2013) is:

$$i_t = i_f + (i_0 - i_f)e^{-kt} \tag{3.6}$$

where i_t is the infiltration capacity at time t in cm/min, i_0 is initial infiltration capacity in cm/min, i_f is final infiltration capacity in cm/min, t is the time in min, and k is empirical constant in 1/min.

The Horton model was fitted with the observed data from all experiments under the three initial water contents and it was accomplished by using SigmaPlot 11.0 (Systat software, Inc.). A similar type equation (exponential decay equation with three parameters) to Horton model was selected from the program. The R^2 values of best fitted infiltration rate vs. time curve were reported in this study. The fitting equation can be expressed as:

$$i_t = i_f + a * e^{-b*t} \tag{3.7}$$

where a is difference between initial and final infiltration rates (i_o-i_f) and b is equal to k in Eq. 3.6.

3.4. Results and discussion

3.4.1. Sensor data quality checking

The soil water content sensors were calibrated manually and the relationship between the volumetric soil water contents and dielectric permittivity numbers for one of the six sensors is shown in figure 9. The R^2 value of the dataset was 0.98, which indicated a good agreement

between the actual θ_v and the dielectric permittivity numbers obtained from the sensor. After six infiltration experiments, the actual volumetric water contents, measured by the manufacturer recommended method used in the standard sensor calibration procedure, and the calculated volumetric water contents for one of the six sensors are compared and shown in figure 10. The calculated volumetric water contents were obtained from the calibration relationship between volumetric water contents and di-electric permittivity numbers of the sensor. In figure 10, the comparisons are shown for two phases: (1) before all experiments (phase 1) and (2) after six experiments (phase 2). The R^2 values were 0.97 and 0.98 for phases 1 and 2, respectively. The good R^2 values for both phases indicated that the calculated volumetric soil water contents were close to the actual or measured volumetric water contents. So, it can be assumed that the soil water sensors measured volumetric water contents accurately throughout the nine experimental periods.

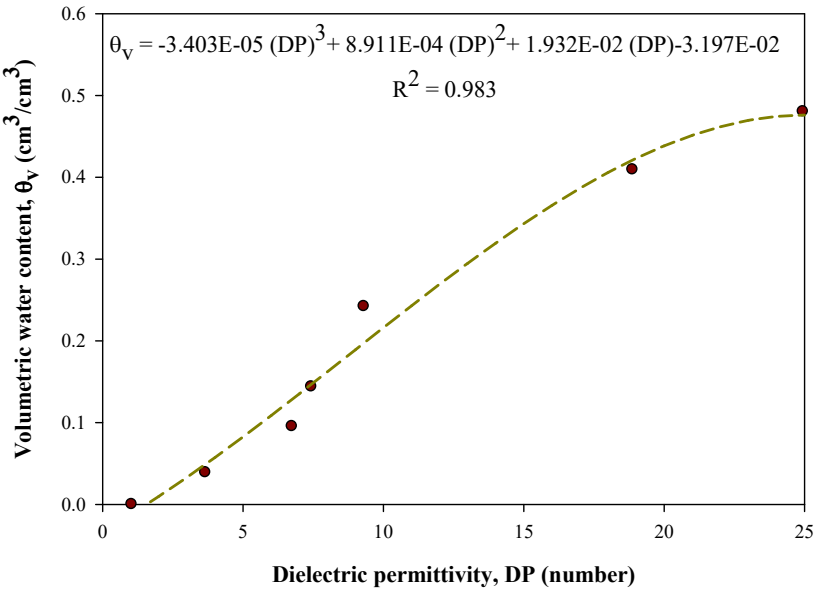

Figure 9. Volumetric water content (θ_v) vs. dielectric permittivity (DP) relationship during 5TE sensor calibration (Sensor 1).

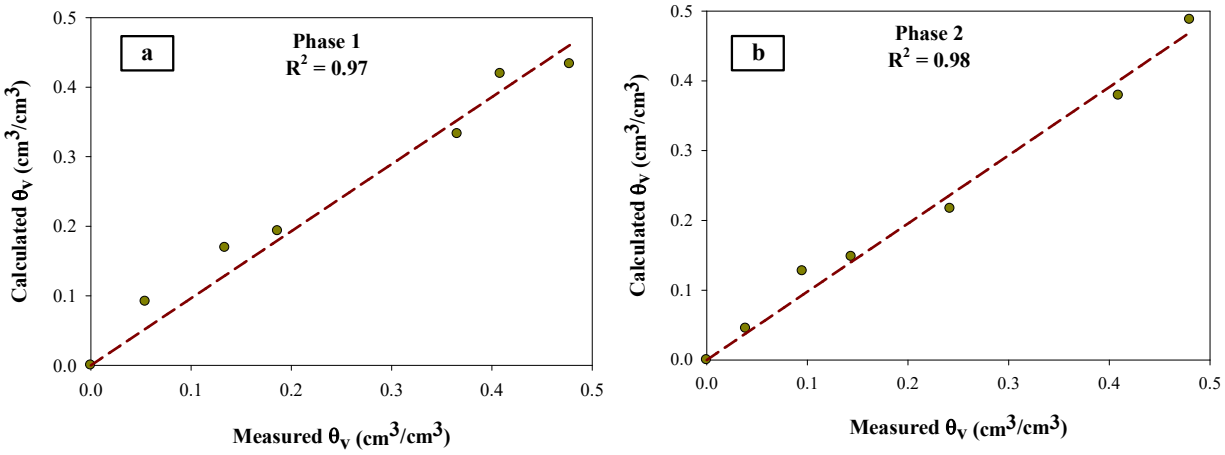

Figure 10. Comparison between measured and calculated volumetric water content for Sensor 4 for (a) before all experiments, phase 1 and (b) after six experiments, phase 2.

3.4.2. Infiltration rate over time

The simulated rainfall rate in the Cornell sprinkler infiltrometer varied from 0.56 to 0.76 cm/min in the experiments for initial water content at θ_{pwp}, from 0.26 to 0.50 cm/min in the experiments for initial water content at θ_{mid}, and from 0.30 to 0.88 cm/min in the experiments for initial water content at θ_{fc}. The comparisons of the infiltration rates for the three initial water content conditions are shown in figure 11. The soil for initial water content θ_{pwp} was comparatively dry compared with the soil with other initial water contents. The water infiltrated rapidly at the beginning until the infiltration rate reached a stable rate. It is probably due to large soil pore spaces; the total amount of infiltrating water was higher in this soil than that for the other soils with higher initial water contents. It could be possible that the soil with an initial water content of θ_{mid} had a higher ice content than that of θ_{pwp}. The melted ice during the infiltration experiment contributed more water to the soil than the soil with an initial water content of θ_{pwp}. Water infiltration decreased slowly after soil surface saturation and it took longer time to reach a steady infiltration rate or infiltration capacity.

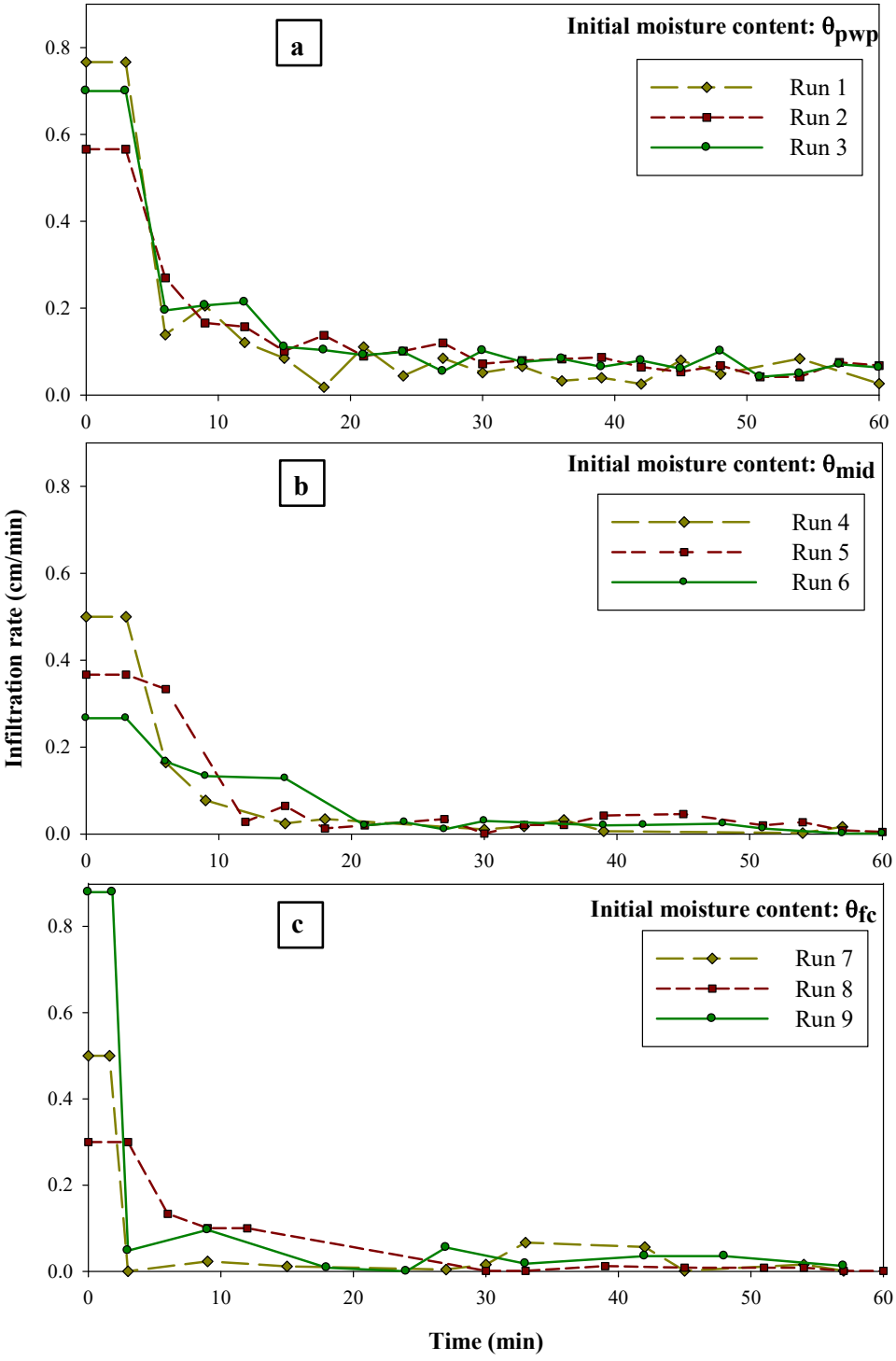

Figure 11. Infiltration rate vs. time over 60-minute duration of experiments for: (a) Run 1, 2, and 3 with initial water content of permanent wilting point (θ_{pwp}); (b) Run 4, 5, and 6 with initial water content between θ_{pwp} and field capacity (θ_{fc}); and (c) Run 7, 8, and 9 with initial water content θ_{fc}.

The initial water infiltration in the soil with an initial water content of θ_{fc} was very slow after the surface saturation, compared with the other infiltration experiments. The soil for the initial water condition at θ_{fc} had the highest soil water content among all soils having different initial water contents. During freezing, due to high soil water content in the soil profile, ice formation and expansion might have blocked the soil pore space and restricted the water movement. During the experiments, it was observed that, after reaching the steady infiltration rate, the infiltration rate went higher sometimes and then became stable again (Fig. 6). As ice was melting due to infiltrated water during the experiments, the pore spaces were blocked by ice lens became open and easy for water to flow through, which might have increased the infiltration rate as well as the infiltrating water amount. As the opened pore spaces were filled with water, the infiltration returned to a steady rate again. Since the soil water content was at a level of field capacity, the soil had very limited pore spaces to reach saturation and the water infiltration was slower in the soil with an initial water content of θ_{fc}.

3.4.3. Observed data fitting with Horton infiltration model

Using equation (3.7), the observed infiltration rates with time were fitted with Horton model for soils under each initial water content condition and for all three replications. The results are shown in Eq. 3.8, Eq. 3.9, and Eq. 3.10:

(i) initial water content, θ_{pwp}: $i_t = 0.060 + 0.68 * e^{-0.16*t}$, $R^2 = 0.87$ (3.8)

(ii) initial water content, $\theta_{mid:}$ $i_t = 0.010 + 0.42 * e^{-0.12*t}$, $R^2 = 0.84$ (3.9)

(iii) initial water content, θ_{fc}: $i_t = 0.027 + 0.53 * e^{-0.54*t}$, $R^2 = 0.75$ (3.10)

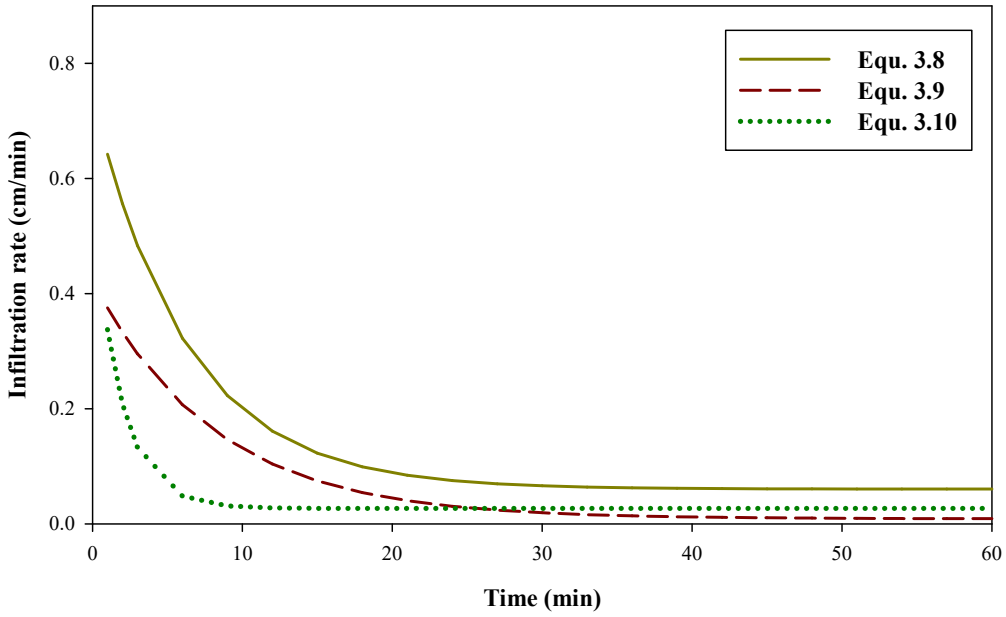

Figure 12. Infiltration rate vs. time by Horton infiltration model, plotted for different initial water contents at permanent wilting point, between permanent wilting point and field capacity, and field capacity in Eq. 3.8, Eq. 3.9, and Eq. 3.10, respectively.

Figure 12 represents the fitted equations for soils under the three initial water content conditions. The high R^2 values showed that the model fitted values were in good agreement with the observed data. Figure 12 indicated that the magnitude of the fitted infiltration curves over time moved downward according to soil initial water contents, from θ_{pwp} to θ_{fc} before the final infiltration rate were achieved. The initial infiltration rate was higher for dry soil but then decreased when soils became wetter. The average final infiltration rate for each initial water content condition was calculated from the average value of the observed data for the last 30 minutes of the 60-min experiment duration. It was found that the final infiltration rates were 0.062 cm/min, 0.017 cm/min, and 0.019 cm/min for the soils with the initial water contents of θ_{pwp}, θ_{mid}, and θ_{fc}, respectively. The measured average final infiltration rate was very close to the model predicated value (0.062 cm/min vs. 0.060 cm/min) for the initial water content of θ_{pwp}. However, for the soil with the initial water content of θ_{mid}, the measured value (0.017 cm/min)

was higher than that of model predication (0.010 cm/min). For the soil with the initial water content of θ_{fc}, the measured final infiltration rate (0.019 cm/min) was lower than the model predicated value (0.027 cm/min). The difference between the initial and final infiltration rates in the soils with θ_{pwp} was the highest (0.68 cm/min) compared to the two other soils with θ_{mid} and θ_{fc}. However, the difference was found lower in the soil with θ_{mid} (0.42 cm/min) than that in the soil with θ_{fc} (0.53 cm/min). Lee (1983) reported that frozen dry soil enhanced infiltration capacity, so the final infiltration rate was higher in dry soil compared to the final infiltration rate in a wet soil when frozen. It was also found that the infiltration rate decreased with the higher initial water contents in frozen soil. In this study, similar results were found while both the actual and predicted final infiltration rates in the dry soil with the initial soil water content of θ_{pwp} were found higher than those in the soil with the initial water content of θ_{mid}. The unusual higher final infiltration rate, and the difference between the initial and final infiltration rates for the wetter soil with θ_{fc} compared to the soil with θ_{mid} were probably due to the unique swelling and shrinkage soil properties in this region. When preparing the soils for the infiltration experiments, the soils were packed according to the designated bulk density, but swelling problem occurred in wet soil with θ_{fc}. As reported by Ito and Azam (2010), a silty clay soil could have a maximal change in soil volume by 24% at the plastic limit. The higher final infiltration rate for the soil with the initial water content of θ_{fc} may be caused by the soil property changes due to compression, freeze and thaw, or measurement errors. Further research is needed to explore the swelling and shrinkage relationships during infiltration of water into frozen soil.

3.4.4. Soil water changes with temperature

Figure 13 shows the θ_v and temperature measurements over the total period for one experiment with the initial water content of θ_{mid}. After soil packing and stabilization, the box was

placed in the freezer and at the same time, datalogging started at 14:00 on 10/30/2015. The box was kept in the freezer until 12:00 on 11/02/2015. The infiltration experiment was started at 13:10 and continued for 10 hours 30 minutes. After the experiment was completed, the box was left in the open space at room temperature and the datalogging continued until 11:00 on 11/04/2015.

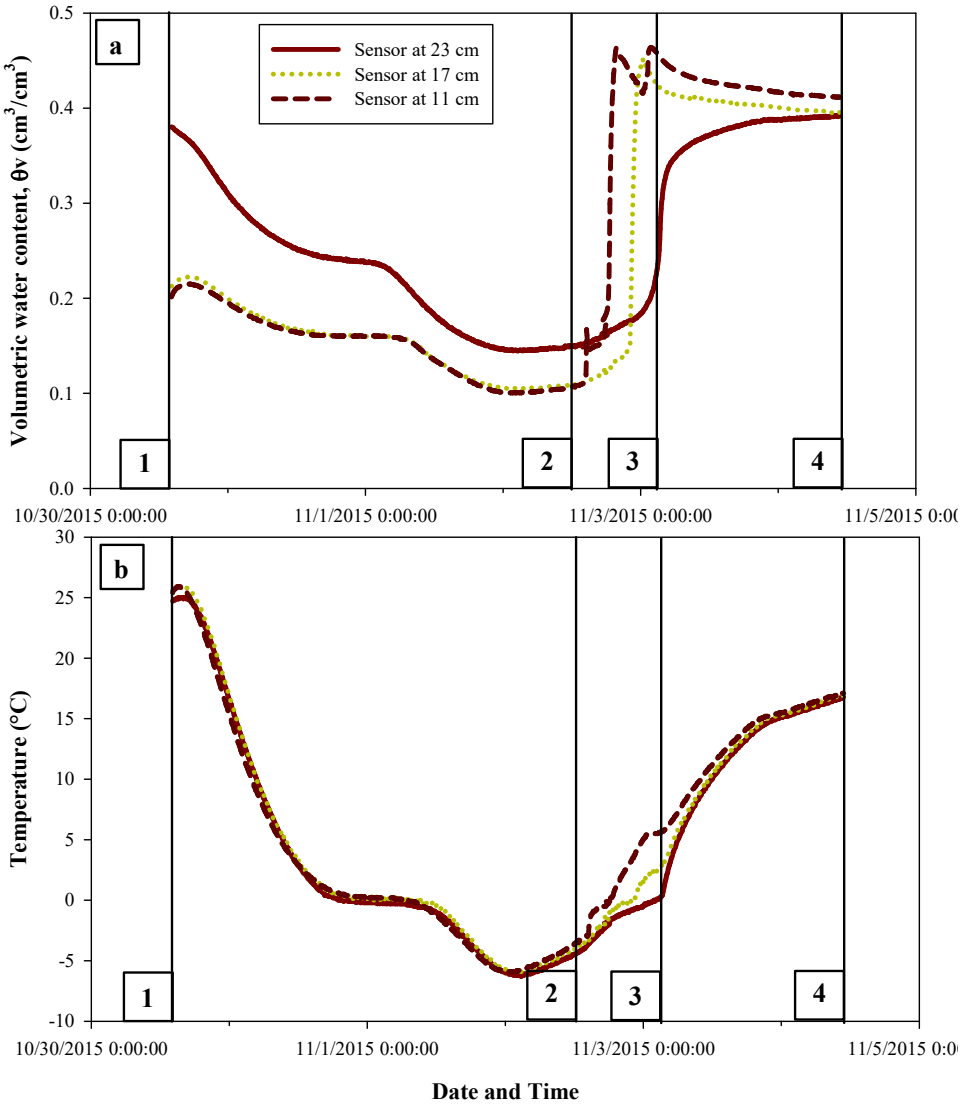

Figure 13. (a) Volumetric soil water content (θ_v) vs. time and (b) soil temperature vs. time, plotted for experimental Run 6 with initial water content condition between permanent wilting point (θ_{pwp}) and field capacity (θ_{fc}). The vertical straight lines indicate: (1) starting time of soil freezing and datalogging, (2) starting time of experimental run, (3) ending time of experimental run, and (4) ending time of datalogging.

Figure 13 gives a detailed picture about the changes of the θ_v and temperature over the entire experimental duration of five days or 119 hours. The figure showed that, though the soil was packed with initial water content of θ_{mid}, which was about 0.25 cm^3/cm^3, the θ_v dropped to 0.2 cm^3/cm^3 at the depths of 11 cm and 17 cm, but rose to 0.38 cm^3/cm^3 at the depth of 23 cm. The box was left for few hours for stabilization after soil packing. Within that time, the water moved vertically from the top to the bottom of the box. This movement of water resulted in soil water content variation along the soil profile. After the freezing process started, the θ_v started to decrease as the liquid water was converted to ice while the di-electric permittivity counts of the sensors were also decreasing. When the infiltration experiment started, the θ_v started increasing along the depth from the soil surface. The θ_v at 11 cm first, and then θ_v at 17 cm started to rise over time. The θ_v at 23 cm stayed constant during the infiltration experiment, but started to increase near the end of the experiment. Infiltration into the frozen soil first filled up the macropores in dry soil with water, causing a high initial infiltration rate. After saturating the macropores, the water moved to micropores where soil temperature is the major governing factor for water movement through small pores (Granger et al., 1983; Bengtesson et al., 1992). When water started infiltrating through the soil profile, the movement of water was governed by the existing soil water content and available soil pore space (Ireson et al., 1999). The time required for water to move vertically through the soil was also subject to water content distribution and pore spaces along the soil profile. Because of the differences in water travel time, the θ_v readings at different depths of the soil profile varied with time. As shown in figure 13, the θ_v at 23 cm continued to increase even after the experiment, while the θ_v at two other depths (11 cm and 17 cm) started decreasing. After the experiment was completed, the soil at the depth of 11 cm started drying immediately due to evaporation, but water was still moving downward, which

increased the θ_v at the depth of 23 cm. From the soil surface to the deep layer, heat was transported from 0 to 30 cm by convection or advection, which changed the phase from ice to melted water. The freshly melted water moved the thawing front downward by the soil matric potential difference between the thawing front and the frozen soil layer (Mackay, 1983). The θ_v changing at all depths was caused by the combined effects of infiltrating water addition and melting ice content contribution along the soil profile. The temperature changing at all depths followed the same decreasing pattern as that for θ_v until the experiment started. After starting the experiment, the temperature at 11 cm rapidly started rising followed by the temperature at 17 cm as the infiltrating water transported heat with it. The temperature at 23 cm started increasing slowly, compared to the temperatures at two other depths. It was observed from figure 13 that after the temperature rose to 0°C, the temperatures at 17 cm and 23 cm made a sharp increase. After the infiltration experiment, the temperatures at all depths also followed the same rising pattern to reach the room temperature. The temperature at 11 cm was higher than those at two other depths as this point received more heat transported by water than two other depths. It also caused more ice melting, which resulted in a sharp rise in the θ_v at the same depth (Figure 13).

Figure 14 showed the θ_v changes with temperature for all initial water contents at the depths of 11 cm, 17 cm, and 23 cm. For the initial water content of θ_{pwp}, the soil was comparatively dry, so the θ_v changed gradually with the temperature increase at all depths. At 23 cm, θ_v started increasing with higher temperature compared to the other depths as infiltrating water reached this depth later than two other depths. As the soil was dry, there was less melting ice content contribution during the phase changing of water at 0°C. During the experiments for the initial water content of θ_{mid}, it was observed that the θ_v increased sharply at 0°C because at

this temperature, water changed its phase from ice to water and the melted water was added into the soil along with infiltrating water.

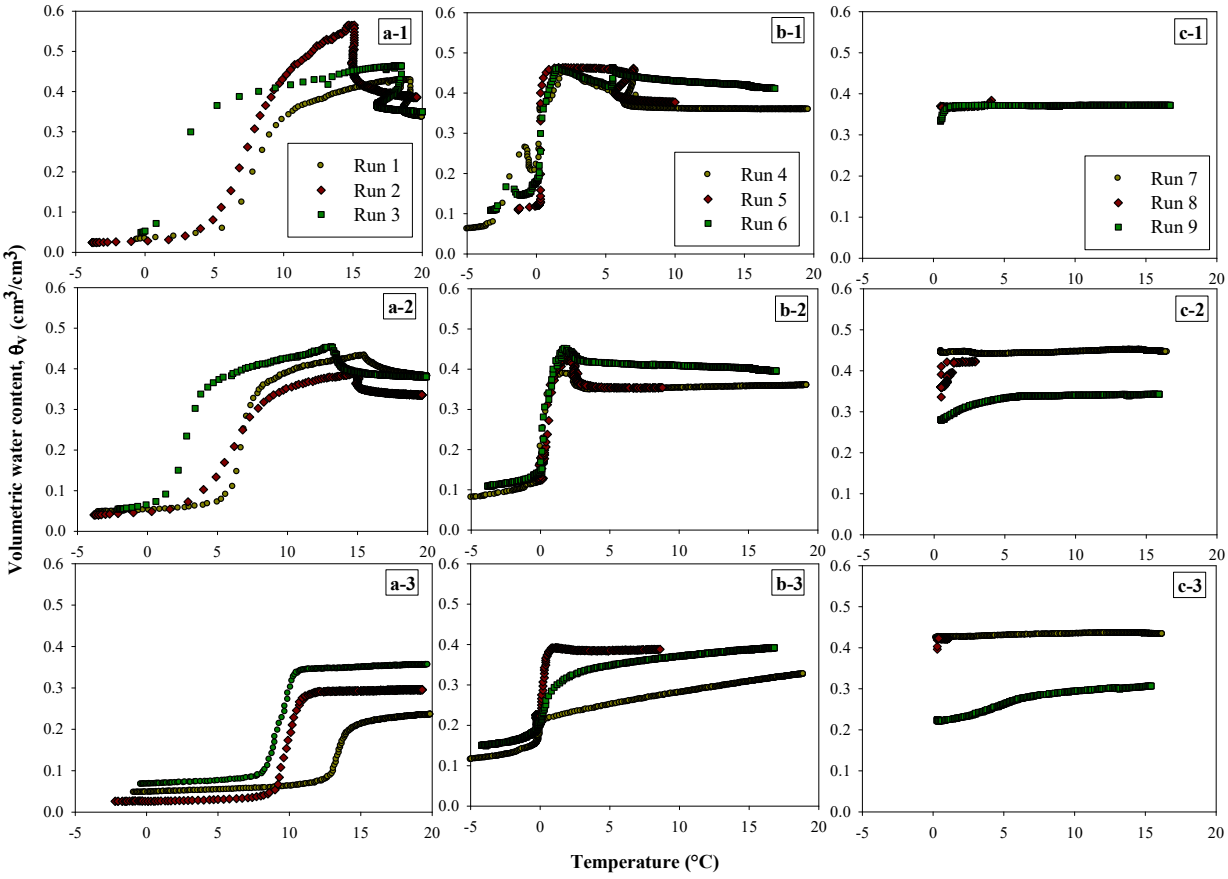

Figure 14. Volumetric soil water content (θ_v) vs. temperature, plotted for (a) Run 1, 2, and 3 with initial water content of permanent wilting point (θ_{pwp}); (b) Run 4, 5, and 6 with initial water content between θ_{pwp} and field capacity (θ_{fc}); and (c) Run 7, 8, and 9 with initial water content θ_{fc} at depths of 11 cm, 17 cm, and 23 cm.

In the experiments for the initial water content of θ_{fc}, the change of θ_v with temperature was not considered compared to two other initial water contents (i.e., θ_{pwp} and θ_{mid}). Since the soil water had already reached the field capacity, there was less pore space for additional water, which caused little change in the θ_v with temperature. The soil reached saturation quickly as melting ice contributed water along with the infiltrating water. Also, it was observed that soil with the initial water content of θ_{fc} needed more time to freeze compared to the other

experiments with drier soils. Higher water content in the soil pore space could increase soil heat capacity (AL-Kayssi et al., 1990), which might delay the freezing process and sometimes, soil temperature did not go below 0°C.

3.4.5. SWRC comparison: before and after experiments

The two SWRCs, developed before and after the frozen soil infiltration experiments (named as pre-experiment SWRC and post-experiment SWRC, respectively), were compared to each other, as shown in figure 15. From the post-experiment SWRC, it was observed that the saturated water content (θ_s) was 0.55 cm^3/cm^3, residual water content (θ_r) was 0 cm^3/cm^3, air entry point (α) was -1.02 /kPa, soil water retention parameters *n* and *m* were 1.15 and 0.14, respectively, field capacity at -33 kPa was 0.32 cm^3/cm^3, and permanent wilting point at -1500 kPa was 0.18 cm^3/cm^3. Comparing to the soil hydraulic properties of the pre-experiment SWRC (Table 5), it was found that both the θ_s and θ_r decreased slightly. The air entry point, reciprocal to air entry Ψ (Tuller and Or, 2004), also increased in the post-experiment SWRC. This indicated that, probably due to repeated freeze and thaw as well as the wet and dry cycles, the post-experiment soil lost the original pore distribution so that small suctions could able to bring air into the soil matrix (Degesse, 2013; Ireson et al., 2013). Also, the smaller value of *n*, the pore size distribution parameter (Tuller and Or, 2004), in the post-experiment SWRC than that in the pre-experiment SWRC implied that the soil aggregates and pore distribution changed in the post-experiment soils. The θ_v differences between the pre-experiment SWRC and the post-experiment SWRC from 0 to -100 kPa (Figure 15) revealed that the macropores in the post-experiment soil were reduced considerably. The macropore reduction might affect the experiment results, because the distribution of air-filled pores, i.e., mostly micropores, within the depth of 0-30 cm

of the soil determined the soil infiltration capacity (Granger et al., 1984; He et al., 2015). Also, the soil drying process in the frozen soil was governed by pore size distribution.

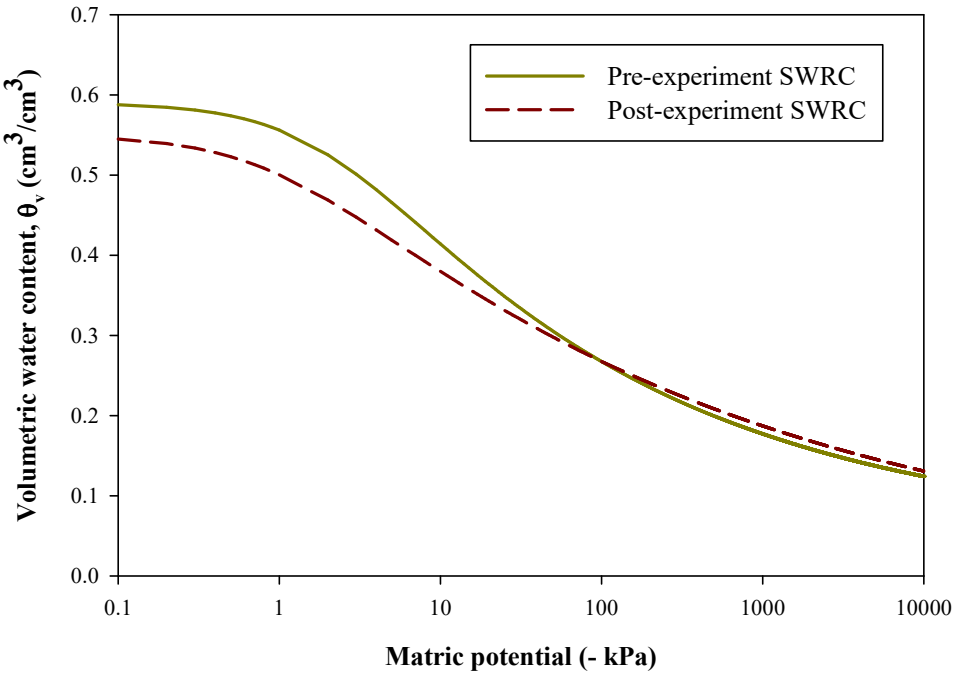

Figure 15. Comparison between pre-experiment and post-experiment soil water release curves (SWRC).

It could be assumed that during freezing, water froze from macropores to micropores, which created strong negative matric potentials, and hence liquid water moved to the freezing front and made the soil drier (Dagesse, 2013; Flerchinger et al., 2005; Ireson et al., 2013). During the experiments, the soil was subject to extensive packing and dry-wet and freeze-thaw cycles, which broke the soil aggregates, destroyed soil structures, and reduced the amount of pore space. Degesse (2013) reported that the freeze-thaw cycles altered the aggregate stability by creating continuous stress on soil structure, which resulted in the change in soil hydraulic properties and soil erosion. It was also found that at a low soil water content, the freeze-thaw cycle could increase the aggregate stability, but at a high-water content, the freeze-thaw process degraded the

soil stability. Soil pore size distribution, i.e., distribution of macropores and micropores, controlled the soil water freezing point in both the large and small pores (Ireson et al., 2013). The freeze-thaw cycles could destroy the soil structure and changed the soil hydraulic properties. The reduction in soil macropores caused a decrease in the soil water contents from saturation (0 kPa) to field capacity (-33 kPa). During the infiltration experiments for the initial water content of θ_{fc}, due to the limited available macropores, the soil was saturated quickly so that the θ_v did not change much with an increase in temperature (Figure 14) compared to other infiltration experiments. In figure 11, probably due to the same reason, the water infiltration reached a steady rate much earlier than that in other experiments for the initial water contents of θ_{pwp} and θ_{mid}, due to the limited pore space for water infiltration at initial water content of θ_{fc}.

3.5. Conclusion

The infiltration rates in a frozen silty clay loam soil of RRB for the initial water contents of θ_{pwp}, θ_{mid}, and θ_{fc} were measured in this study. The soil with θ_{pwp} had less ice content and was comparatively drier than other soils, which resulted in a higher initial infiltration rate and less contribution from ice melting to soil water content. The initial infiltration rate was comparatively lower in the soil with the initial water content of θ_{mid}, due to the combined effect of ice melting and water infiltration. The soil with the initial water content of θ_{fc} reached saturation quickly after starting water infiltration.

The observed infiltration data were fitted with a nonlinear regression model. The fitted equations were: $i_t = 0.060 + 0.68 * e^{-0.16*t}$ with $R^2 = 0.87$ for θ_{pwp}; $i_t = 0.010 + 0.42 * e^{-0.12*t}$ with $R^2 = 0.84$ for θ_{mid}; and $i_t = 0.027 + 0.53 * e^{-0.54*t}$ with $R^2 = 0.75$ for θ_{fc}. The infiltration curves over time shifted downwards from dry soil to wet soil before the infiltration rate became steady. The average final infiltration rate was close to the predicted rate for the dry

soil with θ_{pwp}, higher than the predicted rate for the soil with θ_{mid}, and lower than the predicted rate for soil with θ_{fc}.

Soil water changed in different ways with temperature according to the initial water contents. In the soil with θ_{pwp}, the θ_v changed with temperature gradually due to less water addition from melted ice. But in the soil with θ_{mid}, the θ_v changed rapidly after temperature reached 0°C as the ice was melted to liquid water and added to the existing soil water content. The θ_v in the soil with θ_{fc} did not change with temperature due to the limited pore space for additional water.

Multiple soil packing and freeze-thaw cycles tended to destroy the soil aggregates, resulting in fewer macropores, which in turn reduced the soil water holding capacity used for the experiments. The changed soil hydraulic properties may result in reduced infiltration rate and expedite the soil saturation process in the soil with the initial water content of θ_{fc}.

3.6. Acknowledgement

The research study was supported by NASA ROSES Project NNX15AC47G, USDA National Institute of Food and Agriculture project 2015-68007-23193, Sustainable Agriculture Research and Education project LNC11-332, ND Soybean Council, ND Water Resources Research Institute, ND Agricultural Experimental Station, and USDA Hatch project ND01475. The authors would like to express heartfelt gratitude to Dr. Dongqing Lin, Mr. James Moors, Mr. Mojtoba Ahmadi, Mr. Connor Yaggie and Ms. Qiang Li for their kind support and help throughout the study.

3.7. References

Al-Kayssi, A, W., Al-Karaghouli, A.A., Hasson, A.M. and Beker, S.A. (1990). Influence of soil moisture content on soil temperature and heat storage under greenhouse conditions. *J. Agric. Engng Res.* 45:241.252.

Assouline, S., Narkis, K., Tyler, S.W., Lunati, I., Parlange, M.B., and Selker, J.S. (2010). On the diurnal soil water content dynamics during evaporation using dielectric methods. *Vadose Zone J.* 9(3):709–718. doi:10.2136/vzj2009.0109.

Bengtsson, L., Seuna, P., Lepisto, A., and Saxena, R. K. (1992). Particle movement of melt water in a subdrained agricultural basin. *Journal of Hydrology*. 135: 383-398.

Bouyoucos, G. J. (1951). A recalibration of the hydrometer method for making mechanical analysis of soils. *Agron. J.* 43:434-438.

Cornell Sprinkler Infiltrometer. (2015). User's Manual: Field Procedures and Data Analysis for the Cornell Sprinkle Infiltrometer. Department of Crop and Soil Sciences Research Series R03-01, College of Agriculture and Life science, Cornell University, NY.

Dagesse, D.F. (2013). Freezing cycle effects on water stability of soil aggregates. *Can. J. Soil Sci.* 93:473-483.

Decagon Devices, Inc. (2015). 5TE water content, EC and temperature sensors, operator's manual, Decagon, Pullman, WA.

Decagon Devices, Inc. (2016). Custom Soil Calibration for Volumetric Water Content Sensors. Available at: https://www.decagon.com/en/support/videos/soil-calibration-video/. Accessed 15 December 2016.

Engelmark, E. (1988). Rates of infiltration into frozen and unfrozen fine sand. *Can. J. Earth Sci.* 25:343-347.

Flerchinger G.N., Lehrsch, G.S., and McCoo, D.K. (2005). Freezing and thawing processes. In D. Hillel (ed.) *Encyclopedia of Soils in the Environment* (pp. 104-110). Oxford, UK: Elsevier Ltd.

Fouli, Y., Cade-Menun, B.J., and Cutfort, H.W. (2013). Freeze-thaw cycles and soil water content effects on infiltration rate of three Saskatchewan soils. *Can. J. Soil. Sci*. 93:485-496.

Granger, R.J., Gray, D. M., and Dyck, G.E. (1984). Snowmelt infiltration to frozen Prairie soils. *Can. J. Earth. Sci*. 21:669-677.

Gray, D.M., Toth, B., Zhao, L., Pomeroy, J. W., and Granger, R. J. (2001). Estimating areal snowmelt infiltration into frozen soils. *Hydrological Processes*. 15: 3095-3111.

Horton, R.E. (1940). An approach to the physical interpretation of infiltration capacity. *Proc. Soil Sci. Soc. Am.* 5:399-417.

He, H., Dyck, M.F., Si, B.C., Zhang, T., Lv, J., and Wang, J. (2015). Soil freezing-thawing characteristics and snowmelt infiltration in Cryalfs of Alberta, Canada, *Geoderma Regional.* 5:198-208.

Huffman, R. L., Fangmeier, D. D., Elliot, W. J., Workman, S. R., and Schwab, G. A. (2011). *Soil and Water Conservation Engineering*. (6th ed.). St. Joseph, Mich.: ASABE.

HYPROP® User manual, Version 01/2010, UMS.

Ito, M., and Azam, S. (2010). Determination of swelling and shrinkage properties of undisturbed expansive soils. *Geotech Geol Eng*, 28(4): 413-422.

Ireson, A.M., van der Kamp, G., Ferguson, G., Nachshon, U., and Wheater, H.S. (2013). Hydrogeological processes in seasonally frozen northern latitudes: Understanding, gaps and challenges. *Hydrogeology Journal*, 21:53-66.

Iwata, Y., Nemoto, M., Hasegawa, S., Yanai, Y., Kuwao, K., and Hirota, T. (2011). Influence of rain, air temperature and snow cover on subsequent spring-snowmelt infiltration into thin frozen soil layer in northern Japan. *Journal of Hydrology*. 401:165-176.

Kane, D. L. and Stein, J. (1983). Water movement into seasonally frozen soils. *Water Resour. Res.* 19: 1547–1557.

Kizito, F., Campbell, C.S., Campbell, G.S., Cobos, D.R., Teare, B.L., Carter, B., and Hopmans, J.W. (2008). Frequency, electrical conductivity and temperature analysis of a low-cost capacitance soil moisture sensor. *J. Hydrol*. 352(3–4):367–378.

Lee, H. W. and Molnau. M. P. (1982). Infiltration into frozen soils using simulated rainfall. ASABE Paper No. 82–2048. St. Joseph, Mich.: ASAE.

Lee, H.W. (1983). Determination of infiltration characteristics of a frozen Palouse silty loam soil under simulated rainfall. PhD diss. Moscow, ID, USA: University of Idaho, Department of Agricultural Engineering.

Lundberg, A.L., Ala-Aho, P., Eklo, O., Klove, B., Kvaerner, J., and Stumpp, C. (2015). Snow and frost: Implication for spatiotemporal infiltration patterns- a review. *Hydrol. Process.* 30:1230-1250.

Mackay, J.R. (1983). Downward water movement into frozen ground, western arctic cost, *Canada. Can. J. Earth Sci.* 20:120-134.

Maček M., Smolar, J., and Petkovšek. A. (2013). Extension of measurement range of dewpoint potentiameter and evaporation method. *Proc. 18th International Conference on Soil Mechanics and Geotechnical Engineering,* 1137-1142, Paris, France: The French Society for Soil Mechanics and Geotechnical Engineering (CFMS).

MPRnews. (2013). Why was the Fargo flood forecast off by so much? Fargo, North Dakota: Minnesota Public Radio. Available at: http://minnesota.publicradio.org/display/web/-2013/05/01/regional/fargo-flood-forecast. Accessed 15 December 2016.

Parkin, G., von Bertoldi, A.P., and McCoy, A. J. (2013). Effect of tillage on soil water content and temperature under freeze-thaw conditions. *Vadose Zone J.*:1-9.

Rosenbaum, U., Huisman, J.A., Weuthen, A., Vereecken, H., and Bogena, H.R. (2010). Sensor-to-sensor variability of the ECH(2)O EC-5, TE, and 5TE sensors in dielectric liquids. *Vadose Zone J*. 9(1):181–186. doi:10.2136/vzj2009.0036.

Roy, D., Jia, X., Steele, D. and Lin, D. (2018). Development of soil water release curves for three soils in the Red River of the North, USA. *Soil Sci. Soc. Am. J.* doi: 10.2136/sssaj2017.09.0324

Saito, K., Kimoto, M., Zhang, T., Takata, K., and Emori, S. (2007). Evaluating a high-resolution climate model: Simulated hydrothermal regimes in frozen ground and their change under the global warming scenario, *J. Geophys. Res*. 112: 1-19 doi: 10.1029/2006JF000577.

Saito, T., Fujimakib, H., Yasudac, H., and Inoue, M. (2009). Empirical temperature calibration of capacitance probes to measure soil water. *Soil Sci. Soc. Am. J.* 73(6):1931–1937. doi:10.2136/sssaj2008.0128.

Six, J., Bossuyt, H., Degryze, S., and Denef, K. (2004). A history of research on the link between (micro) aggregates, soil biota, and soil organic matter dynamics. *Soil Tillage Res.* 79:7-31.

Topp, G.C., Davis, J.L., and Annan, A.P. (1980). Electromagnetic determination of soil water con- tent: Measurements in coaxial transmission lines. *Water Resour. Res.* 16(3):574–582. doi:10.1029/WR016i003p00574.

Tuller, M., and D. Or. (2004). Water retention and characteristic curve. In D. Hillel (Ed.), *Encyclopedia of Soils in the Environment* (Vol. 4, pp. 278-289). Oxford, United Kingdom: Elsevier Ltd.

Van Genuchten, M. T. (1980). A closed form equation for predicting the hydraulic conductivity of unsaturated soils. *Soil Sci. Soc. Am. J.* 44:892–898.

Vaz, C.M.P., Scott, J., Mercer, M., and Tuller. M. (2013). Evaluation of standards calibration functions for eight electromagnetic soil moisture sensors. *Vadose Zone. J.* 12(2):1-16 doi:10.2136/vzj2012.0160.

Water content, EC and Temperature sensor (5TE). (2015). Decagon Devices, Inc.

Williams, P.J. and T.P. Burt. (1974). Measurement of hydraulic conductivity of frozen soils. *Can. Geotech. J.* 11:647-650

WP4 dew-point potentiometer operator manual, version 2.1, Decagon devices.

Wraith, J. M. and D. Or. (1998). Nonlinear parameter estimation using spreadsheet software. *J. Nat. Resour. Life Sci. Educ.* 27:13-19.

Zheng, X., Van Liew, M. W., and Flerchinger, G. N. (2001). Experimental study on infiltration into a bean stubble field during seasonal freeze-thaw period. *Soil Science*. 166(1):3-10.

Zuzel, J.F. and Pikul, J.L. (1987). Infiltration into a seasonally frozen agricultural soil. *Journal of Soil and Water Conservation*. 42:447-450

4. HYDRAULIC CONDUCTIVITY MEASUREMENT OF THREE SOILS IN THE RED RIVER OF THE NORTH BASIN IN FROZEN AND UNFROZEN CONDITIONS BY USING MINIDISK INFILTROMETER[3]

4.1. Abstract

Hydraulic conductivity plays a key role in the water movement through the soil profile. It is a vital design factor for subsurface water management system design and installation. In the seasonally frozen Red River Valley of the North Basin (RRB), soils are unique, and information source of frozen soil hydraulic properties are limited and unreliable. The Minidisk infiltrometer is an easy handling and portable instrument that can be used to measure hydraulic conductivity in the field. In this study, minidisk infiltrometer was used to measure hydraulic conductivities of three soils from the RRB (Colvin silty clay loam, Fargo silty clay and Hecla sandy loam soils) with five different initial soil water contents (oven dry, permanent wilting point, field capacity, midway between permanent wilting point and field capacity, and saturation) in frozen and unfrozen conditions. In general, hydraulic conductivity (k) of frozen soils decreased with increased initial soil water contents. Hydraulic conductivity values were higher in dry soils and lower in wet soils due to ice that blocked the pore space and reduced the water movement. Sand

[3] The material in this chapter was co-authored by Debjit Roy and Xinhua Jia, Dean Steele, Xuefeng Chu and Zhulu Lin, will undergo further revision for possible publication in a refereed journal. Debjit Roy participated in data collection effort and had primary responsibility for analyzing the data collected, interpreting the results, and developing the conclusions that are advanced here. Debjit Roy drafted and revised all versions of this chapter. Co-authors served as technical and editorial consultants in the development of the manuscript represented by this chapter.

and clay contents in soils caused the variations in the measured k values. Hecla soil had higher k values and Fargo soil had lower k values. Three nonlinear regression equations for three soils were fitted with measured k values with a reasonable R^2 values of 0.67, 0.79, and 0.43 for Colvin silty clay, Fargo silty clay, and Hecla sandy loam soils, respectively. The k values were also estimated using the Motivilov model. The RMSE between the predicted and the measured k values were 0.013, 0.022, and 0.063 in cm/min for the fitted nonlinear regression models while RMSE were 0.017, 0.031, and 0.036 in cm/min for the Motivilov model, for the Colvin, Fargo and Hecla soil, respectively. Considering the simplicity, the fitted models predicted k values better than the Motivilov model for the Colvin and Fargo soils. The k values decreased with an increased number of the freeze and thaw cycles that changed the soil properties.

4.2. Introduction

Hydraulic conductivity of frozen soil is one of the governing factors that affects the infiltration capacity of water along the soil profile with ice (Stahli, 1999). The frozen soil hydraulic conductivity is considered very low but may not be that low at temperature just below 0°C (Mackay, 1983). Near or at 0°C, hydraulic conductivities are similar in both frozen and unfrozen soils, but with temperature fall, hydraulic conductivity decreases due to ice content formation that restricts water flow through pore space. If the soil is unsaturated during freezing, the soil can conduct water through it. When water freezes continuously from macro-pores to micro-pores, ice content forms within soil pores and hydraulic conductivity also decreases for the frozen soil. During freezing, with the ice formation in pores, matric potential increases and hydraulic conductivity decreases. As a reverse process, during thawing, soil matric potential decreases as ice melts in small pores with temperature increment, the hydraulic conductivity increases (Ireson et al., 1999).

The movement of soil water to freezing zone and ice accumulation is governed by unsaturated hydraulic conductivity of the soil. Water cannot move, or it can move less to freezing front if the soil unsaturated hydraulic conductivity is low. Very dry and coarse-grained soils have low unsaturated hydraulic conductivity compared to fine textured soil (Flerchinger et al., 2005). During frozen soil infiltration, unsaturated hydraulic conductivity can be calculated from available porosity of soil assuming that hydraulic conductivity and soil water retention characteristics of frozen soil is similar to those of unfrozen soil (Flerchinger et al., 2005). The hydraulic conductivity of frozen soil mostly depends on the conditions of soil before it freezes, or a snow cover occurs on the soil surface (Fouli et al., 2013). In seasonally frozen areas, snowmelt infiltration in spring is subjected to frozen soil condition due to variation of hydraulic conductivity (Lundberg et al., 2015). In a situation, when the soil remains dry or has less soil water content in fall before winter starts, and the soil does not get any released water from snow melting that infiltrates into the soil and refreeze, then the soil will be permeable and can conduct water until it gets saturated from snowmelt in spring. But if the soil is wet or nearly saturated before it freezes (in winter), the soil should have low permeability. In addition to the low permeability of the soil, if snowmelt happens due to sudden temperature rise in winter, the melt water can refreeze into the soil profile after entering the soil. This results in a reduction in infiltration capacity of the soil before spring melt.

In a frozen soil, the frozen active layer can be at saturation or over saturation, but other layers are below saturation and even dry. During freezing, the upper part of frozen active layer is unsaturated and is always subjected to many freeze-thaw cycles (Mackay, 1983). When pore water starts to freeze and form ice, soil water potential drops down and becomes negative. The gradient created between water potential and liquid ice contents moves the soil waters to the

freezing front within the soil profile. A single event of freeze-thaw cycle creates extensive network of cracks and ice lenses in clay soil which increases hydraulic conductivity and it continues to increase with more freeze-thaw cycles. However, it was found that after three cycles, hydraulic conductivity becomes stable (Othman et al., 1993). On the other hand, soil pressure reduces soil cracks during thawing and reduces hydraulic conductivity. Freeze-thaw cycles decrease void ratio of frozen soil by creating soil porosity like micro-pore or micro cracks which also helps to increase hydraulic conductivity in frozen clay soil (Kim and Daniel, 1992). But the scenario is different in granular soils. With ice content increasing close to 100% saturation during freezing, the open pore spaces of frozen granular soil decrease and thus, hydraulic conductivity decreases (Andersland et al., 1996).

Zhang (1997) proposed a two-term numerical solution which also derived from Philips equation for "sorptivity" and "hydraulic conductivity" estimation. The Philip infiltration equation is only valid for vertical water movement and also only for a very short infiltration time. Practically, the very short duration cumulative infiltration measurement is not appropriate to estimate sorptivity. In Zhang's numerical solution, there are two non-dimensional constants which can be determined from soil retention parameters, minidisk infiltrometer parameter and initial water content of soil. He found excellent agreement between the estimated and theoretical values of sorptivity and hydraulic conductivity. The theoretical values were obtained from van Genuchten (1980), Gardner (1958), Russo (1988) and Zhang and van Genuchten (1994) methods. In most comparisons, the relative error was within 5%. But the proposed method can be used only for homogeneous soil. On the other side, Dohnal et. al. (2010) found that Zhang's proposed numerical solution which in now used in minidisk infiltrometer of Decagon Device cannot perform well for the soils having "n" value less than 1.35. They showed that Zhang's

solution actually overestimated hydraulic conductivity values for $n < 1.35$ soils that are mostly clay, sandy loam or silty loam soils. They proposed a newly formulated expression for calculating hydraulic conductivity of soils in the range of $1 < n < 1.35$ based on nonlinear optimization of 16 soils having $n < 1.35$, different disk sizes and disk pressure heads. Li et al. (2005) did steady infiltration rate comparisons among different soil crusts using trickle irrigation method and minidisk infiltrometer. For minidisk infiltrometer, they used Zhang's formula to calculate steady infiltration rate, which is actually hydraulic conductivity component of that formula. They reported that minidisk infiltrometer was a good method to estimate field infiltration rates (i.e. hydraulic conductivity) from laboratory results.

In the Red River Valley of the North Basin (RRB), typically the drainage class of the soils are poorly drained, also those soils have a unique characteristic of shrinking and swelling as they sometimes contain high clay (Caine, 1903; Nikiforoff et al., 1939). The information regarding soil hydraulic properties of RRB region is not readily available due to limited soil specific database. However, hydraulic conductivity is one of the most important design parameter for installing subsurface water management systems. In the last few decades, subsurface drainage and irrigation systems (i.e. tile drainage system) are becoming very popular for agricultural water management in the RRB (Scherer et al., 2013). Agricultural water management through subsurface system now has a significant impact on RRB agriculture, environment and economy. Nowadays, the farmers are very concerned about subsurface water management system as it is giving them higher return on investment. In general, the RRB is the seasonally frozen area, so the frozen soil characteristics as well as its hydraulic properties must be considered when designing, modeling, and installing subsurface drainage or irrigation system in this region. However, the available methods for measuring hydraulic conductivity are mostly

laboratory based and typically time consuming, need intensive preparation and sample collection, and still those are unreliable. On the other hand, minidisk infiltrometer is simple, water infiltration based and portable field-oriented instrument that can give an onsite measurement of hydraulic conductivity easily. Moreover, no study was found regarding hydraulic conductivity measurement using minidisk infiltrometer though some findings reported reliable and reliable results by the min disk infiltrometer (Zhang, 1997; Li et al., 2005; Dohnal et. al., 2010). The objectives of this study were: (i) to measure variation in hydraulic conductivity of three soils of the RRB in both frozen and unfrozen conditions, with different initial soil water contents, (ii) to establish a relationship to predict frozen soil hydraulic conductivity using soil water content; (iii) to compare frozen soil hydraulic conductivities measured by minidisk infiltrometer and predicted by developed and existing models, and (iv) to evaluate the effect of freeze-thaw cycle on hydraulic conductivity measurement.

4.3. Materials and methods

4.3.1. Soils and soil properties

Three RRB soils, Colvin silty clay loam, Fargo silty clay, and Hecla sandy loam soils, were collected for the measurement of hydraulic conductivity in frozen soils. Colvin silty clay loam soil (Fine-silty, mixed, superactive, frigid Typic Calciaquolls) was collected from a tile drained field, located in Clay County, Minnesota (46°59'18.19"N, 96°41'7.25"W), about 20 km northwest of Moorhead. Fargo silty clay soil (fine, smectitic, frigid Typic Epiaquerts) was collected at about 8 km north of Gardner, Cass County (47°10'22.7"N, 96°54'01.3"W) of North Dakota. Hecla sandy loam soil (sandy, mixed, frigid Oxyaquic Hapludolls) sampling site (46°02'47.2"N, 98°06'14.7"W) was at about 4.8 km straight south and about 0.8 km west of the Oakes Irrigation Research Site, Dickey County, North Dakota. The percentages of sand, silt, and

clay were measured by the hydrometer method (Bouyoucos, 1951) and listed in Table 6 with bulk density of each soil.

Table 6. Percent of sand, clay, silt and bulk densities of the soil samples

Soil Series	USDA Soil Textural Classification	Sand (%)	Clay (%)	Silt (%)	Bulk density (g cm^{-3})
Colvin	Silty clay loam	1	37	67	1.25
Fargo	Silty clay	5	48	47	1.09
Hecla	Sandy loam	70	14	16	1.31

4.3.2. Soil water release curve and soil freezing curve

For each of three soils, a soil water release curve (SWRC), showing the relationship between the volumetric water contents and the soil matric potentials, was constructed using the combined datasets from the HYPROP® evaporation method (UMS GmbH, Germany) and the WP4 Dewpoint potentiometer (Decagon Devices, Pullman, WA, USA) method (Maček et al., 2013; Roy et al., 2018). The van Genuchten (1980) equation was used to construct SWRC of each soil and the equation can be expressed as:

$$\theta_v(\Psi) = \theta_r + (\theta_s - \theta_r)[1 + (\alpha|\Psi|)^n]^{-m} \quad (4.1)$$

where θ_v is the volumetric water content in cm^3/cm^3, Ψ is the matric potential in kPa, θ_r is the residual water content in cm^3/cm^3, θ_s is the saturated water content in cm^3/cm^3, α is the air entry point in 1/kPa, *n* and *m* are soil water retention parameters. The values of α, *n* and *m* are directly dependent on the shape of the $\theta_v(\Psi)$ curve. In Eq. 4.1, m=1-1/n. The van Genuchten equation was fitted with combined measured dataset of HYPROP and WP4 methods by Wraith and Or (1998) parameter estimation procedure using Excel® Solver. The hydraulic properties of each soil determined from the respective SWRC are listed in Table 7. The SWRCs of Colvin, Fargo and Hecla sandy loam soils are presented in figure 16(a), 16(b) and 16(c), respectively.

Table 7. Soil hydraulic properties from soil water release curve

Soil property	Symbol	Colvin Silty clay loam soil	Fargo Silty clay soil	Hecla Sandy loam soil
Saturated water content (cm^3/cm^3)	θ_s	0.59	0.56	0.51
Residual water content (cm^3/cm^3)	θ_r	0.05	0.10	0.06
Field capacity at -33 kPa (cm^3/cm^3)	θ_{fc}	0.33	0.29	0.16
Permanent wilting point at -1500 kPa (cm^3/cm^3)	θ_{pwp}	0.17	0.14	0.06
Halfway between FC and PWP (cm^3/cm^3)	θ_{mid}	0.25	0.22	0.11

Soil freezing curve (SFC), the relationship between the soil below zero-degree temperature and unfrozen water contents, can be obtained thermodynamically from the soil water release curve using a generalized form of the Clausius-Clapeyron equation (Miller, 1980):

$$\frac{P_w}{\rho_w} = \frac{P_i}{\rho_i} = \left(\frac{L}{K}\right) T \tag{4.2}$$

where P_w and P_i are pore water and pore ice pressure, respectively, in kN/m^2, ρ_w and ρ_i are density of water and ice, respectively, in kg/m^3, L is the latent heat of fusion in kJ/kg, K is the freezing temperature of pure water in °K (273.15°C), and T is the below-zero temperature in °C. Karvonen (1988) assumed that P_i in unsaturated soil is equal to zero (Kinosita and Ishizaki, 1980). So, Karvonen (1988) modified Eq. 4.2 by replacing the numerical values of variables (i.e. $P_i = 0$, $\rho_w = 1000$ kg/m^3, L = 333 kJ/kg and K = 273.15°C). After that, the equation 4.2 can be obtained as:

$$T = \frac{h}{122} \tag{4.3}$$

where h is the soil matric potential in meter of H_2O. Luo et al. (2000) used the same mathematical expressions to get SFC from SWRC during their DRAINMOD modification for the cold region. For this study, the matric potential values in SWRC were converted from kPa to m of water (1 kPa = 0.10199773 m of H_2O) for convenient application of Eq. 4.3. SFC of a soil

was used to measure the ice content of that soil for a specific below-zero temperature. The SFCs of Colvin, Fargo and Hecla soils are shown in figures 16(d), 16(e) and 16(f), respectively.

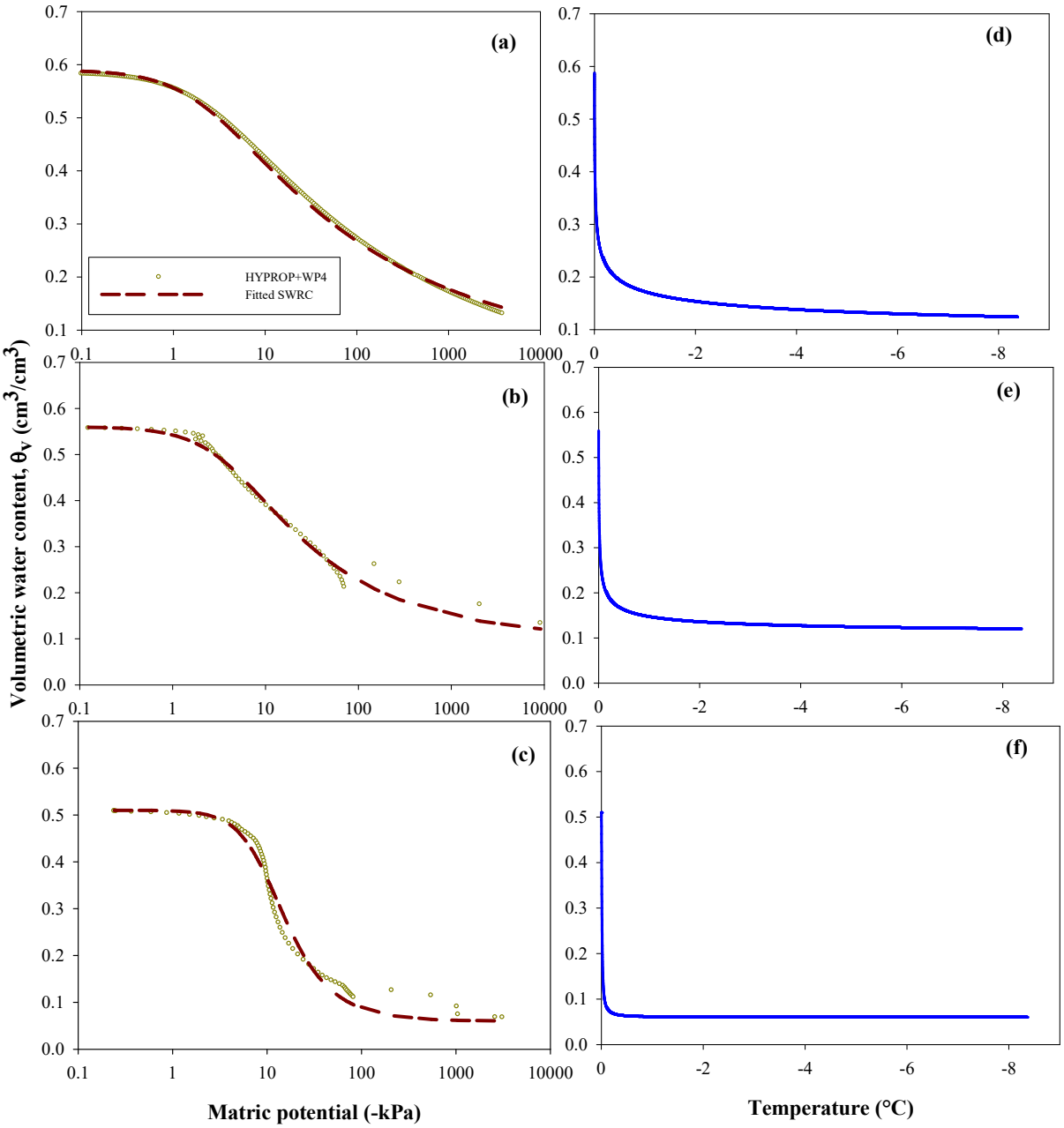

Figure 16. Soil release curves (SWRC) developed by HYPROP+WP4 combined methods for (a) Colvin soil, (b) Fargo soil, and (c) Hecla soils; Soil freezing curves (SFC) for (d) Colvin soil, (e) Fargo soil, and (f) Hecla soils.

4.3.3. Experiment conditions

For each soil, hydraulic conductivity measurement by the minidisk infiltrometer was conducted on both frozen and unfrozen conditions under five initial soil water contents. Each soil was prepared and packed to achieve one of the five initial water contents. The initial soil water contents ($\theta_{initial}$) were: (i) soil water content around permanent wilting point (PWP), designated in this study as θ_{pwp}; (ii) soil water around field capacity (FC), designated as θ_{fc}, (iii) soil water content around halfway between PWP and FC, designated as θ_{mid}, (iv) soil water content at oven dry, designated as $\theta_{ovendry}$, and (v) soil water content at saturation, designated as θ_{sat}. The θ_{mid} was calculated using the difference between PWP and FC values retrieved from SWRC of each soil. The θ_{mid} values are listed in Table 7, for Colvin, Fargo, and Hecla soils, respectively. A total of 90 infiltration experiments by minidisk infiltrometer were conducted for three soils in both frozen and unfrozen conditions under five initial water contents with three replications.

The effect of freeze-thaw (FT) cycles on hydraulic conductivity was assessed for Colvin soil after three, six and nine FT cycles. The soil was packed at the initial water content of θ_{mid} and hydraulic conductivity of soil was measured by the minidisk infiltrometer in unfrozen condition after completing a set of specific number FT cycles. Total nine experiments (three replications for one set of FT cycles) were conducted for this part of the study.

4.3.4. Instrumentation

A 5TE soil water and temperature sensor (Decagon Devices, Inc. Pullman, WA) was used in this study to record soil water content and temperature at any time between the soil packing and end of the experiment. The sensor (10 x 3.2 x 0.7 cm) can be functional between the temperature -40 and 60°C. As the sensor gives the reading of soil water content in number of dielectric permittivity, so a calibration relationship was developed to get volumetric

measurement from the dielectric permittivity number of soil water content. Though factory setup calibration was using Topp et al. (1980) relationship to obtain volumetric water contents from the dielectric permittivity numbers, further studies reported (Vaz et al., 2013) low accurate measurements when using this relationship. So, a soil specific calibration was performed according to the standard procedure described in manufacturer's website (http://www.decagon.com/en/support/videos/soil-calibration-video/). Instead of a linear equation (Rosenbaum et al. 2010), the θ_v vs dielectric permittivity relationship was found best fitted with quadratic equation. Many researchers (Kizito et al., 2008; Assouline et al., 2010; Saito et al., 2009) found that the accuracy of temperature measurement by this sensor was very high and did not vary too much as soil water content. To verify the temperature measurement and in case of any measurement error by the 5TE sensor, one thermocouple was also used to record temperature along with the sensor. Both 5TE soil water and temperature sensor and the thermocouple were connected to a CR 1000 data-logger. The data recording interval was programmed five minutes in CR 1000 data-logger.

4.3.5. Experiment preparation: soil packing and freezing

An experiment unit, made from PVC tube, was used for each experiment of hydraulic conductivity measurement. The diameter, height and thickness of the tubes were 20 cm, 22.8 cm, and 0.6 cm, respectively. The unit was attached to an octagonal base of 1.2 cm thick. A small hole was created at the bottom center of the base to drain any excess water moving down vertically during the experiment. A 2.54 cm thick layer of gravel was placed at the bottom of the unit. The gravel layer was separated from the soil by two mesh screens at the top and the bottom of the gravel layer (Figure 17). A small freeboard of 1.5-2.5 cm was maintained between the top edge of the unit and the packed soil surface.

When soils were packed for different initial water contents, six experiment units or columns (i.e. PVC tubes) were packed with one type of soil at one initial water content at a time. Three columns were used for unfrozen condition experiments while the other three were placed into the freezer for frozen condition. The three soils, collected from different locations, were air-dried first to remove excess soil water before starting the experiments. Before the soil packing, existing soil water content was measured using the 5TE soil water sensor. Then using the bulk density and existing water content, required amounts of soil and water (to get the expected initial water content) were calculated. During the soil packing, soil was packed layer by layer consistently to maintain the bulk density close to the field bulk density. Also, extra care was taken to mix the soil thoroughly to get uniform soil water distribution in the packed soil. After finishing the soil packing, the entire soil was kept sitting on a flat surface untouched for soil settling and soil water stabilization. The soil was also covered by a plastic film to prevent water loss from soil by evaporation.

To conduct experiments on oven dried soils in frozen and unfrozen conditions, soils were dried in a laboratory drying oven at 105°C temperature for 2-3 days to completely remove water form soils as much as possible. Then, the soil was packed in the experiment unit following the same procedure stated earlier. After finishing the experiments for oven dry soil, the packed-soil units were placed in water tubs to saturate the soil. Water was applied to the tub so that the water level inside the tub reached half of the unit height. The experiment units, used for oven dry and saturated soils experiments, had some extra holes at the bottom. Those holes helped the capillary rise of water inside the packed soil after placing in the tub filled with water. To saturate the soil, no water was applied from the top, while water moved upward only by capillary action to saturate the soil. The units were kept inside the tub for few days to saturate the soil completely.

For the freezing of the soil-packed units, a chest freezer (120.3 x 76.8 x 84.8-cm, MAYTAG) was used in the laboratory. The temperature was monitored continuously from the real-time sensor recording for all units after placing inside the freezer. Besides the automatic monitoring, all the dielectric numbers and temperature from sensor and thermocouple readings before freezing and the experiment (both for unfrozen and frozen condition) as well as freezing starting time, experiment starting and ending times were recorded manually.

For the FT cycle experiments, all columns were packed with Colvin soil at initial water of θ_{mid}. Soil packing procedure was same as the packing of soil for different initial water contents. One complete FT cycle consisted of 12-hr freezing and 12-hr thawing. After freezing a unit for 12-hr (below or at 0°C), the unit was left open at room temperature (around 22-25°C) for the next 12-hr. The time limit (12-hr period) was strictly maintained for all sets of FT cycles (i.e. 3, 6, and 9 FT cycle).

4.3.6. Experiment setup and measurement

The schematic diagram of hydraulic conductivity measurement by the minidisk infiltrometer experiment setup is shown in figure 17. The setup was the same for all conditions, i.e. frozen, unfrozen, oven dry or saturated soils. During soil packing, the 5TE soil water and temperature sensor, and the thermocouple were placed at 8-10 cm depth from the packed soil surface, along the vertical center line of the experiment unit. As stated earlier, all the sensors and thermocouple were connected to a data-logger which recorded soil water and temperature continuously after the soil packing and until the experiment ended. A time lapse camera, TimelapseCam® (WINGSCAPES®), was used to take pictures during the experimental period for all experiments. This camera helped to record any unforeseen incident and facilitated water level measurement during any unattended period of the experiment.

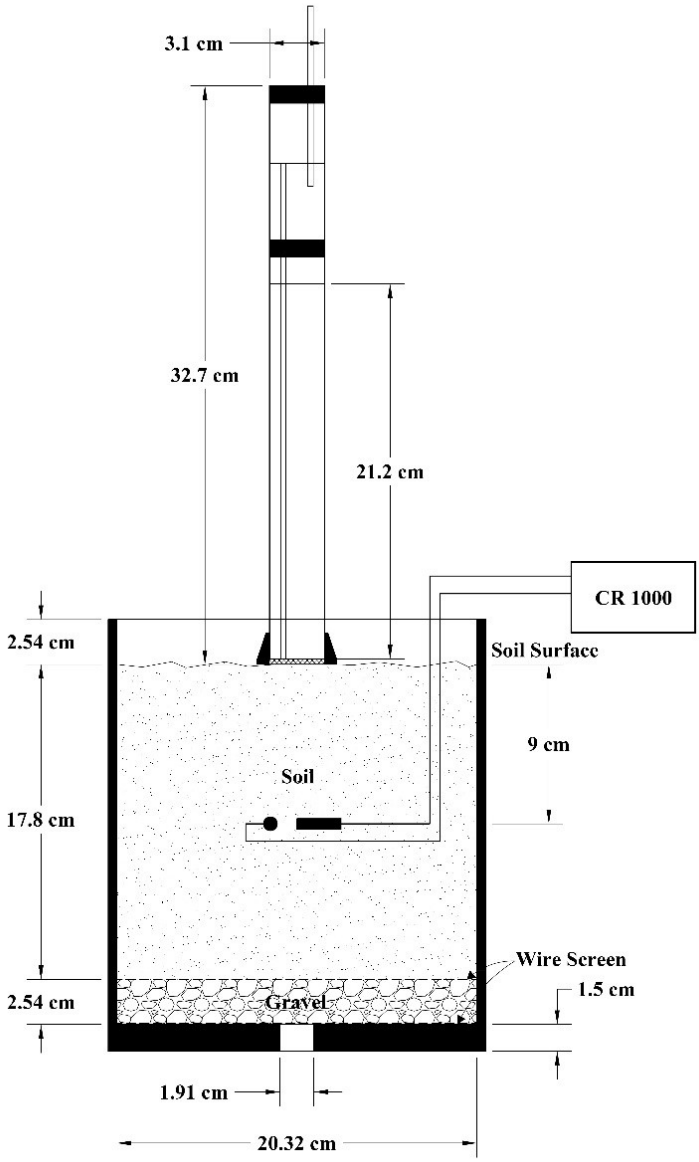

Figure 17. Schematic of experimental setup.

The hydraulic conductivity was calculated from the infiltration experiment conducted by minidisk infiltrometer. Minidisk infiltrometer is a smaller version of tension infiltrometer (Decagon Devices, Inc., Pullman, WA). It is a portable type tension infiltrometer, used for quick measurements of infiltration and hydraulic properties of soil, and good for laboratory experiments. The length of the minidisk infiltrometer was 32.7 cm and diameter of the tube was

3.1 cm. It had a 4.5 cm diameter disk with 3 mm thickness. The suction range of minidisk infiltrometer varied from 0.5 to 7 cm. According to the user's manual (Decagon Device, 2011), a suction rate of 2 cm was selected for Colvin and Fargo soils. But, for Hecla soil, the suction was adjusted to 6 cm as suggested by the manufacturer as the infiltration occurred very quickly in that soil when 2 cm suction used. The suction control section consisted of a single tube combined with bubble tower and water reservoir. The device was divided into upper and lower chambers. Both chambers had to be filled with water for infiltration measurement. The upper chamber, or bubble tower, controlled suction. The water from the lower chamber infiltrated into soil under a selected suction. The infiltration rate measurement was obtained from labeled lower chamber. The infiltration rate and hydraulic properties of a soil was then calculated. With Minidisk infiltrometer, the infiltration rates were calculated with the help of a spreadsheet available from Decagon Devices, which was based on Zhang (1997) by fitting the parameters C_1 and C_2 of the Phillip equation. The equation modified by Zhang (1997) is:

$$I = C_1\, t\ + C_2\, \sqrt{t} \tag{4.4}$$

where I is the cumulative infiltration (cm), t is time (min), the slope of the curve C_1 is a function of the hydraulic conductivity k (cm/min), and C_2 is a function of sorptivity (cm/min$^{1/2}$). The hydraulic conductivity (k) is then calculated from following equation:

$$k = \frac{C_1}{A} \tag{4.5}$$

where A, a value relating the van Genuchten parameters for a given soil type to the suction rate and radius of the infiltrometer disk, is obtained from:

$$A = \frac{11.65(n^{0.1} - 1)\ e^{[2.92(n-1.9)\alpha h]}}{(\alpha r_d)^{0.91}}\ if\ \ n \geq 1.9 \tag{4.6}$$

$$A = \frac{11.65(n^{0.1} - 1)\ e^{[7.5(n-1.9)\alpha h]}}{(\alpha r_d)^{0.91}}\ if\ \ n < 1.9 \tag{4.7}$$

in which h (cm) is a given suction, r_d (cm) is the radius of the disk, and α and n are van Genuchten parameters based on the soil type.

4.3.7. Relationship between k and θ_v: nonlinear regression model

To establish a relationship between k and corresponding volumetric water contents (θ_v) of frozen soil, the pooled measured data were fitted with a nonlinear regression model using SigmaPlot 11.0 statistical software (Systat software, Inc.). Depending on the nonlinear arrangement of the measured data, an exponential decay equation with two parameters was selected from the program. The fitted equation can be described as:

$$k_{predicted} = a * e^{(-b*\theta v)} \tag{4.8}$$

where $k_{predicted}$ is the hydraulic conductivity of frozen soil in cm/min predicted by the fitted model, θ_v is the unfrozen volumetric water content of frozen soil in cm^3/cm^3, and *a* and *b* are fitting parameters. The model was fitted with measured data of each soil separately.

4.3.8. Comparison to Motivilov model

Motivilov (1978) proposed a mathematical model for calculating hydraulic conductivity of frozen soil. The simplified form (Luo et al., 2000) of the Motivilov model can be expressed as:

$$k(\theta_i) = \frac{k(\theta_w)}{(1+8\theta_i)^2} \tag{4.9}$$

where θ_i and θ_w are volumetric contents of ice and unfrozen water in soil, respectively, and $k(\theta_i)$ and $k(\theta_w)$ are hydraulic conductivities for frozen soil with ice and unfrozen soil without ice, respectively. The Motivilov model was used in this study to calculate the frozen soil hydraulic conductivity for all frozen soil experimental conditions described earlier. For the calculation of

the $k(\theta_i)$ at a specific experimental condition (e.g. Colvin soil and θ_{pwp}), the corresponding mean measured k value of unfrozen soil at the same conditions was taken as the $k(\theta_w)$. The θ_w was obtained from SFC curve of the related soil for the temperature recorded by 5TE sensor just before the experiment started. Then the difference between the $\theta_{initial}$ and θ_w was considered as the θ_i (i.e. $\theta_i = \theta_{initial} - \theta_w$). The calculated $k(\theta_i)$ values of Motivilov model were later compared to the measured k values and the estimated values of $k_{predicted}$ by the fitted model.

4.3.9. Goodness of fit and root mean square error

The agreement between the predicted values by a model and measured values, i.e. the goodness of fit, was obtained by the coefficient of determination (R^2). The R^2 value of two datasets indicates how well the predicted values fitted with the measured value overall. Also root mean square error (RMSE) was calculated to evaluate the error between the two datasets. RMSE usually compares predicted values and corresponding observed values. The R^2 and RMSE values can be determined by using following equations:

$$R^2 = \left[\frac{\sum_{i=1}^{N} (Observed\ value - Observed\ mean)(Measured\ value - Measure\ \ mean)}{\sqrt{\sum_{i=1}^{N} (Observed\ value - Observe\ \ mean)^2} \sqrt{\sum_{i=1}^{N} (Measued\ value - Measure\ \ mean)^2}} \right]^2 \quad (4.10)$$

$$RMSE = \sqrt{\frac{\sum_{i=1}^{n} (Predicted\ value - Measure\ \ value)^2}{Number\ of\ measurement,\ \ n}} \quad (4.11)$$

4.4. Results and discussion

Mean measured k values with standard deviations are listed in Table 8 with corresponding soil type, different $\theta_{initial}$ (θ_{pwp}, θ_{mid}, θ_{fc}, $\theta_{ovendry}$, and θ_{sat}, respectively), and frozen/unfrozen conditions.

Table 8. Mean measured hydraulic conductivity, k (cm/min) for different soil types, initial soil water contents (θ_{inital}), and frozen/unfrozen conditions

Soil	θ_{inital}	Frozen soil		Unfrozen soil	
		Mean Measured k (cm/min)	Standard deviation	Mean Measured k (cm/min)	Standard deviation
Colvin silty clay loam	$\theta_{ovendry}$	0.137	0.046	0.225	0.052
	θ_{pwp}	0.073	0.016	0.064	0.015
	θ_{mid}	0.027	0.003	0.021	0.006
	θ_{fc}	0.017	0.005	0.014	0.012
	θ_{sat}	0.013	0.005	0.008	0.005
Fargo silty clay	$\theta_{ovendry}$	0.101	0.037	0.491	0.040
	θ_{pwp}	0.069	0.012	0.051	0.022
	θ_{mid}	0.031	0.017	0.011	0.008
	θ_{fc}	0.002	0.003	0.001	0.001
	θ_{sat}	0.014	0.004	0.011	0.004
Hecla Sandy loam	$\theta_{ovendry}$	0.163	0.037	0.120	0.043
	θ_{pwp}	0.223	0.010	0.205	0.006
	θ_{mid}	0.085	0.003	0.063	0.011
	θ_{fc}	0.031	0.004	0.016	0.006
	θ_{sat}	0.012	0.004	0.066	0.024

4.4.1. k comparison: frozen and unfrozen conditions

From Table 8, it could be observed that Hecla soil had comparatively higher k and Fargo soil had lower k in both frozen and unfrozen conditions among the three soils. The k of Colvin soil in both frozen and unfrozen condition was ranked in between Hecla soil and Fargo soil.

In Table 8, the mean k (cm/min) values and standard deviation among the replications are presented for different soil types with initial soil water contents at $\theta_{ovendry}$, θ_{pwp}, θ_{mid}, θ_{fc}, and θ_{sat}, respectively. It is generally assumed that the soil k value decreases with increase in soil water content, the drier the soil, the higher the k (Lundberg et al., 2015; Flerchinger et al., 2005; Ireson et al., 1999; Mackay, 1983; Fouli et al., 2013). The mean k values were found higher for dry soil (θ_{pwp}) and then decreased with higher soil water content (θ_{mid} and θ_{fc}) in both frozen and unfrozen condition. It was observed that the k for frozen soil at any soil water content was higher than that of unfrozen soil. But the mean k values reduced greatly at θ_{fc} for any soil, which implied that

there was very small or no water movement in the frozen soil. The presence of high water in soil pores might block the flow paths after freezing. It could be anticipated that soil water contents changed from liquid phase to ice phase, created more paths for water movement when the soil was not saturated or at field capacity. Fargo soil had lower mean k at any initial soil water contents for both frozen and unfrozen soils compared to the mean k values of the other two soil types. Fargo soil had higher clay content among the three soils, and higher clay amount could hold more water. In frozen Fargo soil, the higher soil water content could result in high amount of ice in the soil profile, which also restricted water movement and decreased the k value. The mean k values of Hecla sandy soil for initial soil water content at θ_{pwp} were found highest (Table 8) among all measured k values. Hecla soil had higher percentage of sand particles, which might help the water moving faster through the soil profile with a higher k value when it was dry.

In oven dried soil, the soil was not completely dry and it had a minimum soil water content after drying (i.e. nearly oven dry soil having soil water content same as residual water content, θ_r, Table 7). In saturated soil, the situation was completely opposite from oven dry soil (soil with saturated water contents, θ_s, Table 7). So, the mean k values were found very high in oven dry soil compared to those in saturated soils (Table 8). In saturated soil, it was be expected that, after freezing, all possible macro-pores and micro-pores were blocked by ice lenses. The water phase change from liquid to solid ice could reduce the water flow path and consequently decreased the k in saturated frozen soil with time. For oven dry soil (or, nearly oven dry soil), mean k values were lower for frozen condition than those of unfrozen soils for Colvin and Fargo soils, respectively. But, it was found the opposite in Hecla soil, the mean k value of frozen oven dry Hecla soil was higher than that of unfrozen soil.

4.4.2. Relationship between k and θ_v: fitted model

The measured k values were fitted with Eq. 4.8 for each soil, from which k could be predicted for any frozen soil water content. The fitted models are shown in Eq 4.11, Eq 4.12 and Eq 4.13, for Colvin, Fargo, and Hecla soils:

Colvin silty clay loam: $k_{predicted} = 0.4399 * e^{(-31.8127*\theta v)}$, $R^2 = 0.67$ (4.12)

Fargo Silty clay: $k_{predicted} = 0.2790 * e^{(-20.8253*\theta v)}$, $R^2 = 0.79$ (4.13)

Hecla sandy loam: $k_{predicted} = 0.3134 * e^{(-21.3948*\theta v)}$, $R^2 = 0.43$ (4.14)

Figure 19 shows the fitted equations with measured k values for Colvin soil, Fargo soil, and Hecla soil, respectively. The relationship between the measured k value and the corresponding θ_v, was not linear which indicated that k would be higher in frozen dry soil and the k was decreased with higher frozen soil water content, gradually becoming stable or lower after a certain θ_v in frozen soil. The relationship was very simple in terms of parameter, because k value could be predicted by using a single parameter, θ_v of frozen soil.

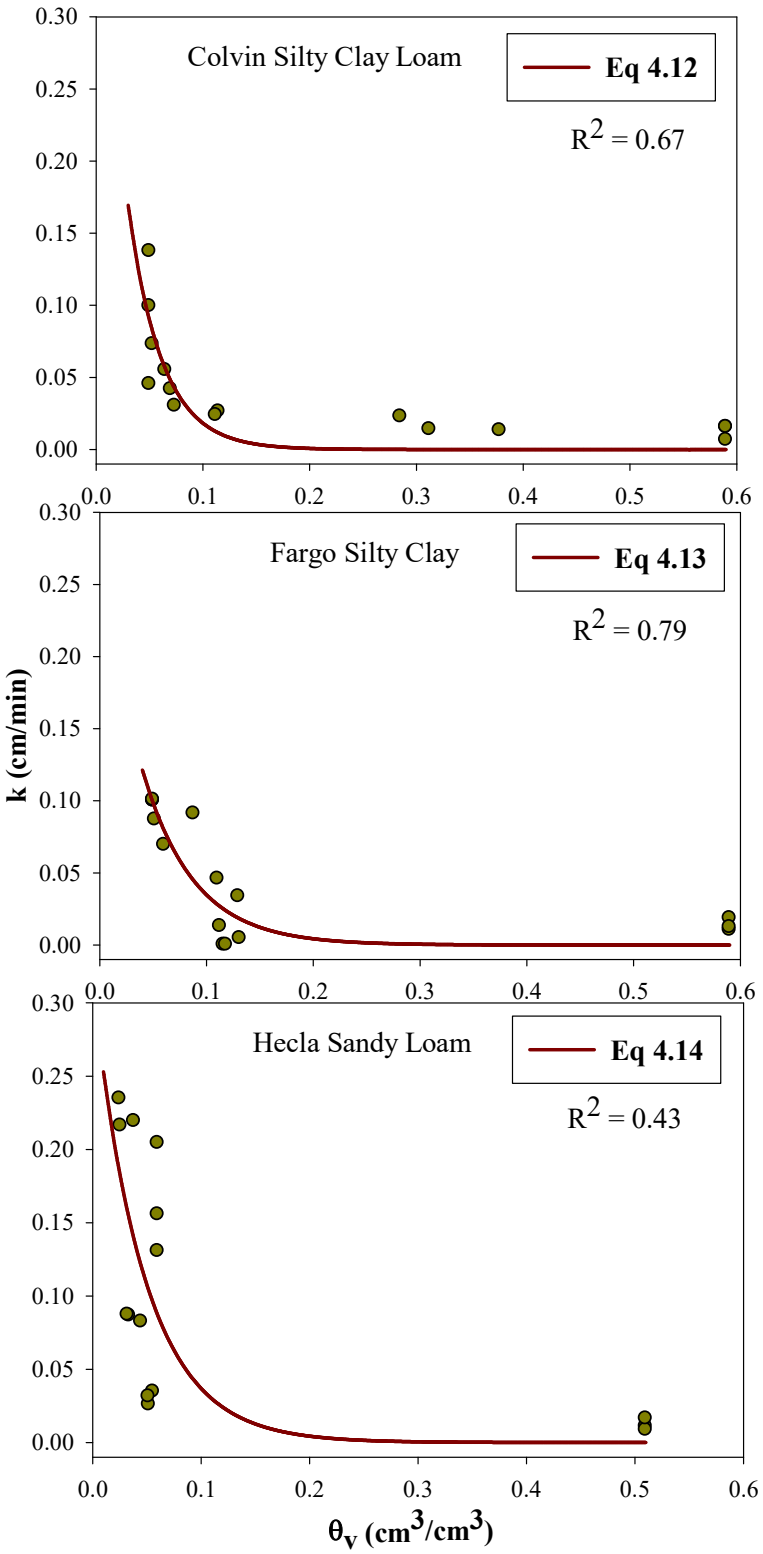

Figure 18. Hydraulic conductivity (k) vs. volumetric water contents (θ_v) relationship by Eq. 4.12, Eq. 4.13, and Eq. 4.14, plotted for Colvin, Fargo and Hecla soils, respectively.

4.4.3. Fitted model vs. Motivilov model

All predicted k values by fitted model and calculated k values by Motivilov model are presented in figure 20 with a 1:1 line. The RMSE of measured k values and predicted k values by fitted equations were found 0.013, 0.022, and 0.063 cm/min for Colvin soil, Fargo soil, and Hecla soil, respectively. Similarly, the RMSE of measured k values and calculated k values by Motivilov model were found 0.017, 0.031, and 0.036 cm/min, for Colvin soil, Fargo soil, and Hecla soil, respectively. In figure 20, it could be seen that the predicted k values by fitted model were widely spread compared to those by the Motivilov model. The calculated k values by Motivilov showed a linear increase, consistent along the 1:1 line compared to calculated k values by the fitted models, though those did not match perfectly with 1:1 line. The predicted k values by fitted models showed reasonable agreement for Colvin soil between the predicated values and 1:1 line, relatively close to the 1:1 line for Fargo soil, but had a poor relationship or matching for Hecla soil along the 1:1 line. However, the Motivilov model, although very complicated to use, gave a better estimation of k values for Hecla soil. The calculation procedure included complex estimation of unfrozen soil water content from SFC, ice content of soil and equivalent hydraulic conductivity of unfrozen soil. Compared to the Motivilov model, the fitted models were simple and needed a single parameter (θ_v of frozen soil) to predict the k values. Considering the variability between the predicted and the measured k values, the overall performance of fitted models was comparatively better than that of Motivilov model.

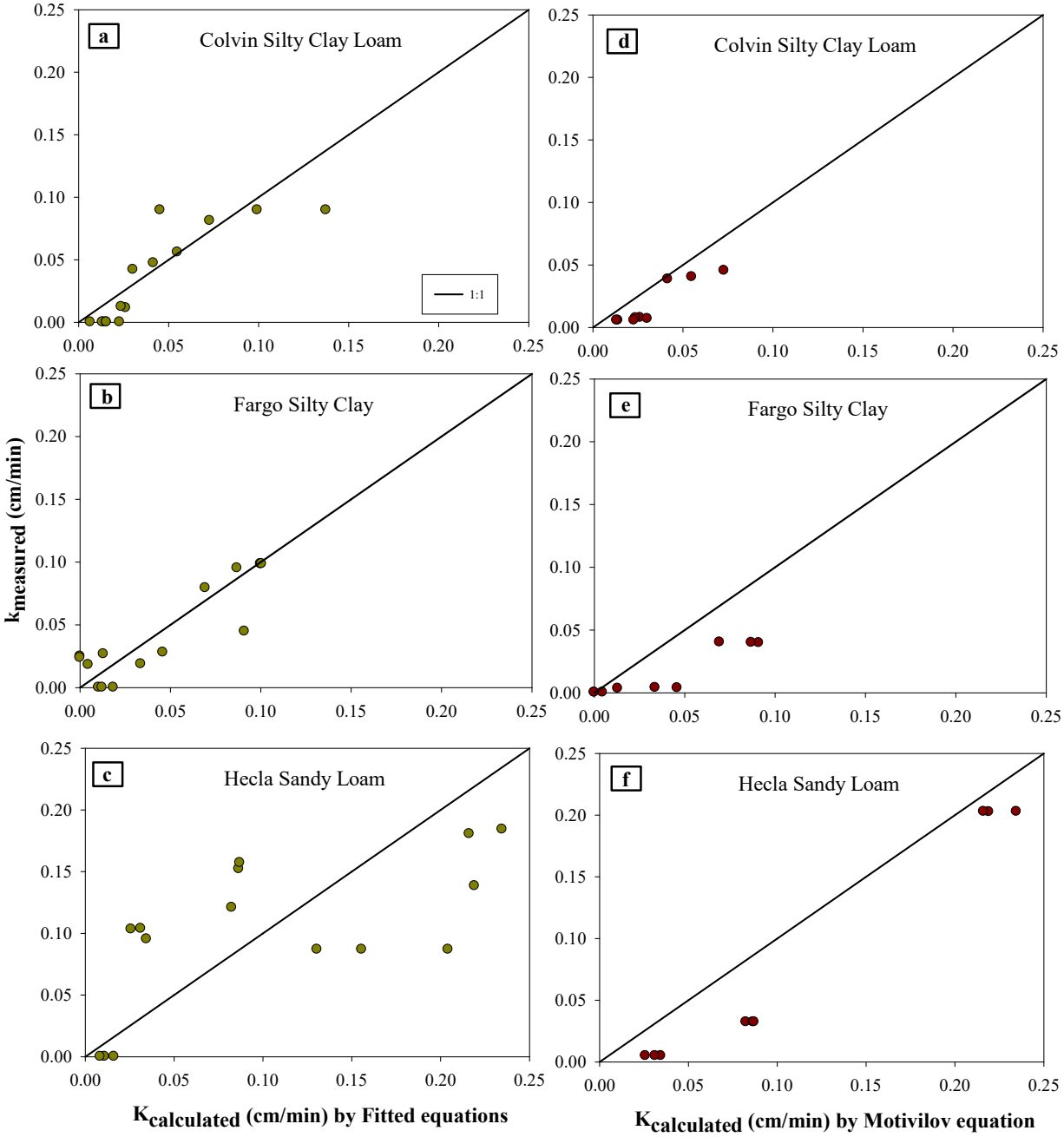

Figure 19. Measured k values by minidisk infiltrometer plotted against calculated k values by Eq. 4.12, Eq. 4.13, and Eq. 4.14 in 1:1 plot for (a) Colvin, (b) Fargo, and (c) Hecla soils, respectively. Measured k values by minidisk infiltrometer plotted against calculated k values by Motivilov model in 1:1 plot for (d) Colvin, (e) Fargo, and (f) Hecla soils, respectively.

4.4.4. Freeze-thaw effect on k measurement

Figure 21 shows the mean k values with standard deviation after 3 FT, 6 FT, and 9 FT cycles on Colvin soil with an initial water content at θ_{mid}. The figure indicated that, after 6 FT cycle, the mean k (0.009 cm/min) decreased than that (0.013 cm/min) after 3 FT cycle, and then the mean k (0.007 cm/min) again decreased after 9 FT cycle than that after 6 FT cycle. Fouli et al. (2013) conducted infiltration experiment with three Saskatchewan soils for different FT cycles. Their procedure for attaining a FT cycle was similar to the procedure in this study (12 hr freezing and 12 hr thawing). They reported a decrease in infiltration rate with increased number of FT cycles. The final or steady state infiltration rate can be considered same or close to hydraulic conductivity of that soil. The decrease in infiltration rate might be the indication of hydraulic conductivity for FT cycles variations. The results of this study agreed with his findings, showed a decreasing pattern of hydraulic conductivity with increased number of FT cycles. Also the change in mean k values indicated that even a short duration FT cycles (24 hr freezing and thawing) affected the soil aggregates, i.e. soil pore distribution. The alteration of soil pore distribution could be the reason of decreasing the mean k values after different FT cycles. The concluding remarks of Fouli et al. (2013) findings also highlighted the change in soil porosity and structural changes due to number of FT cycles. Othman et al. (1993) indicated that hydraulic conductivity could be stable after three FT cycles. For Colvin soil in this study, the hydraulic conductivity was not found stable after 6 and 9 FT cycles. The k values of laboratory experiments might differ from the actual field value. Because, in the laboratory experiment, only 12 hours freezing, and 12 hours thawing was applied as one FT cycle, but in real world, a wide variation could be found in freezing and thawing duration. Therefore, the laboratory testing procedure for the duration of a FT cycle that was not representing field situation. It might be a

reason for a difference in mean k values. However, the findings gave a directional understanding about the effect of FT cycles on hydraulic conductivity of frozen soil.

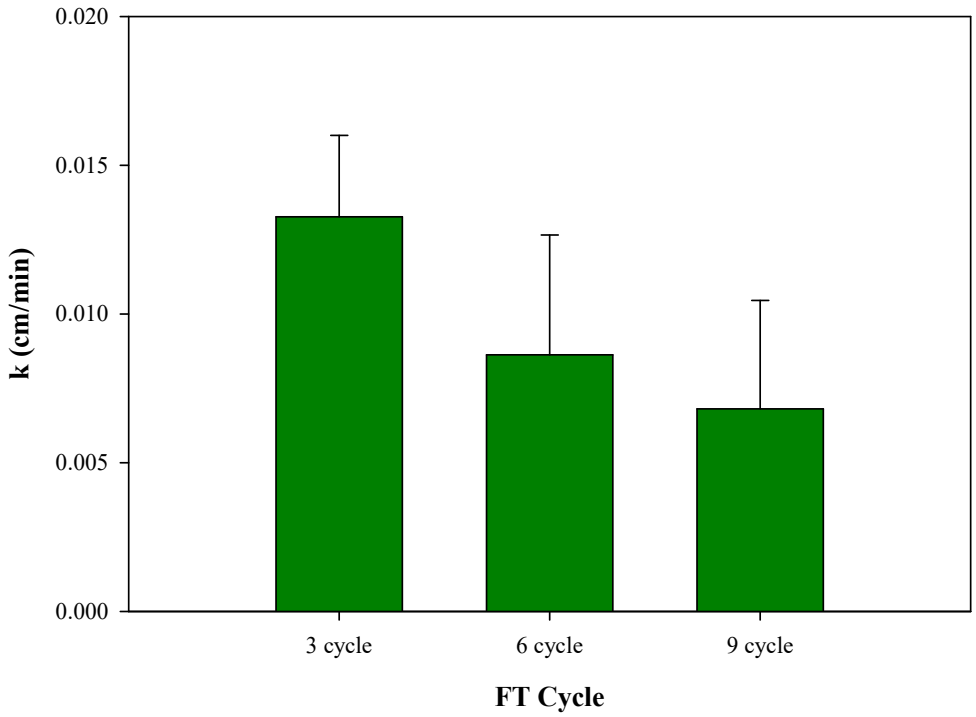

Figure 20. Mean hydraulic conductivity (k) values plotted for 3, 6, and 9 freeze-thaw (FT) cycles for Colvin soil with initial soil water content in between permanent wilting point and field capacity (θ_{mid}).

4.5. Conclusion

Three soils of RRB, Colvin silty clay loam, Fargo silty clay, and Hecla sandy loam, were used in this study. An easy handling, field-oriented, and portable instrument, the Minidisk infiltrometer, was used to measure hydraulic conductivity. Hydraulic conductivity was measured in frozen and unfrozen soils with five initial soil water contents of oven dry, permanent wilting point, halfway between permanent wilting point and field capacity, field capacity, and saturation ($\theta_{ovendry}$, $\theta_{pwp,}$ θ_{mid}, θ_{fc}, and θ_{sat}, respectively). Soil water release curve (SWRC) and soil freezing

curve (SFC) were constructed for each soil to obtain related values of soil hydraulic properties in frozen and unfrozen conditions.

Fargo soil had low hydraulic conductivity and Hecla soil had higher hydraulic conductivity among the three soils, irrespective of frozen/unfrozen condition, and $\theta_{initial}$. Hydraulic conductivity of both frozen and unfrozen Fargo soils for soil water content at field capacity (θ_{fc}) was lower than those of the other two soils. Generally, k values varied from higher to lower with the increment of $\theta_{initial}$. The higher clay content of Fargo soil might hold more water than other soils, and produced more ice in the soil pores, which restricted the water movement in frozen soil, i.e. reduced the hydraulic conductivity. The frozen saturated soil reduced the pore space with blocked ice contents, and might result in lower k than other $\theta_{initial}$ conditions. Hecla soil had higher sand percentage compared to other soils, which contributed to greater k values than other two soils. Due to higher sand content, it had low water holding capacity, which actually resulted high k value in dry frozen soil and even in saturated unfrozen soil. The measured k values were fitted with three nonlinear regression equations for three different soils. The equations were: $k_{predicted}=0.4399*e^{(-31.8127*\theta_v)}$ for Colvin soil, $k_{predicted}=0.2790*e^{(-20.8253*\theta_v)}$ for Fargo soil, and $k_{predicted}=0.3131*e^{(-21.3948*\theta_v)}$ for Hecla soil with a considerable agreement between predicted and measured k values (R^2 values were 0.67, 0.79 and 0.43, respectively). The frozen soil k values were also estimated by using Motivilov model and compared to measured k values. The RMSE between measured and predicted values by fitted models were obtained 0.013, 0.022, and 0.063 cm/min for Colvin soil, Fargo soil, and Hecla soil, respectively. On the other hand, the RMESE were 0.017, 0.031, and 0.036 cm/min for Colvin, Fargo and Hecla soil, respectively. The fitted models were simple in terms of parameters, could predict better k values compared to Motivilov model for Colvin and Fargo soils, though both

models had limitation to predict k values perfectly close to measured k values. The k value measurements of increasing FT cycles showed a decrease in hydraulic conductivity, agreed with the previous study findings where it was indicated that k decreased with increased frequent FT cycles. Also the k variation with different FT cycles gave evident observation that soil properties changed with increased FT cycles, supported earlier research study remarks.

4.6. Acknowledgement

The research study was supported by NASA ROSES Project NNX15AC47G, USDA National Institute of Food and Agriculture project 2015-68007-23193, Sustainable Agriculture Research and Education project LNC11-332, ND Soybean Council, ND Water Resources Research Institute, ND Agricultural Experimental Station, and USDA Hatch project ND01475. The authors would like to express heartfelt gratitude to Dr. Dongqing Lin, Mr. James Moors and Mr. Mojtoba Ahmadi, for their physical and technical support and help throughout the study.

4.7. References

Andersland, O.B., Wiggert, D.C., & Davies, S.H. (1996). Hydraulic conductivity of frozen granular soils. *Journal of Environmental Engineering*. 122(3):212-216

Assouline, S., Narkis, K., Tyler, S.W., Lunati, I., Parlange, M.B., and Selker, J.S. (2010). On the diurnal soil water content dynamics during evaporation using dielectric methods. *Vadose Zone J.* 9(3):709–718. doi:10.2136/vzj2009.0109.

Bouyoucos, G. J. (1951). A recalibration of the hydrometer method for making mechanical analysis of soils. *Agron. J.* 43:434-438.

Caine, T.A. (1903). Soil survey of the Fargo area, North Dakota. Field Operation of the Bureau of Soils, USDA.

Decagon Devices, Inc. (2015). 5TE water content, EC and temperature sensors, operator's manual, Decagon, Pullman, WA.

Decagon Devices, Inc. (2016). Custom Soil Calibration for Volumetric Water Content Sensors. Available at: https://www.decagon.com/en/support/videos/soil-calibration-video/. Accessed 15 December 2016.

Dohnal, M., Dusek, J., & Vogel, T. (2010). Improving hydraulic conductivity estimates form minidisk infiltrometer measurements for soils with wide pore size distributions. *Soil Sci. Soc. Am. J.* 74:804-811

Flerchinger, G.N., Lehrsch, G.S., McCool, D.K. (2005). Freezing and Thawing processes. In *Encyclopedia of Soils in the Environment*, Hillel D (ed.). Elsevier: Ltd, Oxford, UK: 104-110

Fouli, Y., Cade-Menun, B.J., & Cutforth, H.W. (2013). Freeze-thaw cycles and soil water content effects on infiltration rate of three Saskatchewan soils. *Can. J. Soil. Sci.* 93:485-496

Gardner, W.R. (1958). Some steady-state solutions of the unsaturated moisture flow equation with application to evaporation from a water table. *Soil Sci.* 85:228-232

Ireson, A.M., van der Kamp, G., Ferguson, G., Nachshon, U., & Wheater, H.S. (2013). Hydrogeological processes in seasonally frozen northern latitudes: Understanding, gaps and challenges. *Hydrogeology Journal*. 21:53-66

Karvonen, T. (1988). A model for predicting the effect of drainage on soil moisture, temperature and crop yield. Ph.D. diss. Helsinki, Finland: Helsinki Univ. of Technol.

Kim, W. & Daniel, D.E. (1992). Effects of freezing on hydraulic conductivity of compacted clay. 1992. *J. Geotech. Eng*. 118(7):1083-1097

Kizito, F., Campbell, C.S., Campbell, G.S., Cobos, D.R., Teare, B.L., Carter, B., & Hopmans, J.W. (2008). Frequency, electrical conductivity and temperature analysis of a low-cost capacitance soil moisture sensor. *J. Hydrol*. 352(3–4):367–378.

Li, X., Gonzalez, A., & Sole-Benet, A. (2005). Laboratory methods for the estimation of infiltration rate of soil crusts in the Tabernas Desert badlands. *Catena*. 60:255-266

Lundberg, A.L., Ala-Aho, P., Eklo, O., Klove, B., Kvaerner, J., & Stumpp, C. (2015). Snow and frost: Implication for spatiotemporal infiltration patterns- a review. *Hydrol. Process*. 30:1230-1250

Luo, W., Skaggs, R.W. & Chescheir, G.M. (2000). DRAINMOD modification for cold conditions. *Transaction of the ASABE*, 43(6): 1569-1582

Maček M., Smolar, J., & Petkovšek. A. (2013). Extension of measurement range of dewpoint potentiameter and evaporation method. *Proc. 18th International Conference on Soil Mechanics and Geotechnical Engineering,* 1137-1142, Paris, France: The French Society for Soil Mechanics and Geotechnical Engineering (CFMS).

Mackay, J.R. (1983). Downward water movement into frozen ground, western arctic cost, *Canada. Can. J. Earth Sci*. 20:120-134

Miller, R.D. (1980). Freezing phenomenon in soils. *Application of Soil Physics*, Ch. 11, ed. D. Hillel. New York, N.Y.: Academic Press, Inc.

Motovilov, Y.G. (1978). Mathematical model of water infiltration into frozen soil. *Soviet Hydrol.* 17: 62-66

Nikiforoff, C.C., Hasty, A.H., Swenson, G.A., Gray, A.L., Fieger, E.A., Hill, S., Newman, H.C., Mattson, C.H., Hide, J.C., & Kneen, E. (1939). Soil survey (Reconnaissance) of the Red River Valley area, Minnesota. Bureau of Chemistry and Soils, USDA, Series 1933, No 25, April.

Othman, M.A. & Benson, C.H. (1993). Effect of freeze-thaw on the hydraulic conductivity and morphology of compacted clay. *Can. Geotech. J.* 30:236-246

Rosenbaum, U., Huisman, J.A., Weuthen, A., Vereecken, H., and Bogena, H.R. (2010). Sensor-to-sensor variability of the ECH (2) O EC-5, TE, and 5TE sensors in dielectric liquids. *Vadose Zone J.* 9(1):181–186. doi:10.2136/vzj2009.0036.

Roy, D., Jia, X., Steele, D. and Lin, D. (2018). Development of soil water release curves for three soils in the Red River of the North, USA. *Soil Sci. Soc. Am. J.* doi: 10.2136/sssaj2017.09.0324

Russo, D. (1988). Determining soil hydraulic properties by parameter estimation on the selection of a model for the hydraulic properties. *Water Resour. Res*. 24:453-459

Saito, K., Kimoto, M., Zhang, T., Takata, K., and Emori, S. (2007). Evaluating a high-resolution climate model: Simulated hydrothermal regimes in frozen ground and their change under the global warming scenario, *J. Geophys*. Res. 112: 1-19 doi: 10.1029/2006JF000577.

Scherer, T., Kandel, H., Sands, G., & Hay, C. (2013). Frequently asked questions about subsurface (tile) drainage. AE1690: North Dakota State University.

Soil Survey Staff, Natural Resources Conservation Service, United States Department of Agriculture. Web Soil Survey. Available online at the following link: https://websoilsurvey.sc.egov.usda.gov/. Accessed [01/20/2018].

Stahli, M. (1999). Soil moisture redistribution and infiltration in frozen sandy soils. *Water Resour. Res.* 35(1):95-103

Topp, G.C., Davis, J.L., and Annan, A.P. (1980). Electromagnetic determination of soil water con- tent: Measurements in coaxial transmission lines. *Water Resour. Res.* 16(3):574–582. doi:10.1029/WR016i003p00574.

van Genuchten, M. Th. (1980). A closed form equation for predicting the hydraulic conductivity of unsaturated soils. *Soil Sci. Soc. Am. J.* 44:892–898.

Vaz, C.M.P., Scott, J., Mercer, M., and Tuller. M. (2013). Evaluation of standards calibration functions for eight electromagnetic soil moisture sensors. *Vadose Zone. J.* 12(2):1-16 doi:10.2136/vzj2012.0160.

Wraith, J. M. and D. Or. (1998). Nonlinear parameter estimation using spreadsheet software. *J. Nat. Resour. Life Sci. Educ.* 27:13-19.

Zhang, R., and van Genuchten, M. Th. (1994). New models for unsaturated soil hydraulic properties. *Soil. Sci.* 158:77-85

Zhang. R. (1997). Determination of soil sorptivity and hydraulic conductivity from the disk infiltrometer. *Soil Sci. Soc. Am. J.* 61:1024-1030

5. GENERAL CONCLUSIONS

The combined HYPROP and WP4 produced good quality data over the entire wet and dry soil moisture range and constructed a better SWRC because of the improved measurement ranges for estimating van Genuchten fitting parameters. Glyndon silty loam and Hecla sandy loam soils had the best fitted SWRCs by combined HYPROP and WP4 method in terms of shape and slope. Fargo soil did not produce a good SWRC due to the presence of clay and its swelling and shrinkage nature in the Red River Valley. It saves at least half the time, applies simpler procedures, and could be considered as an acceptable approach for replacing the traditional laboratory method.

For the initial water contents of θ_{pwp}, θ_{mid}, and θ_{fc}, the infiltration rates in a frozen silty clay loam soil of RRB were measured. The soil with θ_{pwp} was comparatively drier that resulted in a higher initial infiltration rate, the initial infiltration rate was comparatively lower in the soil with the initial water content of θ_{mid}, and the soil with the initial water content of θ_{fc} reached saturation quickly. The infiltration curves over time shifted downwards from dry soil to wet soil before the infiltration rate became steady. The average final infiltration rate was close to the predicted rate for the dry soil with θ_{pwp}, higher than the predicted rate for the soil with θ_{mid}, and lower than the predicted rate for soil with θ_{fc}. In the soil with θ_{pwp}, the θ_v changed with temperature gradually, the θ_v changed rapidly in the soil with θ_{mid}, and the θ_v in the soil with θ_{fc} did not change with temperature due to the limited pore space.

In this study, the average temperature and electrical conductivity (EC) of the water, used in the infiltration experiment, were 18°C and 985 μs/cm. In future research, variation of temperature and EC of infiltrating water into frozen soil could be investigated. The outcomes

might help to understand the changes in frozen soil hydraulic properties due to temperature and EC difference.

Three soils of RRB, Colvin silty clay loam, Fargo silty clay, and Hecla sandy loam, in frozen and unfrozen conditions with initial soil water contents of $\theta_{ovendry}$, $\theta_{pwp,}$ θ_{mid}, θ_{fc}, and θ_{sat} were used to measure hydraulic conductivity (k) by minidisk infiltrometer. The k values were varied from higher to lower with the increment of $\theta_{initial}$. Higher clay content of Fargo soil might hold more water, produced more ice, and reduced the hydraulic conductivity. Due to higher sand content of Hecla soil, high hydraulic conductivity values, in dry frozen soil and even in saturated unfrozen soil, were found. The frozen soil k values were also estimated by using Motivilov model and compared to measured k values. The fitted models were simple in terms of parameters. Those equations could predict better k values compared to Motivilov model for Colvin and Fargo soils, though the predicted k values were somewhat off from the measured k values.

Multiple soil packing and freeze-thaw cycles destroy the soil aggregates, resulting in fewer macropores, may result in reduced infiltration rate and expedite the saturation process in the soil with the initial water content of θ_{fc}. The k variation with different FT cycle might indicate that soil hydraulic properties changed with increased FT cycles.

APPENDIX. INFILTRATION MEASUREMENT IN FROZEN AND UNFROZEN SOILS

Total 20 field experiments were conducted by using Cornel Sprinkler infiltrometer at two locations of the Red River of North Basin (RRB): (1) North Moorhead, Morken Township, Clay County, MN, and (2) Fairmount, Richland County, ND. The infiltration rates were measured in both frozen and unfrozen conditions of the soils in fall, spring and summer of 2014, 2015, and 2016. All field test results were summarized according to soil frozen/unfrozen conditions and time of the year when the experiments were executed. These measured datasets can be used as reference for future frozen soil studies such as infiltration modeling, simulated or measured results validation, and comparison.

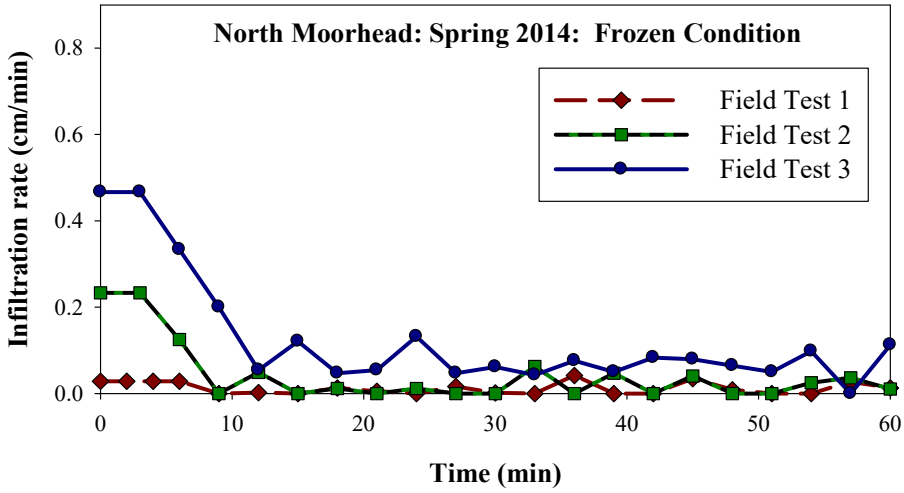

Figure A1. Field tests in frozen condition (North Moorhead, spring 2014).

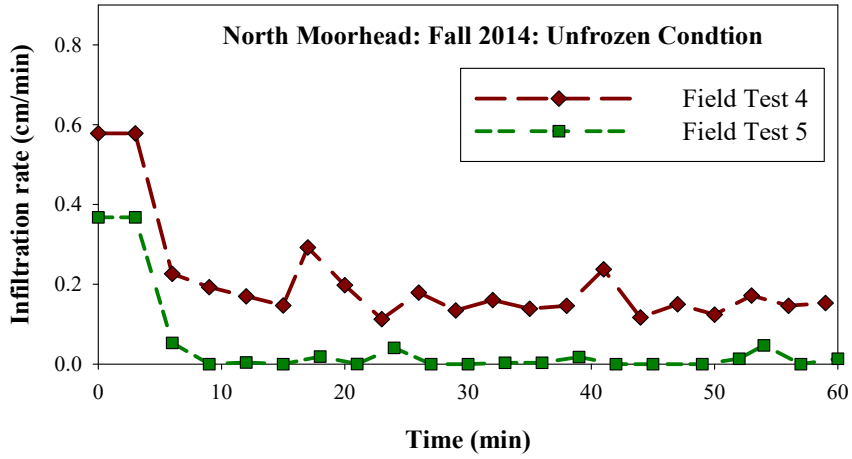

Figure A2. Field tests in unfrozen condition (North Moorhead, fall 2014).

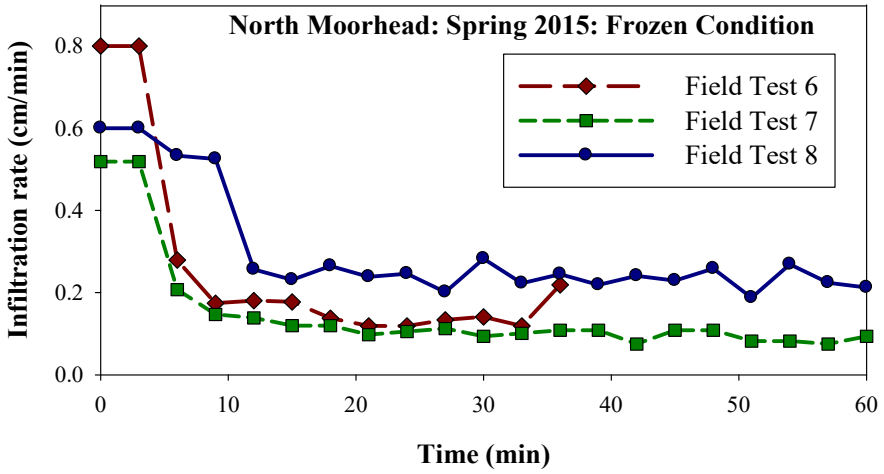

Figure A3. Field tests in frozen condition (North Moorhead, spring 2015).

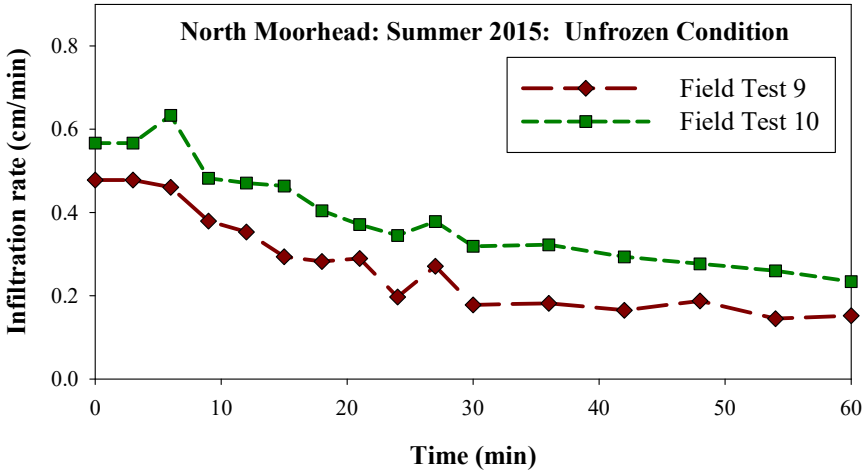

Figure A4. Field tests in unfrozen condition (North Moorhead, summer 2015).

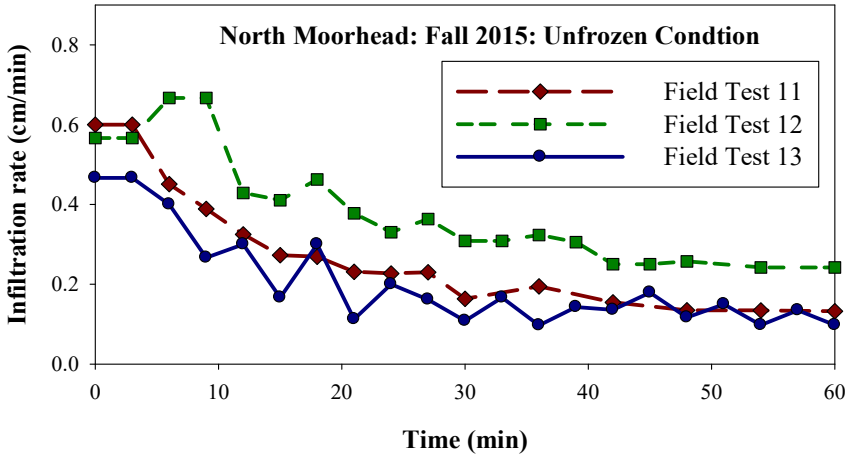

Figure A5. Field tests in unfrozen condition (North Moorhead, fall 2015).

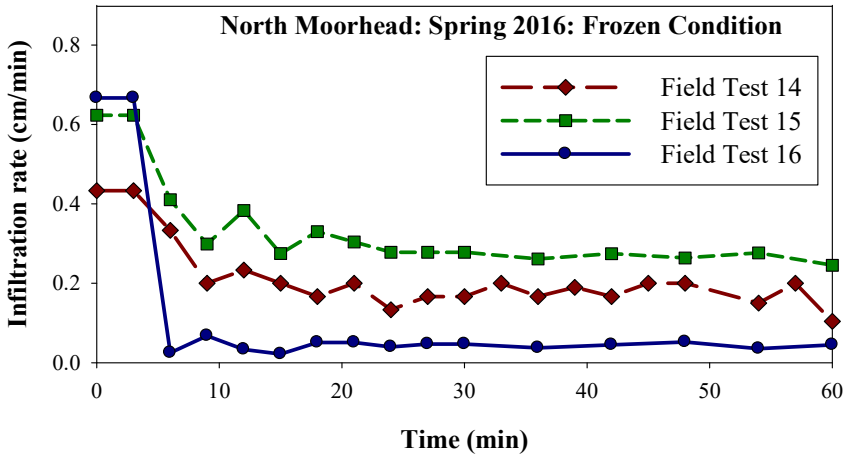

Figure A6. Field tests in frozen condition (North Moorhead, spring 2016).

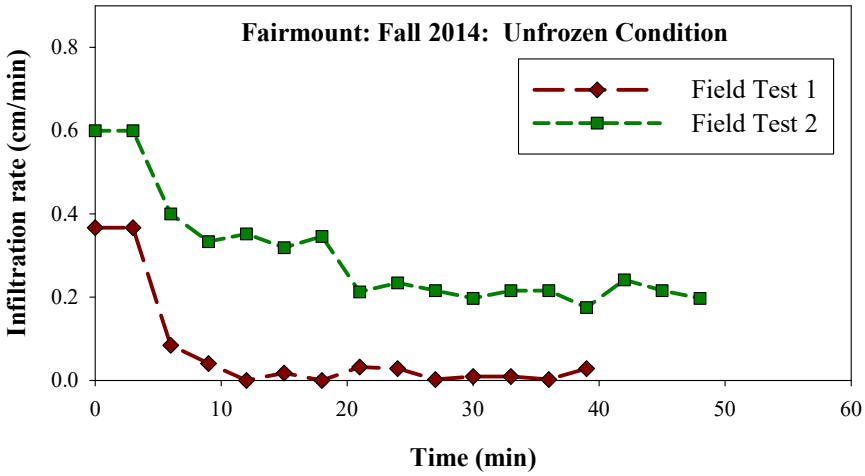

Figure A7. Field tests in frozen condition (Fairmount, fall 2014).

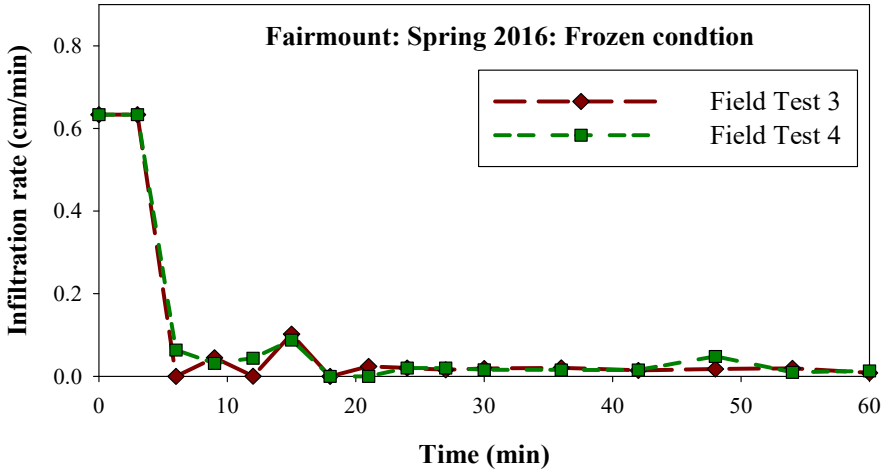

Figure A8. Field tests in frozen condition (Fairmount, spring 2016).

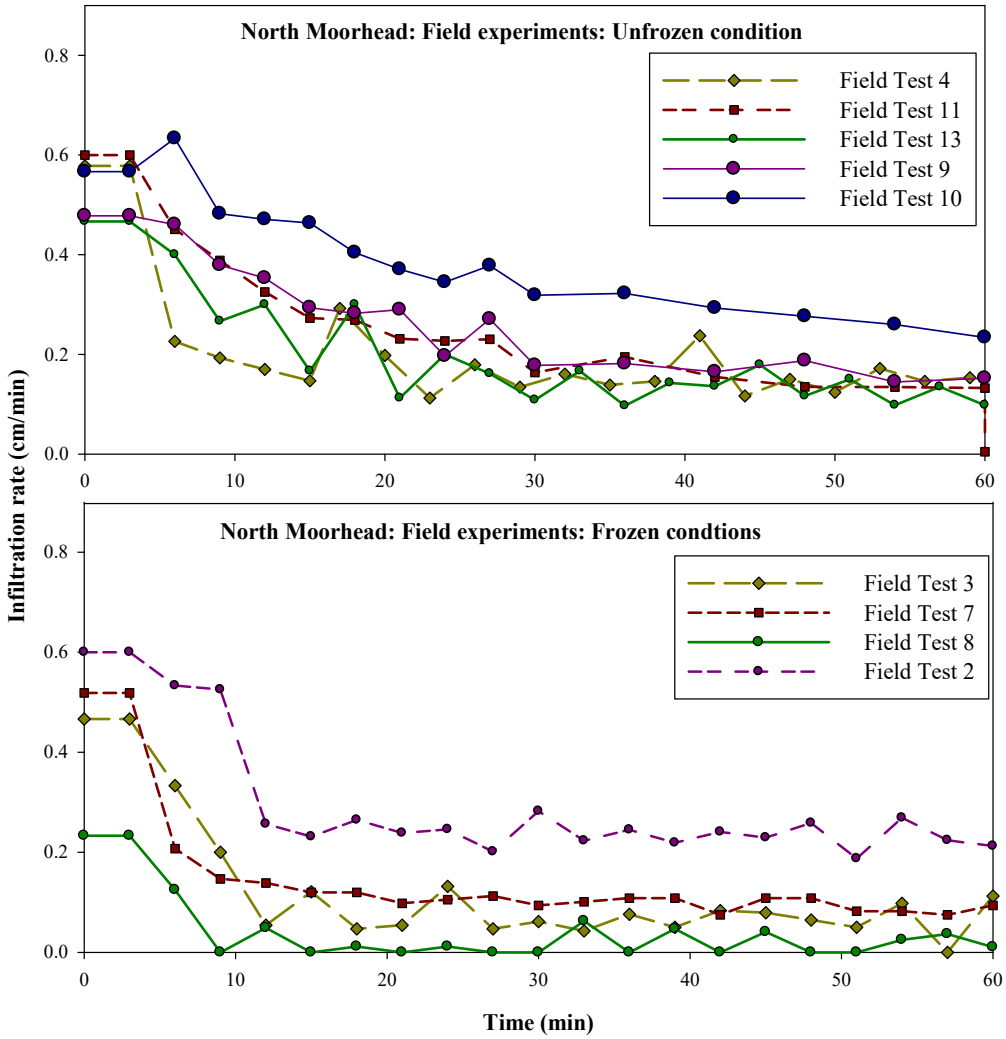

Figure A9. Field experiments: unfrozen vs frozen condition (North Moorhead, all years).